

1 **TITLE**

2

3 **CSF1R inhibitor levels determine sex-specific phenotype of resilient microglia and**
4 **neurofunctional rescue leading to extended survival in tauopathy mice**

5

6 **AUTHORS**

7 Noah R. Johnson^{1,2†}, Peng Yuan^{1,3†}, Erika Castillo¹, T. Peter Lopez¹, Weizhou Yue¹, Annalise
8 Bond¹, Brianna M. Rivera¹, Miranda C. Sullivan¹, Masakazu Hirouchi^{1,4}, Kurt Giles^{1,5}, Atsushi
9 Aoyagi^{1,4}, and Carlo Condello^{1,5†*}

10 ¹ Institute for Neurodegenerative Diseases, UCSF Weill Institute for Neurosciences, University
11 of California, San Francisco, CA 94158, USA.

12 ² University of Colorado Alzheimer's and Cognition Center, Linda Crnic Institute for Down
13 Syndrome, Department of Neurology, University of Colorado Anschutz Medical Campus,
14 Aurora, CO 80045, USA.

15 ³ Department of Rehabilitation Medicine, Huashan Hospital, State Key Laboratory of Medical
16 Neurobiology, Institute for Translational Brain Research, MOE Frontiers Center for Brain
17 Science, Fudan University, Shanghai 200032, China.

18 ⁴ Daiichi Sankyo Co., Ltd., Tokyo, 140-8710, Japan.

19 ⁵ Department of Neurology, UCSF Weill Institute for Neurosciences, University of California, San
20 Francisco, CA 94158, USA.

21

22 †N.J., P.Y. and C.C. contributed equally to this work. *Correspondence to:
23 carlo.condello@ucsf.edu

24

25

26

27 **ABSTRACT**

28 Microglia are central to pathogenesis in many neurological conditions. Drugs targeting colony-
29 stimulating factor-1 receptor (CSF1R) to block microglial proliferation in preclinical disease
30 models have shown mixed outcomes, thus the therapeutic potential of this approach remains
31 unclear. Here, CSF1R inhibitors were evaluated in tauopathy mice using multiple dosing
32 schemes, drug analogs, and longitudinal measurements in the brain and plasma. A sex-
33 independent reduction in pathogenic tau was seen in several models and non-microglial gene
34 expression patterns reverted toward a normal wild type signature. Surprisingly, despite greater
35 drug exposure in male mice, functional rescue and extended survival was only observed in
36 female mice. A dose-dependent upregulation of immediate early genes and neurotransmitter
37 dysregulation were observed in the brains of male mice only, indicating that excitotoxicity may
38 have precluded functional benefits. Drug-resilient microglia in male mice exhibited
39 morphological and gene expression patterns consistent with increased neuroinflammatory
40 signaling, suggesting a mechanistic basis for sex-specific excitotoxicity. These data argue that
41 complete microglial ablation is neither required nor desirable for neuroprotection and that
42 therapeutics targeting microglia must consider sex-dependent effects on functional outcomes.

43

44 **INTRODUCTION**

45 Microglia, the resident innate immune cells of the central nervous system (CNS), are important
46 for neurodevelopment and homeostasis, and are a fundamental component to pathogenesis in
47 many neurological conditions. We now appreciate that microglia are heterogeneous cells, are
48 influenced by the periphery, have sex-dependent biology, and can be helpful or harmful
49 depending on the disease stage or specific pathology¹⁻⁴. Gene mutations affecting the
50 expression and sequence of microglial genes (e.g. *TREM2*, *CD33*, and *MS4A*) increase risk for
51 Alzheimer's disease (AD), and implicate microglia in several disease pathways including toxic
52 protein aggregation (A β and tau) and neuroinflammation^{5,6}. Thus, for the first time, there is
53 unequivocal evidence in humans that certain microglial functions are robustly involved in the
54 pathogenesis of neurodegenerative disease. However, the precise mechanisms governing
55 microglia function in disease are still not well understood.

56 In tauopathy (a family of neurodegenerative disorders characterized by tau inclusions in neural
57 cells), there is growing evidence that microglia play an early and constant role in tau

58 aggregation and neuronal loss. Disease-activated microglia can secrete pro-inflammatory
59 cytokines that regulate neuronal kinases and phosphatases causing tau hyperphosphorylation,
60 aggregation and consequent neurodegeneration⁷⁻⁹. Genome-wide transcriptomic studies have
61 identified innate immune pathways that implicate early and robust involvement of microglia in
62 human tauopathy^{10,11} and related mouse models^{12,13}. Deletion of microglia-specific genes or
63 genetic ablation of microglial cells in rodents have been useful approaches to dissect microglia-
64 mediated mechanisms in disease models, but pharmacologic tools to more dynamically
65 manipulate microglial function have been limited. Recently developed small-molecule drugs
66 targeting colony-stimulating factor-1 receptor (CSF1R), a receptor kinase critical for survival and
67 proliferation of CNS microglia, peripheral tissue macrophages and blood myeloid cells¹⁴, are
68 approved for clinical use in various oncology indications¹⁵, and have now been adopted by the
69 neuroscience community to study microglia biology. In the past few years, there have been
70 numerous studies using CSF1R inhibitors in models of neurological disease, but only a few
71 studies in models of primary tauopathy¹⁶⁻¹⁹. While important first steps, these studies only
72 explored single, static time points of treatment, or used only one sex. Given the dynamic nature
73 and complexity of microglial activation, the timing of CSF1R inhibition in tauopathy and its
74 translational relevance is still an open question.

75 Thus, the goal of our study was to define a therapeutic window that not only reduced
76 pathological markers, but also led to functional improvement. Moreover, we questioned whether
77 complete or continuous microglial ablation using CSF1R inhibitors was necessary given the
78 important and diverse roles these cells play in brain health and disease. Here, we systematically
79 test CSF1R inhibition using multiple drug analogs at several time points in transgenic mice
80 developing spontaneous tauopathy, and in an inoculation model of induced tauopathy. We
81 demonstrate a reduction of tau pathology in multiple dosing schemes without complete
82 microglial ablation; drug exposure levels correlated with the extent of tau-prion²⁰ and microglial
83 reduction. Surprisingly, we observed suppressed plasma biomarkers of neurodegeneration,
84 rescue of aberrant behavior, and extended survival in female mice only. These data reveal a
85 previously unrecognized sex-dependent therapeutic benefit of pharmacological CSF1R
86 inhibition. Transcriptome analyses showed that treated tauopathy mice exhibited a restored
87 gene expression profile similar to wild type mice; however, we observed a specific module of
88 sex- and drug concentration-dependent gene expression that might explain the lack of
89 functional rescue in male mice. Interestingly, residual microglia had a morphology similar to wild
90 type microglia and their gene expression pattern indicated a unique, sex-specific signature in

91 response to CSF1R inhibition. These data highlight yet another context for microglial
92 heterogeneity with implications for novel microglial biology, and argue that tempering microglial
93 activation with drugs, rather than cellular ablation, is a better therapeutic strategy with clinical
94 relevance.

95 **RESULTS**

96 **CSF1R inhibition reduces pathogenic tau in the brains of Tg2541 mice**

97 Building on previous findings¹⁶⁻¹⁹, we first evaluated the effect of CSF1R inhibition on the levels
98 of pathogenic tau in the brains of transgenic mice expressing human tau, using a cell-based tau-
99 prion bioassay, enzyme-linked immunosorbent assay (ELISA), and immunohistochemical (IHC)
100 analysis. To deplete microglia, Tg2541 mice were dosed with one of two potent, orally
101 bioavailable, and brain-penetrant CSF1R inhibitors: PLX3397 (pexidartinib), which binds
102 receptor tyrosine kinases CSF1R, and to lesser extent, KIT and FLT3²¹, and PLX5622, which
103 selectively binds CSF1R²². Three different treatment paradigms were evaluated: acute (2–4
104 months old), chronic (2–7 months old), and terminal (2 months old until death) (Fig. 1a–c).
105 Transgenic B6-Tg(Thy1-MAPT*P301S)2541 mice²³, referred to here as Tg2541 mice, express
106 the 0N4R isoform of human tau with the familial frontotemporal lobar degeneration (FTLD)-
107 linked P301S mutation²⁴, which increases its aggregation propensity and prion-like
108 characteristics^{25,26}. We previously demonstrated that the levels of pathogenic tau in hindbrain
109 regions of Tg2541 mice were greater than in forebrain regions²⁷. This observation is consistent
110 with the neuropathological staging of human FTLD and specifically of progressive supranuclear
111 palsy (PSP) where tau deposition begins and predominates in subcortical and brainstem
112 nuclei²⁸. Therefore, the forebrain and hindbrain regions were examined separately in this study
113 (Fig. 1d).

114 We confirmed that CSF1R inhibition effectively reduced microglial markers Iba1 and P2yr12 by
115 an average of ~60% in both the forebrains and hindbrains of Tg2541 mice compared to vehicle
116 treatment, and that they had similar effects in the brains of C57BL/6J wild type mice
117 (Supplementary Fig. 1a–p). Principal component analysis of all Iba1 and P2yr12 data combined
118 showed that sex did not have a significant effect on the extent of microglial depletion by CSF1R
119 inhibitors (Supplementary Fig. 1q and Supplementary Data File 1), and therefore male and
120 female mice were grouped together for analysis unless otherwise noted.

121 We next employed a reproducible and rapid cell-based bioassay^{27,29,30} to measure the activity of

122 replication-competent tau-prions in brain homogenates from Tg2541 mice. To ensure an
123 appropriate dynamic range in this bioassay, we optimized for dilution factor and assay duration
124 using aged Tg2541 mouse brain samples, which showed greater than 100-fold higher signal
125 than wild type mouse brain samples (Supplementary Fig. 2). Following acute, chronic, or
126 terminal treatment with PLX3397 or PLX5622, tau-prion activity in the forebrains of Tg2541 mice
127 was significantly decreased compared to vehicle-treated mice (Fig. 1e–g).
128 Hyperphosphorylation and aggregation of tau occurs first in hindbrain regions of Tg2541 mice,
129 especially in the brainstem and spinal cord, leading to motor deficits caused by severe
130 paraparesis²³. This is consistent with our previous report of early and aggressive tau-prion
131 activity in hindbrain regions of Tg2541 mice²⁷; as such, we found that acute CSF1R inhibition
132 was insufficient to reduce tau-prion activity in the hindbrain (Fig. 1e). However, chronic or
133 terminal treatment with PLX3397 did significantly reduce tau-prion activity in hindbrain regions
134 (Fig. 1f,g) and the spinal cords of Tg2541 mice (Supplementary Fig. 3). To examine other
135 markers of pathogenic tau, we measured the levels of tau phosphorylated at Ser396 (pS396) by
136 ELISA, and tau phosphorylated at Ser202/Thr205 (pS202/T205) by IHC. Acute, chronic, or
137 terminal PLX3397 treatment robustly reduced pS396 tau in both forebrain and hindbrain regions
138 of Tg2541 mice (Fig. 1h–j), and also reduced pS202/T205 tau in forebrain regions (Fig. 1k–m)
139 and in the spinal cord (Supplementary Fig. 3d). Since the various measures of tau pathology
140 represent different steps of tau pathogenesis (hyperphosphorylation vs. oligomerization vs.
141 filament formation), they may be differentially impacted by CSF1R inhibition with different
142 treatment regimens. Thus, to consider all tau measurements and both brain regions together,
143 we performed principal component analysis which revealed that pathogenic tau was reduced by
144 both CSF1R inhibitors, and that there was no significant effect of sex on drug efficacy (Fig. 1n
145 and Supplementary Data File 1).

146 Having verified the benefits of microglial depletion at an early disease stage, we next wondered
147 whether initiating CSF1R inhibition at a more advanced stage of disease would have similar
148 effects, simulating an interventional drug treatment. Thus, we dosed Tg2541 mice with PLX3397
149 in a delayed treatment paradigm (4–7 months old). Similar to terminal treatment, interventional
150 treatment also significantly reduced tau-prion activity in both the forebrain and hindbrain
151 (Supplementary Fig. 4a,b). Although pS396 tau levels were unchanged after interventional
152 treatment, levels of tau phosphorylated at Thr231 (pT231) were reduced in the forebrain
153 (Supplementary Fig. 4c,d). Considering the potential off-target effects of continuous, long-term
154 microglial depletion on brain function, we also wondered whether periodic CSF1R inhibition

155 might provide a safer, yet similarly efficacious therapy. Thus, we also tested PLX3397 dosed
156 intermittently by repeating dosing cycles of three weeks on followed by three weeks off. The
157 intermittent dosing interval was selected based on prior studies showing that there is rapid
158 microglial repopulation of the brain, and that morphological and transcriptional changes in the
159 microglia return to baseline levels within 21 days of removing PLX³¹. Intermittent treatment
160 produced similar reductions in the levels of microglial markers in both brain regions as for
161 continuous treatment (Supplementary Fig. 1r-t), but tau-prion activity and pT231 levels were
162 reduced only in the forebrain (Supplementary Fig. 4e-h). Taken together, these data suggest
163 that intermittent/interventional dosing is sufficient to reduce pathogenic tau in the forebrain of
164 Tg2541 mice, likely due to slower disease kinetics; however, continuous CSF1R inhibition is
165 necessary for the extended reduction of pathogenic tau in the hindbrain.

166 Tau has been shown to propagate throughout the brain in a prion-like fashion along
167 interconnected neural networks^{32,33}. To test the hypothesis that microglial depletion may reduce
168 the propagation of tau-prions²⁰ in the brains of Tg2541 mice, we inoculated fibrils of the
169 microtubule-binding repeat domain of tau, referred to as K18 fibrils³⁴, into the hippocampus and
170 overlying cortex (forebrain regions) of Tg2541 mice and then treated them with PLX3397.
171 Compared to un-inoculated mice, K18-inoculated mice had significantly increased tau-prion
172 levels in the ipsilateral (inoculated) forebrain, as well as in the contralateral forebrain and in the
173 hindbrain (Supplementary Fig. 5), which suggests that tau-prions had propagated from the
174 inoculation site to those brain regions. However, acute PLX treatment was sufficient to
175 significantly reduce tau-prion levels in the ipsilateral forebrain and hindbrain, as well as in the
176 contralateral forebrain. Furthermore, tau-prion levels in the contralateral forebrain of PLX-
177 treated mice were not significantly different from the forebrain of un-inoculated, vehicle-treated
178 mice (Supplementary Fig. 5), which indicates that CSF1R inhibition prevented the spreading of
179 tau-prions from the inoculation site to this brain region.

180 CSF1R inhibition can affect peripheral immune cells such as blood myeloid cells and tissue
181 macrophages, in addition to microglia^{17,35}. To determine if the effects of PLX3397 and PLX5622
182 on pathogenic tau in the brain are due, at least in part, to depletion of peripheral CSF1R-
183 expressing cells we dosed Tg2541 mice with PLX73086³⁶, a non-brain penetrant CSF1R
184 inhibitor analog of PLX3397 and PLX5622. Chronic treatment with PLX73086 had no significant
185 effect on microglial markers Iba1 and P2yr12, or on levels of tau-prions or pTau[S396] or
186 pTau[T231] in the forebrain or hindbrain of Tg2541 mice (Supplementary Fig. 6). Therefore, the
187 effects of CSF1R inhibitors in peripheral compartments do not significantly contribute to their

188 reduction of pathogenic tau in the CNS. We also evaluated the numbers of Iba1⁺/CD206⁺
189 perivascular macrophages (PVMs) and found that PLX3397 treatment did not significantly
190 deplete this cellular population, although there was a trend ($P = 0.0947$) towards reduced PVMs
191 in female Tg2541 mice (Supplementary Fig. 7). Lastly, because there is limited data for CSF1R
192 expression in neurons after injury³⁷, we considered whether PLX3397 or PLX5622 might affect
193 neurons or their expression of tau protein in Tg2541 mice. Acute, chronic, and terminal CSF1R
194 inhibition did not significantly reduce levels of neuronal nuclei (NeuN), detected by IHC, or total
195 tau, detected by ELISA (Supplementary Fig. 8). Therefore, CSF1R inhibitors do not directly
196 affect measures of neuronal viability or tau expression, consistent with a prior report using
197 PLX3397 in cultured primary neurons¹⁷. Together, these data confirm that drug effects on
198 biological and functional end points are due to inhibition of CSF1R in CNS microglia.

199 **CSF1R inhibition extends survival in female Tg2541 mice**

200 We next focused on the terminal treatment paradigm with PLX3397 to evaluate the long-term
201 effects of CSF1R inhibition on lifespan and behavior. Tg2541 mice develop paraparesis from
202 5–6 months of age which makes feeding difficult, resulting in a loss of body weight and thus, a
203 greatly reduced lifespan compared to wild type mice. We found that terminal PLX treatment
204 significantly extended the median survival of female Tg2541 mice [16.5 days longer median
205 survival; $P = 0.0004$], but not male Tg2541 mice, compared to vehicle treatment (Fig. 2a,b). The
206 extended survival in PLX-treated female mice was preceded by significantly reduced weight
207 loss, which was not observed in male mice (Fig. 2c). Body weight at 180 days of age,
208 irrespective of treatment, was predictive of lifespan in female mice but not in male mice, with
209 less weight loss being correlated with longer survival (Fig. 2d). Lower forebrain tau-prion levels
210 were also correlated with longer survival in female mice but not in male mice (Fig. 2e),
211 suggesting that Tg2541 mice have a sex-specific physiological response to tauopathy. To
212 confirm the effect of PLX treatment on survival in a different experimental paradigm, we used a
213 midbrain inoculation model. Since Tg2541 mice spontaneously develop substantial tau
214 pathology in the midbrain²⁷, we predicted that K18 inoculation in the midbrain would accelerate
215 and synchronize the disease course, which would be ideal for studying mouse survival. Indeed,
216 female Tg2541 mice inoculated with K18 tau fibrils died significantly earlier than mice inoculated
217 with diluent, though no difference was observed in male mice (Fig. 2f,g). Consistent with our
218 prior result, PLX treatment significantly extended the median survival of female mice inoculated
219 with K18 tau fibrils [29.5 days longer median survival; $P = 0.0095$], but not male mice, compared
220 to vehicle treatment (Fig. 2h). Taken together, these data indicate that CSF1R inhibition robustly

221 extends the lifespan of female Tg2541 mice, even during an accelerated disease course.

222 **CSF1R inhibition reduces aberrant behavioral phenotypes in Tg2541 mice**

223 To examine the relationship between drug exposure and markers of disease progression more
224 closely, we collected blood plasma at monthly intervals from mice receiving terminal treatment
225 with PLX3397 or vehicle (Fig. 3a). Consistent with previous reports¹⁷, male Tg2541 mice had
226 higher plasma (25.3%; $P < 0.0001$) and brain (44.9%; $P = 0.0250$) concentrations of PLX than
227 did female mice (Fig. 3b and Supplementary Fig. 9a–c); we also observed this difference in wild
228 type mice (Supplementary Fig. 9d,e). Male and female mice had *ad libitum* access to food, and
229 had similar rates of food consumption relative to body weight, independent of whether it
230 contained PLX or vehicle (Supplementary Fig. 10a,b). However, female mice were consistently
231 more active than male mice (Supplementary Fig. 10c,d). Thus, the reduced PLX exposure in
232 female mice is likely due to a higher metabolic and drug clearance rate compared with male
233 mice. In line with the hypothesis that drug exposure was excessive in male mice, we observed a
234 trend towards reduced body weight in male wild type mice receiving terminal PLX treatment, but
235 not in female wild type mice (Supplementary Fig. 9f). In spite of this sex-specific difference in
236 PLX exposure, we found that higher plasma concentrations of PLX were correlated with greater
237 microglial depletion in both forebrain and hindbrain regions, independent of sex (Fig. 3c).
238 Furthermore, higher PLX exposure was correlated with reduced tau-prion levels in the forebrain
239 regions of both male and female mice (Fig. 3d). Together, these data indicate that PLX has
240 dose-dependent on-target effects in both male and female mice.

241 Previous studies have demonstrated a common hyperactive phenotype in the early stages of
242 tauopathy in transgenic rodent models^{38,39}. While the precise mechanism that leads to this
243 deficit is unclear, this phenotype is causally linked with tau aggregate burden⁴⁰. Based on the
244 reduction of tau deposition we observed with PLX treatment, we sought to also examine its
245 effect on this hyperactive phenotype. Using an automated home-cage monitoring system, we
246 longitudinally tracked the activity levels in Tg2541 mice at different ages, measuring their
247 amounts of rearing, locomotion, and wheel running. We confirmed the previous reports, finding
248 that at early ages the Tg2541 mice displayed a hyperactive phenotype relative to wild type mice
249 (90–150 days old in females, 90–120 days old in males), while at later ages their activity was
250 significantly reduced (Fig. 3e), likely due to the accumulation of pathogenic tau in brain regions
251 associated with motor function. PLX treatment led to a consistent reduction in Tg2541 mouse
252 hyperactivity, but did not change their hypoactivity at later ages (Fig. 3e), indicating the activity

253 reduction is not due to a general weakening effect. Detailed examination of the individual activity
254 measurements revealed that PLX treatment normalized the amounts of wheel running (Fig. 3f)
255 and active time (Fig. 3g). These data indicate that PLX treatment corrects the aberrant behavior
256 of Tg2541 mice towards that of wild type mice.

257 **Sex-dependent effects of CSF1R inhibition on a biomarker of CNS injury**

258 To further interrogate CNS damage caused by tauopathy, or potentially caused by the observed
259 sex-dependent PLX exposure, we also evaluated the plasma levels of neurofilament light chain
260 (NfL). NfL is a validated blood-based biomarker of neuronal injury⁴¹ which correlates with
261 disease progression and tau burden in human tauopathy^{42,43}. Female PLX-treated mice had
262 reduced levels of NfL compared to vehicle-treated mice (Fig. 4a,b), consistent with reduced
263 CNS injury due to tauopathy. Conversely, NfL levels were increased in male mice following PLX
264 treatment (Fig. 4c), suggestive of PLX-induced toxicity. Consistent with these findings, PLX
265 treatment resulted in significantly increased NfL levels in male mice that received midbrain
266 inoculation of K18 tau fibrils, but not female mice (Fig. 4d-f). We found no correlation between
267 NfL level and survival in female mice, but in male mice, higher NfL levels were strongly
268 correlated with reduced survival in both PLX and vehicle treatment groups (Fig. 4g,h).
269 Furthermore, the concentrations of NfL in both the forebrain and hindbrain at death were
270 positively correlated with PLX3397 concentration in the brains of male, but not female, Tg2541
271 mice (Fig. 4i,j). Interestingly, intermittent treatment, resulting in a 50% lower total dosage of
272 PLX, produced a significant decrease in NfL levels in male mice, but had no effect in female
273 mice (Fig. 4k-m). Taken together, these data suggest that in female Tg2541 mice, tauopathy
274 drives CNS injury and its reduction by PLX effectively masks any effect of PLX toxicity, whereas
275 in male mice, excessive exposure causes CNS injury that supersedes any benefit of PLX.
276 Consistent with this premise, we found that PLX treatment increased plasma NfL levels in male
277 wild type mice, as expected, but also in female wild type mice (Fig. 4n-p), albeit at substantially
278 lower levels than tau-induced NfL in Tg2541 mice.

279 **Peripheral CSF1R inhibition does not cause therapeutic or adverse effects in the CNS**

280 CSF1R inhibitors have known adverse effects in the periphery including anemia, leukopenia,
281 and hepatotoxicity, which have been observed in human clinical trials⁴⁴. To determine if
282 peripheral PLX toxicity was causing NfL release or reducing drug efficacy, we evaluated mice
283 receiving chronic treatment with PLX73086, the non-brain penetrant CSF1R inhibitor analog of
284 PLX3397 and PLX5622. We observed no effect of PLX73086 treatment on body weight or

285 plasma NfL levels in either male or female Tg2541 mice (Fig. 5a–d), indicating that peripheral
286 CSF1R inhibition does not impact tauopathy-driven phenotypes. Furthermore, we observed no
287 effect of PLX73086 treatment on body weight or plasma NfL levels in wild type mice (Fig. 5e–h),
288 demonstrating that the drug-induced toxicity indicated by NfL rise is dependent on the drug
289 entering the brain. Histopathological evaluation of liver sections of PLX3397-dosed Tg2541
290 mice stained with hematoxylin and eosin (H&E), Masson’s trichrome, or Picosirius red did not
291 reveal any overt signs of liver injury or fibrosis (Fig. 5j), nor did quantification of the Picosirius
292 red-stained liver sections (Fig. 5k). Alkaline phosphatase (ALP) in the plasma, a different
293 indicator of liver damage, was elevated in Tg2541 mice following PLX3397 treatment; however,
294 the ALP levels were elevated in both male and female mice (Fig. 5l), indicating that the sex-
295 specific toxicity of PLX3397 in male mice likely occurs in the brain rather than in the periphery.
296 Taken together, these data further confirm that the drug exposure of brain-penetrant CSF1R
297 inhibitors was appropriate for female Tg2541 mice to reduce tauopathy and significantly extend
298 survival; however, the drug exposure was too high for male Tg2541 mice, and the resulting
299 neurotoxicity outweighed its therapeutic benefit.

300 **CSF1R inhibition shifts gene expression patterns in Tg2541 mice towards wild type**

301 To better characterize global molecular changes in the CNS due to CSF1R inhibition, we used
302 the Nanostring platform to analyze a curated panel of gene transcripts related to
303 neuroinflammation, myeloid cell function and neuropathology in bulk brain tissue following
304 chronic treatment of Tg2541 mice with PLX5622. The chronic treatment group was selected for
305 this analysis because the collection time point was synchronized (unlike in the terminal
306 treatment group) and seven months of age is close to the average lifespan of Tg2541 mice. We
307 measured mRNA transcripts of 1,841 genes, many of them shown to be regulated by tau or A β
308 pathology in previous genome-wide gene expression studies^{12,13}. To validate the Nanostring
309 approach, we identified 53 genes with a broad range of expression level changes and measured
310 mRNA transcripts with quantitative reverse-transcription PCR (RT-qPCR) in the same sample
311 used for sequencing. The RT-qPCR results generally matched the trends shown in the
312 Nanostring data (Supplementary Fig. 11), supporting the validity of our transcriptomic data.

313 Since microglial cells are directly impacted by PLX treatment, we first excluded the microglial-
314 specific genes (see Methods) and examined the general trend of expression patterns among
315 different treatment groups. Pearson’s correlation matrix showed high similarity among wild type
316 brains with or without PLX treatment (Fig. 6a), indicating that the gene expression pattern we

317 measured is not affected by the treatment itself. In contrast, PLX treatment in Tg2541 mice
318 caused a distinct shift in the gene expression pattern away from the vehicle-treated group.
319 Interestingly, the gene expression patterns of PLX-treated Tg2541 mice showed a stronger
320 correlation with wild type mice than with vehicle-treated Tg2541 mice (Fig. 6a dashed boxes
321 and Fig. 6b). To further quantify this shift, we performed partial-least squares (PLS) regression
322 analysis using the gene expression data from vehicle-treated Tg2541 and wild type mice (Fig.
323 6c filled circles), and projected the data from PLX-treated mice onto the PLS dimensions (Fig.
324 6c empty circles). This allowed us to represent the transgene-specific gene expression pattern
325 in a relatively low-dimensional space, and to quantify the changes associated with treatment by
326 calculating the population vector distances and angles in this space. We found that PLX
327 treatment significantly normalized gene expression patterns in Tg2541 mice towards those of
328 wild type mice (Fig. 6d,e, only two out of five dimensions are shown, covering >95% of the total
329 variance). The normalization in gene expression was further confirmed by similar trends in
330 neuron-specific genes (Supplementary Fig. 12). Importantly, PLX treatment in wild type mice
331 showed negligible changes in the gene expression patterns. These results indicate that PLX
332 treatment specifically suppresses the abnormal transcriptome associated with transgene
333 overexpression, consistent with its effects ameliorating pathogenic tau deposition.

334 **Evidence for excitotoxicity with increased drug exposure**

335 As described above, although we observed consistent reduction in the levels of pathogenic tau
336 in the brains of both male and female Tg2541 mice with PLX treatment, only female mice
337 benefited from extended survival, functional rescue, and reduced NfL levels (Figs. 1–4). We
338 hypothesized that excessive PLX dosing may underlie this sex-specific effect, as male mice
339 consistently had higher drug exposure in the plasma and CNS (Fig. 3 and Supplementary Fig.
340 9), and also benefitted from a lower, intermittent PLX dosing paradigm (Supplementary Fig. 4).
341 Indeed, in our transcriptomic analysis we identified individual genes whose expression was
342 associated with brain PLX5622 concentration or with sex (Fig. 6f). First, we ruled out the
343 possibility that sex-dependent functional benefits were caused by differential expression of the
344 drug target, CSF1R, or its ligand, CSF1 (Supplementary Fig. 13). Using a PLS regression of all
345 non-microglia genes to brain PLX concentration and sex for each sample, we calculated the
346 variable importance score along each of these dimensions. Interestingly, many immediate early
347 genes (IEGs) showed high importance scores (Fig. 6g), suggesting that IEGs might be a
348 module that is altered by CNS drug exposure. To further test this possibility, we examined all
349 IEGs (56 genes overlapped in our dataset) and found that their expression patterns fit closely

350 with the brain PLX concentration (Fig. 6h). Importantly, when we excluded the IEGs and
351 examined the PLX-induced transcriptome shift along the wild type-to-Tg2541 dimension, the
352 correlation of gene expression changes and brain PLX concentration was no longer significant
353 (Fig. 6i), indicating that the IEGs contribute substantially to the PLX treatment effects. Notably,
354 relative to wild type vehicle-treated mice, only male PLX5622-treated Tg2541 mice had
355 significantly upregulated expression of IEGs (Fig. 6j), which we also validated using qPCR of
356 the five most highly expressed IEGs (Supplementary Fig. 14a-c), as well as by *in situ* labeling of
357 *Fos* mRNA (Fig. 6k,l). Furthermore, we observed the same drug-dependent IEG up-regulation in
358 male mice in a completely independent study using PLX3397 (Supplementary Fig. 14d-f),
359 thereby confirming that this is a robust sex-specific effect of CSF1R inhibition. As increased IEG
360 expression can be indicative of neuronal hyperactivity, these data provide a plausible
361 mechanism by which excessive PLX dosing may have led to excitotoxicity, thereby masking its
362 therapeutic effect in male mice.

363 To interrogate this mechanism directly, we performed hydrophilic interaction liquid
364 chromatography tandem mass spectrometry (HILIC-MS/MS)-based metabolomics to measure
365 the levels of relevant neurotransmitters in forebrain lysates of the mice. PLX3397-treated male
366 Tg2541 mice, but not PLX-treated wild type or female Tg2541 mice, had increased brain levels
367 of the excitatory neurotransmitter glutamate (Fig. 7a), the most common cause of neuronal
368 excitotoxicity⁴⁵. Unexpectedly, PLX-treated male Tg2541 mice also had increased levels of the
369 inhibitory neurotransmitter γ -aminobutyric acid (GABA) (Fig. 7b). However, these PLX-induced
370 alterations were not due to general neurotransmitter dysregulation because we did not observe
371 altered levels of acetylcholine, glycine, or histamine in the brains of male Tg2541 mice
372 (Supplementary Fig. 15). These data provide evidence of PLX-induced glutamate-driven
373 excitotoxicity in the brains of male Tg2541 mice which may, in part, underlie the sex-specific
374 benefit of CSF1R inhibition on mouse survival.

375 **CSF1R inhibition ameliorates pathological activation of astrocytes**

376 As suggested by the reduction of tau deposition, we hypothesized that astrocyte-driven
377 neuroinflammation would also be reduced by PLX treatment. Therefore, we examined
378 transcriptome shifts in astrocyte-specific genes upon PLX treatment. Similar to the neuronal-
379 specific genes, we observed a normalization of astrocyte-specific gene expression patterns
380 towards wild type in both forebrain and hindbrain regions (Fig. 8a,b). Using previously described
381 astrocytic gene signatures of disease⁴⁶, we found that PLX treatment led to a dose-dependent

382 reduction in the expression of the A1 astrocytic gene cluster associated with neurotoxic effects
383 (Fig. 8c,d). In addition, we measured astrogliosis over time using longitudinal bioluminescence
384 imaging (BLI) methods based on a previously established transgenic reporter system of glial
385 fibrillary acidic protein (GFAP)-driven luciferase⁴⁷, which we validated by IHC and mRNA
386 analyses (Supplementary Fig. 16). To perform reliable BLI in Tg2541 mice, we intercrossed
387 each transgenic line to an albino background and refined the method, using a synthetic luciferin
388 substrate to increase signal from deep hindbrain regions (see Methods and Supplementary Fig.
389 17). This technique allowed us to non-invasively measure astrogliosis in live mice longitudinally
390 over the course of PLX treatment. In vehicle-treated Tg2541 mice, the BLI signal gradually
391 increased with age (Supplementary Fig. 18), in accordance with the accumulation of tau
392 pathology and gliosis reported in Tg2541 mice^{23,48}. Consistent with our hypothesis and with
393 measurement of GFAP using other methods (Supplementary Fig. 16), CSF1R inhibition
394 suppressed the BLI signal in both the forebrain and the hindbrain (Fig. 8e–g). Together, these
395 data suggest that astrocytic inflammation, in particular the neurotoxic astrocytes, driven by
396 microgliosis was attenuated by CSF1R inhibition, thus leading to a general neuroprotective
397 effect.

398 **CSF1R inhibition preferentially eliminates a highly activated microglia subpopulation**

399 Given reported roles of microglia in driving astrocytic inflammation and neurotoxicity in disease,
400 we next interrogated whether resilient microglial phenotypes could be responsible for the sex-
401 specific neurofunctional effects. Thus, we examined the morphological and transcriptional
402 changes in microglia following CSF1R inhibition. In tauopathy, microglia acquire an activated
403 morphology in brain regions where neurons contain tau aggregates, a phenomenon seen in
404 many focal neuropathologies⁴⁹. Interestingly, the elimination of microglia in the Tg2541 mouse
405 brain following PLX3397 treatment was not uniform nor complete, but was the most effective in
406 the vicinity of tau aggregates (Fig. 9a,b). The microglial density near tau-laden neurons was
407 reduced by more than 60%, but in distal regions (>200 microns) the microglial density was not
408 significantly changed (Fig. 9c), indicating that microglia in the vicinity of the tau aggregates may
409 have increased sensitivity towards CSF1R inhibition. We then compared the morphologies of
410 PLX-resistant (residual microglia in PLX-treated mice) and PLX-sensitive microglia (in vehicle-
411 treated mice). Notably, we found that PLX resistance was associated with more abundant and
412 intricate microglial cell processes, close to the levels seen in wild type mice (Fig. 9d–g). The
413 number of microglial process branches ($P = 0.0075$), process lengths ($P = 0.028$), and territory
414 sizes ($P = 0.011$) in the forebrain were also significantly different between male and female

415 PLX-treated mice, with female mice showing more abundant and intricate microglial processes
416 by all three metrics (Fig. 9d–g). These data suggest that microglia associated with tau pathology
417 may be in an “activated” state, with a reduced number of processes. This view is consistent with
418 previous reports that activated microglia adopt a “disease-associated microglial” (DAM)
419 phenotype, with some of the signature genes associated with inflammatory responses that are
420 detrimental to adjacent neural cells^{50,51}. Interestingly, our data suggests that DAM in tauopathy
421 are more vulnerable to PLX treatment, and that surviving microglia might be neuroprotective,
422 particularly in female mice.

423 In support of this view, transcriptome analyses showed that many microglial-specific genes were
424 upregulated in Tg2541 mice (Fig. 10a), among which the most notable were signature DAM
425 genes such as *Tyrobp*, *Clec7a*, *Trem2* and *CD68*. By correlation analysis among different
426 samples using a generalized Louvain algorithm⁵², we found that the microglia-specific genes in
427 our dataset were clustered into three groups (Fig. 10b and Supplementary Fig. 19). The red-
428 cluster genes showed the highest degree of modulation by transgene overexpression, while the
429 blue-cluster genes showed a moderate degree of modulation, and the green-cluster genes
430 showed almost no difference between Tg2541 and wild type mice (Fig. 10b). Transgene-
431 modulated genes clustered into red and blue groups, consistent with a recent finding that tau
432 pathology activates both immune-activation and immune-suppression gene expression
433 modules¹⁰.

434 We next compared the gene expression patterns in vehicle- and PLX5622-treated brains. We
435 examined all previously reported DAM signature genes⁵¹ and found a partial match with the
436 activation markers in each of our identified gene clusters (Fig. 10c). Regardless of the
437 designation of homeostatic or activation genes reported in previous studies, the red-cluster
438 genes showed a stereotypical pattern of transgene activation and sensitivity to PLX treatment,
439 while green- and blue-cluster genes did not appear to be modulated by these factors. Given that
440 PLX predominantly eliminated microglia in the vicinity of the tau deposits (Fig. 9c), these data
441 suggest that red-cluster genes are preferentially expressed by tau-associated microglia.
442 Interestingly, when we examined PLX-induced expression changes in male and female mice
443 separately, we found that while the expression of red cluster genes were substantially
444 diminished by PLX independent of sex, green cluster genes and some blue cluster genes were
445 markedly increased in treated male mice (Fig. 10d,e). We validated some of the sex-specific
446 microglial genes affected by PLX treatment using real-time PCR as well as *in situ* labeling of
447 mRNA (Fig. 10f,g). To better describe the microglial gene expression in the surviving population

448 and account for the cell number reduction, we calculated the gene expression of resilient
449 microglia by normalization to six microglia-specific housekeeping genes. The normalized data
450 showed a trend towards increased gene expression in male mice, yet most of the male-specific
451 PLX-induced genes belonged to the green cluster (Fig. 10e), many of which are known to be
452 pro-inflammatory. Indeed, subsequent Ingenuity Pathway Analysis revealed a higher activation
453 of inflammation-related pathways in PLX-treated male mice compared to female mice (Fig. 10h).
454 These inflammation-related pathways included tau-activated NF- κ B⁵³ and excitotoxicity⁵⁴
455 pathways, but not amyloid-induced inflammasome genes⁵⁵ (Supplementary Fig. 20). Pathways
456 related to phagocytosis or microglia growth, on the other hand, did not show such consistent
457 sex-specific change (Fig. 10h). Taken together, our data show morphological and transcriptional
458 changes in microglia associated with tau deposition, consistent with a pattern of pathological
459 activation. CSF1R inhibition appears to preferentially eliminate these microglia in female mice,
460 leaving the brain with a more quiescent and less inflammatory microglial population. Male mice,
461 on the other hand, showed a drug-induced inflammatory microglia phenotype, which might
462 contribute to neuronal excitotoxicity and diminished therapeutic effect.

463

464 **DISCUSSION**

465 Our study reveals several major findings from a comprehensive evaluation of CSF1R inhibitors
466 in preclinical models of tauopathy. Importantly, we present the first line of evidence that CSF1R
467 inhibition reduces pathology that leads to functional improvements associated with longer
468 lifespan and reduced behavioral deficits in tauopathy mice (Figs. 2 and 3). Overall, our data
469 showing a reduction of pathogenic tau is consistent with prior studies using a different drug
470 scaffold targeting CSF1R (JNJ-527; edicotinib) in Tg2541 mice¹⁸, or using PLX3397 in a
471 different mouse model of tauopathy (TgPS19)¹⁷. However, in our study, neuroprotection
472 occurred despite incomplete microglia depletion (~60%); upon deeper analysis, we identified
473 distinct microglial-specific gene clusters suggesting subsets of microglia responsive to
474 tauopathy or resilient to CSF1R inhibition (Fig. 10). This finding is in line with the wealth of data
475 demonstrating that microglia exist as unique subsets in different brain regions, sexes, ages or
476 disease states²⁻⁴. From this perspective, our data suggest that it may be possible to target
477 specific subsets of activated microglia in tauopathy, without affecting other beneficial microglia
478 populations. Taken together, we argue that CSF1R inhibition causing complete microglia
479 ablation is unnecessary for therapeutic benefits, and may possibly be detrimental in humans

480 given that microglia are important for brain homeostasis and defending against other insults.
481 Several prior studies have suggested that therapeutic outcomes may only be achieved with
482 complete ablation of microglia, although these studies used different mouse models or dosing
483 regimens^{17,19}. Nevertheless, these disparate findings in prior literature are now more
484 interpretable alongside our study, which sheds light on the intricate relationships between
485 CSF1R inhibitor dosing, microglial depletion and therapeutic outcomes.

486 The precise mechanism of CSF1R inhibitors causing reduced tau pathology is still unclear, but
487 our data indicates that activated microglia are the primary target resulting in reduced numbers of
488 cells producing pro-inflammatory cytokines⁷⁻⁹ and other disease-associated microglial factors
489 (Fig. 10) that stoke tau pathogenesis in neurons, such as apolipoprotein E^{17,56} and complement
490 proteins⁵⁷. In addition, it seems plausible that CSF1R inhibitors may also block microglia-
491 mediated activation of A1 astrocytes⁴⁶, which in turn secrete factors that also drive tau
492 pathogenesis; blocking this cellular feed-forward pathway using a different drug targeting
493 microglia led to neuroprotection in a synucleinopathy model of Parkinson's disease⁵⁸.
494 Consistent with this view, PLX-treated mice exhibited a restored astrocyte phenotype,
495 suggesting that therapeutic benefits in our study may also be due, in part, to quelling neurotoxic
496 astrocytes (Fig. 8). Pharmacological CSF1R inhibition has been reported to also deplete
497 PVMs⁵⁹. Although we did not detect a significant reduction in the numbers of cortical blood
498 vessel-associated PVMs in our studies (Supplementary Fig. 7), their roles in tauopathy remain
499 to be determined. While there is cross-talk between peripheral immune cells and microglia¹, we
500 show that a non-brain penetrant analog, PLX73086, did not affect CNS microglia, tau pathology
501 or NfL levels (Fig. 5 and Supplementary Fig. 6), and it is thus unlikely that CSF1R inhibition in
502 the periphery contributes to the phenotypic rescue observed in our study. Lastly, it is possible
503 that chronic PLX treatment caused depletion of some oligodendrocyte progenitor cells (OPCs)
504 in our study, but we expect that PLX did not affect mature oligodendrocytes or myelination⁶⁰.
505 The relationship between OPC biology and tau pathology in neurons is largely unknown, and
506 thus it remains unclear how CSF1R inhibition in OPCs contributes, if at all, to the mechanism of
507 action. Nevertheless, this topic warrants further investigation.

508 Tau pathology in Tg2541 mice is associated with moderate microgliosis and an up-regulation of
509 transcriptomic signatures of microglial activation^{10,50}. Our transcriptome analysis showed
510 activation of two major clusters of microglial-specific genes in Tg2541 mice. These two clusters
511 had a high degree of overlap with the immune activation and suppression modules recently
512 described in tauopathy mice and FTLN patients¹⁰, indicating a specific reactive transcriptional

513 program of microglia towards tau pathology. Consistent with this view, genes in the activated
514 clusters also matched transcriptome modules described in activated microglia in
515 neurodegeneration models (such as *Itgax* and *Clec7a*), but not in tumor or acute inflammation
516 models⁵⁰. We found an additional cluster of microglial genes that had similar expression in
517 Tg2541 and wild type mice. Intriguingly, this cluster was not affected by PLX treatment in female
518 mice, while in male mice this cluster exhibited marked activation (Fig. 10). Considering that PLX
519 eliminates more than half of the total microglia population, a parsimonious explanation for this
520 sustained gene cluster is that they are preferentially expressed by an inert microglial
521 subpopulation that does not respond to tauopathy or lower dose CSF1R inhibition⁶¹. Consistent
522 with this notion, we found that PLX treatment preferentially eliminates activated microglia in the
523 vicinity of tau deposits, and thus most surviving microglia are not in direct contact with tau-laden
524 neurons (Fig. 9). This is in contrast to A β mice, in which the surviving microglia are usually
525 associated with A β plaques following PLX treatment^{22,62}. We found that surviving microglia in
526 female mice were non-inflammatory, and had longer and more elaborate processes compared
527 to vehicle-treated microglia, showing functional and morphological features more similar to
528 those of wild type microglia (Fig. 9). In sum, our data describe a microglial genetic signature that
529 remains stable in Tg2541 mice with or without PLX treatment, likely representing a “dormant”
530 microglial subpopulation that are less dependent on CSF1R for survival, or are less sensitive to
531 CSF1R inhibition at the doses administered in our study.

532 Sex-specific differences exist in mouse microglial morphology, function, gene expression, and
533 response to tauopathy, and the differences increase with age⁶³⁻⁶⁶. Our data identify a sex-
534 dependent effect on therapeutic exposure and efficacy of CSF1R inhibition in Tg2541 mice. A
535 difference in the plasma levels of PLX3397 during *ad libitum* oral dosing in male and female
536 mice has been noted previously¹⁷; however, only male mice were evaluated further. We
537 examined both male and female Tg2541 mice and found that, despite similar food intake,
538 plasma and brain levels of PLX3397 were higher in male mice compared to female mice (Fig. 3
539 and Supplementary Fig. 9). However, at this level of drug exposure, only female mice received
540 a functional benefit from CSF1R inhibition, an unexpected and clinically relevant outcome that
541 would have been overlooked had our analysis been focused on a single sex. In male Tg2541
542 mice, despite a robust reduction of microglia and pathogenic tau, PLX treatment did not slow
543 weight loss or extend survival, and plasma NfL levels were significantly increased, indicative of
544 neuronal damage⁴¹. Neurodegeneration in Tg2541 mice has been shown to be largely limited to
545 spinal cord motor neurons^{23,67}, and we found that NeuN and total tau immunoreactivity in the

546 brain were largely unchanged by CSF1R inhibition (Supplementary Fig. 8). Thus, the functional
547 deficits we measured are likely caused by neuronal dysfunction rather than neuronal death, but
548 can be rescued by CSF1R inhibition. It has been suggested before that microglia from male
549 animals may exhibit an increased responsiveness to CSF1R depletion compared to microglia
550 from female animals⁶⁸. Our results indicate that despite robust on-target effects for microglial
551 depletion, male mice developed a PLX-induced inflammatory microglial phenotype (Fig. 10).
552 Furthermore, we observed a concentration-dependent activation of IEGs in PLX treated Tg2541
553 mice, suggesting that excessive PLX dosing in male mice may lead to excitotoxicity (Fig. 6),
554 thus masking the beneficial effect of tau reduction. Microglia in male mice adopted a
555 transcriptome and morphological phenotype that have been previously linked to
556 excitotoxicity^{54,69}. Curiously, IEGs were not significantly upregulated in male wild type mice,
557 indicating that their activation may not be due to high concentration of PLX alone, but may also
558 be dependent on tau deposits. Consistent with premise, we identified increased glutamate and
559 GABA neurotransmitter levels in the brains of male Tg2541 mice, but not male wild type mice or
560 any female mice (Fig. 7), indicative of excitotoxicity following PLX dosing. Previous studies have
561 linked tau accumulation and aberrant neural activity *in vivo*⁷⁰. On the other hand, microglia are
562 known to mediate neuroprotection against excitotoxicity^{69,71} and elimination of microglia can
563 exacerbate seizures and related neuronal degeneration⁷². Therefore, the concurrent tau
564 removal and drug-induced inflammation driven by surviving microglia may increase the risk for
565 hyperactivity, resulting in excitotoxicity in male mice with high PLX concentrations. Other sex-
566 specific differences may also contribute to microglial sensitivity to CSF1R inhibition by a
567 currently unknown mechanism. Future translational studies of pharmacological CSF1R
568 inhibitors will need to carefully evaluate the role of sex in both safety and therapeutic outcomes.

569 CSF1R inhibitors were shown to be protective in mouse models of other neurodegenerative
570 diseases, such as AD and Down syndrome^{22,73,74}. However, under different treatment
571 conditions, CSF1R inhibition did not affect A β plaque burden, but did rescue some functional
572 deficits^{62,75}. Therefore, microglia play a dynamic role in the brain's response to A β pathogenesis,
573 and their attenuation may impart distinct benefits at different stages of disease. Our results
574 suggest that, in primary human tauopathies, a subset of microglia play a net negative role
575 before, during, and after disease onset and that their removal may be a viable therapeutic
576 strategy. It remains to be determined if similar benefits should be expected for tauopathy in AD
577 given the preceding comorbid A β pathology, but this may be elucidated in rodent models co-
578 expressing human tau and A β . Nevertheless, because CSF1R inhibition has not been reported

579 to be detrimental in A β mice, CSF1R inhibitors could ameliorate AD-related tauopathy even if
580 caused by different disease mechanisms. Ongoing human clinical trials of CSF1R inhibitors in
581 AD (e.g. NCT04121208) may provide additional mechanistic insights.

582 Primary human tauopathies constitute a class of neurodegenerative diseases caused by tau
583 misfolding and aggregation and include progressive supranuclear palsy (PSP), corticobasal
584 degeneration (CBD) and Pick's disease, among others. When combined with AD, in which tau
585 aggregation follows A β deposition, tauopathies afflict a significant proportion of the human
586 population, and thus novel approaches to directly or indirectly block tau pathogenesis or its
587 downstream effects are urgently needed. Our study highlights several aspects of
588 pharmacological CSF1R inhibition that bolster its therapeutic potential for human tauopathies.
589 First, we observed greater efficacy of early (acute) CSF1R inhibition to restrict tau-prion levels in
590 forebrain regions (Fig. 1e), likely due to reduced disease severity there relative to hindbrain
591 regions. At later stages (chronic and terminal), CSF1R inhibition with PLX3397 did reduce tau-
592 prion levels in the hindbrain, albeit a modest reduction relative to the effects in the forebrain
593 (Fig. 1f,g). These findings suggest that early and long-term CSF1R inhibition (though not
594 necessarily continuous) would most effectively mitigate human tauopathy. Second, we
595 demonstrated that interventional dosing of Tg2541 mice, initiated at a stage when robust tau
596 deposition had already occurred^{23,27}, led to a significant reduction in pathogenic tau
597 (Supplementary Fig. 4). Therefore, our data support some potential clinical benefit of CSF1R
598 inhibitors for treatment, in addition to prevention, of tauopathy. This is important because
599 prophylactic prevention of non-autosomal dominant neurodegenerative diseases may be difficult
600 due to a lack of definitive prognostic biomarkers paired with the fact that aggregation of the
601 causative proteins can occur years or decades prior to symptom onset³⁰. Third, we found that
602 intermittent dosing of Tg2541 mice at three-week intervals produced a significant reduction in
603 pathogenic tau (Supplementary Fig. 4). Despite relatively minimal off-target effects from
604 continuous, long-term dosing of CSF1R inhibitors in mice²², non-human primates⁷⁶, and
605 humans²¹, intermittent dosing would be clinically preferable if a similar therapeutic outcome was
606 achieved, given the important functions for microglia and related peripheral cells in innate
607 immunity. Because neurodegenerative tauopathies are slow, protracted diseases and microglia
608 are long-lived⁷⁷, it is conceivable that breaks in dosing may occur on the order of months or
609 years and be informed by medical imaging probes for microglia activation⁷⁸. Imaging will be
610 highly valuable for guiding intermittent dosing because microglial repopulation in a pathological
611 setting (e.g., disease or normal aging) may not necessarily result in a return to baseline

612 transcriptional profiles. Fourth, we found CSF1R inhibition to extend the survival of female
613 Tg2541 mice (Fig. 2), indicating that the reduction in pathogenic tau in this model system
614 translates to an improved clinically relevant outcome. We postulate that if CSF1R inhibitor
615 dosing was optimized for male Tg2541 mice, any adverse effects in the CNS or periphery would
616 likely be diminished and their survival extended. Fifth, we showed that complete microglial
617 depletion is not necessary, or even desirable, for a therapeutic benefit. As discussed above, the
618 microglia that survive CSF1R inhibition represent a unique microglial sub-population that likely
619 serves important functions in brain homeostasis. Future preclinical studies may pinpoint the
620 precise level, timing, and frequency of CSF1R inhibition such that the detrimental effects of
621 microglial activation are minimized while an appropriate number of homeostatic microglia
622 remain for brain surveillance. Lastly, CSF1R inhibitors applied in conjunction with tau
623 immunotherapy may prove to be a successful combination therapy; because microglia are not
624 needed for antibody effector function⁷⁹, removing tauopathy-activated microglia would slow tau
625 pathogenesis and may also increase the efficacy of tau immunotherapy. Taken together, our
626 data strongly support the therapeutic modulation of microglial activation by CSF1R inhibitors as
627 a promising approach to treating human tauopathies.

628

629 **METHODS**

630 **Animals**

631 The Tg2541 transgenic mouse line expresses the human 0N4R tau isoform under the Thy1.2
632 genetic promoter. Tg2541 mice were originally generated on a mixed C57BL/6J × CBA/Ca
633 background²³ and were then bred onto a congenic C57BL/6J background using marker-assisted
634 backcrossing for eight generations before intercrossing to generate homozygous mice. Albino
635 Tg2541 mice were generated by intercrossing Tg2541 with C57BL/6J mice expressing a
636 spontaneous mutation in the tyrosinase gene (homozygous for Tyr^{c-2J}) causing albinism
637 (Jackson Laboratory; 000058). To generate mice for *in vivo* bioluminescence imaging, we
638 employed Tg(*Gfap-luc*) mice, which express firefly luciferase under the control of the murine
639 *Gfap* promoter (gift from Caliper Life Sciences). These reporter mice were originally on the FVB
640 background, but we backcrossed them to a congenic B6 background, and then crossed them to
641 the B6-albino background. To create bigenic mice, albino Tg2541 mice were crossed with albino
642 Tg(*Gfap-luc*) animals to produce double hemizygotes; next, double hemizygotes were crossed
643 and the progeny were screened for the presence of both transgenes expressed at

644 homozygosity. Animals were maintained in a facility accredited by the Association for
645 Assessment and Accreditation of Laboratory Animal Care International in accordance with the
646 *Guide for the Care and Use of Laboratory Animals*. All procedures for animal use were
647 approved by the University of California, San Francisco's Institutional Animal Care and Use
648 Committee.

649 **PLX compound formulation in mouse chow**

650 PLX3397 was provided by Plexxikon Inc. and was formulated in AIN-76A standard chow by
651 Research Diets Inc. at 275 mg/kg as previously described⁸⁰. PLX5622 was provided by
652 Plexxikon Inc. and was formulated in AIN-76A standard chow by Research Diets Inc. at 1200
653 mg/kg as previously described⁶². PLX73086 was provided by Plexxikon Inc. and was formulated
654 in AIN-76A standard chow by Research Diets Inc. at 200 mg/kg as recommended by Plexxikon
655 Inc.

656 **Immunohistochemistry and slide scanning**

657 Formalin-fixed samples were embedded into paraffin (FFPE) using standard procedures and
658 microtome-cut into 8 µm sagittal brain sections or coronal spinal cord sections and mounted
659 onto slides. To reduce tissue autofluorescence, paraffin slides were photobleached for 48 hours.
660 Slides were deparaffinized in a 61°C oven for 15 minutes and rehydrated through alcohols.
661 Antigen retrieval was performed by autoclaving for 10 minutes at 121°C in 0.01 M citrate buffer.
662 Sections were blocked in 10% normal goat serum (NGS) (Vector Labs) for 1 hour at room
663 temperature. All primary antibodies were used at 1:250 dilution and included rabbit monoclonal
664 anti-Iba1 (Abcam, ab178847), rabbit polyclonal anti-P2yr12 (Atlas, HPA014518), mouse
665 monoclonal anti-NeuN (Millipore, MAB377), chicken anti-GFAP (Abcam, ab4674), and mouse
666 monoclonal anti-pS202/T205 tau (AT8; Thermo Fisher, MN1020). Primary antibodies were
667 diluted in 10% NGS in PBS and allowed to incubate on the slides overnight at room
668 temperature. Primary antibody detection was performed using goat secondary antibodies with
669 conjugated AlexaFluor 488, AlexaFluor 555, or AlexaFluor 647 (Life Technologies) at 1:500
670 dilution. Slides were cover-slipped using PermaFluor mounting medium (Thermo). Whole-
671 section tiled images were acquired with an Axioscan.Z1 slide scanner (Zeiss) at 20x
672 magnification, and quantification was performed with Zen 2.3 software (Zeiss).

673 **Cellular bioassay to measure tau-prion activity**

674 A HEK293T cell line expressing the repeat domain of 4R human tau (aa 243–375) containing

675 the P301L and V337M mutations and C-terminally fused to YFP was previously generated as
676 described²⁹. A stable monoclonal line was maintained in DMEM, supplemented with 10% FBS
677 and 1% penicillin/streptomycin. To perform the bioassay, 3,000 cells (containing 0.1 µg/ml
678 Hoechst 33342) were plated in 70 µl per well into 384-well plates (Greiner) and incubated for 2
679 hours before treatment with samples. Clarified brain lysate at a final concentration of 1.25 µg/mL
680 total protein was first incubated with Lipofectamine 2000 (0.2% final concentration) and
681 OptiMEM (9.8% final concentration) for 90 minutes, and then added to the plated cells in
682 quadruplicate. Plates were incubated at 37°C for 1–3 days, and then the live cells were imaged
683 using an INCell Analyzer 6000 Cell Imaging System (GE Healthcare) and custom algorithms
684 were used to detect fluorescent YFP-positive puncta (aggregates).

685 **Mechanical tissue homogenization**

686 Postmortem brains and spinal cords were thawed and weighed to determine the mass in grams.
687 Brains were bisected into forebrain and hindbrain pieces using a single cut with a scalpel blade
688 between the striatum and hypothalamus. Tissue was homogenized in nine volumes of cold
689 DPBS containing Halt Protease Inhibitor Cocktail (1x, Thermo Fisher Scientific) using a
690 Precellys 24-bead beater (Bertin Instruments) with metal bead lysing matrix (MP Biomedical).
691 Where necessary, brain lysates were clarified by centrifugation at 10,000 × g for 10 min at 4°C.
692 All tissue and samples were stored at –80°C until further use.

693 **Formic acid extraction of insoluble proteins in brain tissue for ELISA**

694 Fifty microliters of formic acid were added to 25 µL of 10% brain homogenate and placed in an
695 ultracentrifuge tube. The samples were vortexed, sonicated for 20 minutes at 37°C in a water-
696 bath sonicator, and then centrifuged at 100,000 × g for 1 hour. Fifty microliters of supernatant
697 were recovered to a low-binding tube and neutralized with 950 µL of neutralization buffer (1 M
698 Tris base and 500 mM dibasic sodium phosphate). Samples were aliquoted into low-binding
699 tubes and flash frozen in liquid nitrogen. The following ELISA kits from Thermo Fisher Scientific
700 were used according to the manufacturer's protocols: total tau (KHB0041), p-tau S396
701 (KHB7031), and p-tau T231 (KHB8051). Each sample was analyzed in duplicate. Raw ELISA
702 values were adjusted to total brain protein (grams) in the clarified 10% brain homogenate as
703 determined by bicinchoninic acid (BCA) assay (Pierce/Thermo Fisher Scientific).

704 **Quantification of total protein in brain homogenate**

705 Total protein content in the PBS-soluble (clarified 10% brain homogenate) and detergent-

706 soluble fractions was quantified using the Pierce BCA Protein Assay Kit (Thermo Fisher
707 Scientific) following the manufacturer's protocol.

708 **Generation of tau K18*P301L fibrils**

709 Production, purification and fibrillization of recombinant tau K18*P301L fibrils were performed as
710 previously described⁸¹.

711 **Stereotaxic injections in Tg2541 mice**

712 Forebrain inoculation: Ten-week-old Tg2541 mice received unilateral inoculations of 10 μ l of 1.5
713 mg/ml tau K18 P301L fibrils using stereotaxic methods. Injections followed a two-step process:
714 the needle was first advanced to the hippocampus (Bregma -2.5mm, Lateral 2.0mm; Depth -2.3
715 mm from the skull surface) to deliver 5 μ l over three minutes, then the Hamilton syringe pump
716 was paused for five minutes to allow for diffusion prior to retracting the needle to the overlying
717 cortex (Depth -1.3 mm) where the remaining 5 μ l was injected. After fibril injection, the needle
718 remained in place for five minutes to allow for diffusion of fibrils before retraction, patching the
719 skull and suturing the scalp. Midbrain inoculation: Ten-week old Tg2541 mice received bi-lateral
720 inoculations of 10 μ l of 1.5 mg/ml tau K18 P301L fibrils using stereotaxic methods. Five
721 microliters was injected at each site in the midbrain (Bregma, -4.3 mm; Lateral, 1.0 mm, Depth, -
722 2.5 mm) and (Bregma, -4.3 mm; Lateral, -1.0 mm, Depth, -2.5 mm).

723 **Automated home cage monitoring of behavior**

724 Total activity measurements of freely moving mice were made every 30 days after PLX dosing
725 in Promethion cages (Sable Systems International). At each time point, mice were first
726 randomized and placed individually in Promethion cages for 4 to 6 days. Real-time cage activity
727 recording was continuous during the entire session using a combination of a running wheel with
728 sensors to measure speed and distance traveled, three balances to measure body weight, food
729 and water consumption, and a matrix of infrared light beams to measure XYZ movements with
730 0.25 cm resolution. Analysis of these metrics was used to detect behaviors such as sleep,
731 rearing and general locomotion. For each mouse, data used for analyses were average
732 readings per light or dark cycle. Data from the first circadian cycle were excluded due to variable
733 behavior during habituation. To calculate the activity scores, wheel use, locomotion and rearing
734 were first normalized to a 0–1 scale by the maximum value in the whole dataset, and then the
735 geometric mean of the normalized values for each session was calculated.

736 **Quantification of PLX compound levels in brain tissue and plasma**

737 Brain homogenates (20% w/v) were prepared in PBS by one 30-second cycle of bead beating at
738 5500 rpm with a Precellys 24-bead beater (Bertin Instruments) or plasma samples were
739 prepared by dilution to 25% with PBS. Compounds were recovered by mixing equal parts of
740 brain homogenate with a 50/50 (v/v) solution of acetonitrile (ACN) and methanol containing 1
741 mM niflumic acid. Precipitated proteins were removed by vacuum filtration (Captiva ND,
742 Agilent). Analysis was performed using a liquid chromatography-tandem mass spectrometry
743 system consisting of an API4500 triple quadra-pole instrument (AB Sciex, Foster City, CA)
744 interfaced with a CBM-20A controller, LC20AD 230 pumps, and a SIL-5000 auto-sampler
745 (Shimadzu Scientific, Columbia, MD). Samples were injected onto a BDS Hypersil C8 column
746 maintained at room temperature. The amount of ACN in the gradient was increased from 75–
747 95% ACN over two minutes, held for one minute, and then re-equilibrated to 75% ACN over 1.4
748 minutes. Data acquisition used multiple reaction monitoring in the positive ion mode. Specific
749 methods were developed for each compound (PLX3397 and PLX5622), enabling the
750 determination of absolute concentrations.

751 **Blood plasma neurofilament light (NfL) protein measurement using SIMOA**

752 At monthly time points, 150 μ l blood was collected in EDTA-coated tubes. The plasma was
753 centrifuged at 1,000 x g for ten minutes to clarify the samples, and was then diluted with sample
754 diluent buffer included in the kit by 25-fold and 100-fold, respectively, prior to the measurement.
755 Plasma NfL concentration was measured and analyzed using the NfL kit (Quanterix) with the
756 SIMOA HD-1 analyzer (Quanterix). Briefly, samples, magnetic beads coated with capture
757 antibody, and biotinylated detector antibodies were combined. Thereafter, the capture beads
758 were resuspended with streptavidin- β -galactosidase (SBG) and resorufin β -D-
759 galactopyranoside (RGP) and transferred to the SIMOA disk. Each bead fit into a microwell in
760 the disk and if NfL was captured then the SBG hydrolysed the RGP substrate which generated
761 a fluorescent signal, and then the concentration was measured against a standard curve
762 derived from known concentrations of recombinant NfL included in the kit. The lower limit of
763 quantification of the assay for plasma was 17.15 pg/mL.

764 **Masson's trichrome and Picosirius red staining**

765 FFPE liver sections (eight μ m) were deparaffinized through xylenes and graded alcohols and
766 then rehydrated in distilled water. The Masson's trichrome staining kit (Abcam #ab150686) was

767 used according to the manufacturer's protocol. The Picro Sirius Red Stain Kit (Abcam
768 #ab150681) was used to stain tissue sections for 60 min at room temperature. The slides were
769 rinsed in two changes of acetic acid, three changes of ethanol, and then mounted using
770 PermaFluor mounting medium (Thermo). Whole-section tiled images were acquired with an
771 Axioscan.Z1 slide scanner (Zeiss) at 20x magnification, and quantification was performed with
772 Zen 2.3 software (Zeiss).

773 **Alkaline phosphatase (ALP) ELISA of plasma samples**

774 Mouse plasma samples were diluted 1:100 in the provided dilution buffer and measured using
775 the ALP ELISA kit (Biovision #E4572-100) according to the manufacturer's protocol.

776

777 **RNA extraction and Nanostring RNA expression measurements**

778 RNAlater-preserved samples were homogenized in PBS and total RNA was extracted from
779 samples using the Quick-RNA Miniprep Kit (Zymo Research). RNA extracts were evaluated for
780 concentration and purity using a Nanodrop 8000 instrument (Thermo Fisher Scientific) and
781 diluted to a concentration of 20 ng/ μ l. Hybridizations were performed for the mouse
782 Neuroinflammation, Myeloid cell, and Neuropathology panels according to the nCounter XT
783 Assay user manual (Nanostring). The hybridizations were incubated at 65°C for 16 hours, and
784 then were added to the nCounter SPRINT Cartridge for data collection using the nCounter
785 SPRINT Profiler. Counts were analyzed using the nSolver Analysis Software.

786 **RNA expression analysis**

787 In total, there were 10 mice in the Tg2541 vehicle group, 10 mice in the Tg2541 PLX5622
788 group, 6 mice in the wild type vehicle group, and 6 mice in the wild type PLX5622 group. Each
789 mouse had separate forebrain and hindbrain samples and three panels of Nanostring
790 sequencing were performed on each sample. Data from the three panels were pooled together
791 to form the final dataset. When pooling data, if a gene appeared in more than one panel then
792 the average read value was used in subsequent analysis, unless one panel failed to detect the
793 gene.

794 To assign cell-type specificity of each gene, we used the transcriptome dataset reported in a
795 previous study⁸², inspired by previously reported approaches in bulk tissue samples⁵⁰. We set a
796 specificity threshold in which a gene qualifies to be cell-type specific if its expression in a cell
797 type is greater than five times the sum in all other cell types. Using this standard, our dataset

798 had 242 microglia-specific genes, 47 astrocyte-specific genes and 70 neuron-specific genes. All
799 cell-type specific gene analyses were repeated with a three-time threshold and all results were
800 consistent (data not shown).

801 We used partial least-square (PLS) regression (MATLAB) to extract the gene expression pattern
802 aligned with Tg2541-wild type axis, using individual gene reads from each mouse as predictors
803 and genotype as responses. Only vehicle groups were used in constructing the PLS regression.
804 Forebrain and hindbrain were calculated separately. Five output dimensions were chosen for all
805 PLS analyses, as they covered 99.99% of the total variance in all cases. The scores in the first
806 two dimensions were plotted. To project PLX3397-treated groups to the PLS dimensions, we
807 used the following formula:

$$808 \text{Score}_{projection} = (\text{Loading}_{predictor} \setminus (\text{raw} - \text{mean}_{predictor}))'$$

809 To calculate population vector distance, we use the “mhal” command in MATLAB. All five
810 dimensions were used for each mouse. The wild type vehicle group was used as a target.

811 To calculate the vector angle, each mouse’s gene expression pattern was regarded as a five-
812 dimension vector in the PLS space, and the angle between each mouse and the average vector
813 of the wild type vehicle group was calculated with the following formula:

$$814 A = \cos^{-1}((u \cdot v) / (|u||v|))$$

815 To calculate the PLS regression along the PLX concentration and sex-correlated dimensions,
816 we constructed regressions using all non-microglial genes or only immediate early genes⁸³ to
817 measured brain PLX concentrations and sex of each sample. We then calculated variable
818 importance in projection to isolate the genes important for the regression. To calculate the
819 projected PLX concentrations, we used the products of gene expression levels and coefficients
820 estimated from PLS regression.

821 To calculate clusters in the microglial-specific genes, we calculated pairwise Pearson’s
822 correlation coefficients across 32 samples among each gene. The resulting similarity matrix was
823 then processed with a generalized Louvain community detection algorithm⁵².

824 To estimate the gene expression levels of the resilient microglia, we used 6 genes (Tmem119,
825 P2ry12, Fcrls, Olfm13, Itgam v1, and Itgam v2) as microglial-specific house-keeping genes⁸⁴ and
826 used their levels relative to the vehicle-treated group to scale the expression levels of other
827 microglial genes. We used these estimated expression levels as input for the Ingenuity Pathway

828 Analysis (QIAGEN).

829 **Gene expression analysis by RT-qPCR**

830 Mouse brains were collected at endpoints and flash frozen in DNA/RNA shield reagent. Tissue
831 was homogenized as described above and total RNA was purified using a commercial isolation
832 kit (Zymo Research). RNA concentration and the RNA integrity number (RIN) were determined
833 using a Bioanalyzer 2100 instrument and an Agilent RNA 6000 Pico Kit (Agilent 5067-1513).
834 Only samples with a RIN score ≥ 7.0 were used for gene expression analysis. To confirm
835 transcriptome profiling results, 2.5 ng of sample mRNA was applied to triplicate RT-qPCR
836 reactions consisting of 1x TaqPath 1-Step Multiplex Master Mix (ThermoFisher Scientific
837 A28526), Taqman primer/probe sets and a normalizing human MAPT Taqman assay. Reactions
838 were run on a QuantStudio 6 and 7 Pro instrument and amplification yielding cycle threshold
839 (C_T) values were corrected with Mustang Purple passive reference dye for each target gene.
840 Gene expression of PLX-treated mice relative to vehicle-treated mice was determined by the
841 comparative C_T method and values were expressed as fold-change.

842 Comparative C_T equation:

843 $2^{-\Delta\Delta C_T} = [(C_T \text{ gene of interest} - C_T \text{ hMAPT internal control})_{\text{PLX-treated mice}} - [(C_T \text{ gene of}$
844 $\text{interest} - C_T \text{ hMAPT internal control})_{\text{vehicle-treated mice}}$

845 ***In situ* mRNA hybridization (RNAscope) analysis**

846 All RNAscope experiments were performed using FFPE tissue sections of age-matched male
847 and female mice from transgenic tau and wild type control lines. The RNAscope Multiplex
848 Fluorescent V2 Reagent Kit (#323100) was used according to the manufacturer's instructions,
849 other than the target retrieval incubation step, which was carried out at 95°C for 20 minutes. The
850 following probes, all from ACD Bio (Newark, CA), were used: *MAPT* (#522491), *Fos* (#506931-
851 C2), and *Csf1r* (#428191-C3).

852 **HILIC-MS/MS metabolomics analysis**

853 HILIC-MS/MS analysis was carried out by the West Coast Metabolomics Center at the
854 University of California, Davis. Briefly, four milligrams of mouse cortex were homogenized with
855 3.2mm stainless steel beads using a bead-beater in 750 μ l of methyl-tertiary butyl ether and 225
856 μ l of methanol. Samples were then vortexed for 10 s, shaken on an orbital shaker at 4°C for 5

857 min, and then 188 μ l of liquid chromatography mass spectrometry (LCMS)-grade water was
858 added. Samples were vortexed again for 20 s and centrifuged for 2 min at 14,000xg. 110 μ l of
859 the lower phase (all polar metabolites) were then moved to a new 1.5 ml tube and dried using a
860 centrivap. Dried samples were resuspended in 100 μ L buffer containing internal standards and
861 then analyzed using an Agilent 1290 ultra-high pressure liquid chromatography (UHPLC)/Sciex
862 Triple-time-of-flight (TOF) 6600 mass spectrometer. Briefly, a Waters Acquity Premier UHPLC
863 bridged ethylene hybrid (BEH) Amide Column (1.7 μ m, 2.1 mm x 50 mm) was used with a
864 mobile phase A of ultrapure water with 10mM ammonium formate (AF) and 0.125% formic acid
865 (FA) (pH 3.0), and a mobile phase B of 95:5 (v/v) acetonitrile:ultrapure water with 10 mM AF +
866 0.125% FA (pH 3.0). A column temperature of 45°C and a gradient of 0 min, 100% B; 0.5 min,
867 100% B; 1.95 min, 70% B; 2.55 min, 30% B; 3.15 min, 100% B; 3.8 min, 100% B, were used
868 with a flow rate of 0.8 ml/min.

869 Following data collection, internal standard chromatograms were examined for consistency of
870 peak height and retention time as quality control measures. Raw data files were then processed
871 using an updated version of the MS-DIAL software⁸⁵ using an in-house mzRT library and
872 MS/MS spectral matching with NIST/MoNA libraries. All MS/MS annotations were then manually
873 curated to ensure that only high-quality metabolite identifications were included.

874 **In vivo bioluminescence imaging**

875 Bioluminescence imaging was performed on the brains and spinal cords of albino bigenic
876 Tg(2541:*Gfap-luc*) homozygous mice after receiving an intraperitoneal injection of 25 mg/kg
877 cyclic luciferin-1 (CycLuc1) sodium salt solution (Aobious; AOB6377) prepared in PBS, pH 7.4.
878 After CycLuc1 injection, mice were placed in an anesthetization chamber and exposed to an
879 isoflurane/oxygen gas mix for ten minutes. During this time, the heads of the mice were shaved
880 to enhance the bioluminescence signal. After anesthetization, mice were placed in an IVIS
881 Lumina III small animal imaging system (PerkinElmer) and were kept under constant
882 anesthesia. Mice were imaged for 60 s duration at three time points (14, 16 and 18 minutes)
883 following CycLuc1 injection as determined in one-hour time-lapse calibration studies. After
884 image acquisition, the mice were allowed to recover in their home cages. Brain and spinal cord
885 bioluminescence values were calculated from images displaying surface radiance using
886 standardized regions of interest and were then converted to total photon flux (photons per
887 second) using Living Image software version 4.4 (PerkinElmer).

888 **Confocal imaging of thick tissue sections**

889 Vibratome-sectioned brain slices (40 μm thick) were immunolabeled with Iba1, AT8, and/or
890 CD206 (Biorad, MCA2235) antibodies using standard protocols for free-floating sections in
891 multi-well plates. Sections were mounted using PermaFluor and #1.5 coverglass. Using a Leica
892 SP8 confocal microscope equipped with HyD detectors and an AOBS, samples were first
893 visualized using Navigator function to acquire an overview image of each slice using a 20 \times
894 water-immersion lens (0.95 NA). From the mosaic image, smaller tiled-ROIs were marked in the
895 forebrain and hindbrain to acquire high-resolution, sequential-scanned image stacks using a
896 63 \times water-immersion lens (1.2 NA). Eight-bit image z-stacks (1 μm steps) were collected at
897 512 \times 512-pixel resolution. Images were processed using custom MATLAB code.

898 **Microglial morphology analysis**

899 Microglia morphology was analyzed using a custom script in MATLAB. Briefly, raw confocal
900 image stacks were smoothed and then maximally projected. Isolated microglia cells were
901 manually selected for analysis. The selected microglia region was binarized with an intensity
902 threshold, and then the cell body was detected by fitting a largest circle in the binary mask. After
903 excluding the cell body region, the remaining microglia processes were skeletonized and branch
904 number, branch length and bounding box were measured using “regionprops” and “bwmorph”
905 commands.

906 **Statistical analysis**

907 Statistical analyses were performed using GraphPad Prism 8. Comparisons between two
908 groups were performed by two-tailed unpaired t test or by Mann-Whitney nonparametric test.
909 For comparisons of more than two groups, one-, two-, or three-way ANOVA was performed with
910 Holm-Šidák post hoc analysis. Following ANOVA, residuals were evaluated for normal
911 distribution using the Anderson-Darling test and the data were evaluated for equal variance
912 using the Brown-Forsythe test. If both assumptions were violated ($P < 0.05$), the data was
913 reanalyzed using Welch’s ANOVA with Dunnett T3 post hoc analysis. For repeated-measures
914 ANOVA, sphericity was not assumed and the Geisser-Greenhouse correction was applied. If
915 any data points were missing, a mixed-effects model (Restricted maximum likelihood; REML)
916 was used instead. Pearson’s correlation tests were performed as one-tailed tests as, in each
917 case, we had a directional hypothesis of either positive or negative correlation. Sample sizes
918 are shown in graphs with each data point representing an individual mouse, or are reported in
919 the figure legends. Experimental replication and exact statistical tests used are detailed in the
920 figure legends.

921

922 **ACKNOWLEDGEMENTS**

923 We thank Plexxikon, Inc for providing the PLX3977, PLX5622 and PLX73086 compounds, and
924 Andrey Reymar and Brian West for consulting on drug dosing and chow formulation. We thank
925 Julian Castaneda, Karina Walker and Lyn Batia (and their staff) at the UCSF Hunter's Point
926 animal facility for coordinating transgenic mouse development, breeding, and drug efficacy
927 studies. We thank Masahiro Inoue (Daiichi Sankyo, Inc.) for insightful discussions on
928 pharmacokinetics and pharmacodynamics in our study. We thank Stanley Prusiner and David
929 Ramsay at the UCSF Institute for Neurodegenerative Diseases (IND) for access to equipment
930 and technical resources critical for the completion of this study. We thank the following UCSF
931 IND staff for technical assistance: Abby Oehler, Rigoberto Roman-Albarran, Julia Becker, Marta
932 Gavidia and Manuel Elepano. The study was funded by grants from the National Institutes of
933 Health: (# RF1 AG061874), the Rainwater Charitable Foundation, the Sherman Fairchild
934 Foundation, the Henry M. Jackson Foundation, the Edward N. & Della L. Thome Memorial
935 Foundation, and Daiichi Sankyo, Inc. P.Y. was funded by Shanghai Municipal Science and
936 Technology Major Project and Shanghai Natural Science Foundation (22ZR1415000).
937 Competing interests: The Institute for Neurodegenerative Diseases (UCSF) had a research
938 collaboration with Daiichi Sankyo, Inc. (Tokyo, Japan).

939

940 **AUTHOR CONTRIBUTIONS**

941 C.C. conceived the study. N.R.J and C.C. designed the experiments. N.R.J., E.C., T.P.L., W.Y.,
942 A.B., B.M.R., M.C.S., H.M., K.G., A.A., and C.C. performed experiments and prepared data.
943 N.R.J., P.Y., and C.C. analyzed and interpreted data. N.R.J., P.Y., and C.C. wrote the paper.
944 C.C. supervised the study.

945

946 **DATA AVAILABILITY**

947 The authors declare that all other data supporting the findings of this study are available within
948 the paper and its supplementary files.

949

950 **CODE AVAILABILITY**

951 The transcriptome data (Nanostring) that support the findings of this study, specifically in
952 Figures 6-9, are available from Github with the following link: [https://gitfront.io/r/user-](https://gitfront.io/r/user-8849465/665dd65fd9d9e78650ed02b9f30236d99240de39/UCSF-PLX-nanostring/)
953 [8849465/665dd65fd9d9e78650ed02b9f30236d99240de39/UCSF-PLX-nanostring/](https://gitfront.io/r/user-8849465/665dd65fd9d9e78650ed02b9f30236d99240de39/UCSF-PLX-nanostring/)

954

955

956

957 **REFERENCES**

- 958 1. Dionisio-Santos, D.A., Olschowka, J.A. & O'Banion, M.K. Exploiting microglial and
959 peripheral immune cell crosstalk to treat Alzheimer's disease. *J Neuroinflammation* **16**, 74
960 (2019).
- 961 2. Masuda, T., *et al.* Spatial and temporal heterogeneity of mouse and human microglia at
962 single-cell resolution. *Nature* **566**, 388-392 (2019).
- 963 3. Kodama, L. & Gan, L. Do Microglial Sex Differences Contribute to Sex Differences in
964 Neurodegenerative Diseases? *Trends Mol Med* **25**, 741-749 (2019).
- 965 4. Stratoulis, V., Venero, J.L., Tremblay, M.E. & Joseph, B. Microglial subtypes: diversity
966 within the microglial community. *EMBO J* **38**, e101997 (2019).
- 967 5. Schwabe, T., Srinivasan, K. & Rhinn, H. Shifting paradigms: The central role of microglia
968 in Alzheimer's disease. *Neurobiol Dis* **143**, 104962 (2020).
- 969 6. Shi, Y. & Holtzman, D.M. Interplay between innate immunity and Alzheimer disease:
970 APOE and TREM2 in the spotlight. *Nat Rev Immunol* **18**, 759-772 (2018).
- 971 7. Maphis, N., *et al.* Reactive microglia drive tau pathology and contribute to the spreading
972 of pathological tau in the brain. *Brain* **138**, 1738-1755 (2015).
- 973 8. Stancu, I.C., *et al.* Aggregated Tau activates NLRP3-ASC inflammasome exacerbating
974 exogenously seeded and non-exogenously seeded Tau pathology in vivo. *Acta*
975 *Neuropathol* **137**, 599-617 (2019).
- 976 9. Ising, C., *et al.* NLRP3 inflammasome activation drives tau pathology. *Nature* **575**, 669-
977 673 (2019).
- 978 10. Rexach, J.E., *et al.* Tau Pathology Drives Dementia Risk-Associated Gene Networks
979 toward Chronic Inflammatory States and Immunosuppression. *Cell Rep* **33**, 108398
980 (2020).
- 981 11. Allen, M., *et al.* Divergent brain gene expression patterns associate with distinct cell-
982 specific tau neuropathology traits in progressive supranuclear palsy. *Acta Neuropathol*
983 **136**, 709-727 (2018).
- 984 12. Wang, H., *et al.* Genome-wide RNAseq study of the molecular mechanisms underlying
985 microglia activation in response to pathological tau perturbation in the rTg4510 tau
986 transgenic animal model. *Mol Neurodegener* **13**, 65 (2018).
- 987 13. Matarin, M., *et al.* A genome-wide gene-expression analysis and database in transgenic
988 mice during development of amyloid or tau pathology. *Cell Rep* **10**, 633-644 (2015).
- 989 14. Stanley, E.R. & Chitu, V. CSF-1 receptor signaling in myeloid cells. *Cold Spring Harb*
990 *Perspect Biol* **6**(2014).

- 991 15. Cannarile, M.A., *et al.* Colony-stimulating factor 1 receptor (CSF1R) inhibitors in cancer
992 therapy. *J Immunother Cancer* **5**, 53 (2017).
- 993 16. Asai, H., *et al.* Depletion of microglia and inhibition of exosome synthesis halt tau
994 propagation. *Nat Neurosci* **18**, 1584-1593 (2015).
- 995 17. Shi, Y., *et al.* Microglia drive APOE-dependent neurodegeneration in a tauopathy mouse
996 model. *J Exp Med* **216**, 2546-2561 (2019).
- 997 18. Mancuso, R., *et al.* CSF1R inhibitor JNJ-40346527 attenuates microglial proliferation and
998 neurodegeneration in P301S mice. *Brain* **142**, 3243-3264 (2019).
- 999 19. Bennett, R.E., *et al.* Partial reduction of microglia does not affect tau pathology in aged
1000 mice. *J Neuroinflammation* **15**, 311 (2018).
- 1001 20. Condello, C., DeGrado, W.F. & Prusiner, S.B. Prion biology: implications for Alzheimer's
1002 disease therapeutics. *Lancet Neurol* **19**, 802-803 (2020).
- 1003 21. Tap, W.D., *et al.* Structure-Guided Blockade of CSF1R Kinase in Tenosynovial Giant-Cell
1004 Tumor. *N Engl J Med* **373**, 428-437 (2015).
- 1005 22. Spangenberg, E., *et al.* Sustained microglial depletion with CSF1R inhibitor impairs
1006 parenchymal plaque development in an Alzheimer's disease model. *Nat Commun* **10**,
1007 3758 (2019).
- 1008 23. Allen, B., *et al.* Abundant tau filaments and nonapoptotic neurodegeneration in transgenic
1009 mice expressing human P301S tau protein. *J Neurosci* **22**, 9340-9351 (2002).
- 1010 24. Bugiani, O., *et al.* Frontotemporal dementia and corticobasal degeneration in a family with
1011 a P301S mutation in tau. *J Neuropathol Exp Neurol* **58**, 667-677 (1999).
- 1012 25. Goedert, M., Jakes, R. & Crowther, R.A. Effects of frontotemporal dementia FTDP-17
1013 mutations on heparin-induced assembly of tau filaments. *FEBS Lett* **450**, 306-311 (1999).
- 1014 26. Sperfeld, A.D., *et al.* FTDP-17: an early-onset phenotype with parkinsonism and epileptic
1015 seizures caused by a novel mutation. *Ann Neurol* **46**, 708-715 (1999).
- 1016 27. Johnson, N.R., *et al.* Evidence for sortilin modulating regional accumulation of human tau
1017 prions in transgenic mice. *Proc Natl Acad Sci U S A* **114**, E11029-E11036 (2017).
- 1018 28. Kovacs, G.G., *et al.* Distribution patterns of tau pathology in progressive supranuclear
1019 palsy. *Acta Neuropathol* **140**, 99-119 (2020).
- 1020 29. Sanders, D.W., *et al.* Distinct tau prion strains propagate in cells and mice and define
1021 different tauopathies. *Neuron* **82**, 1271-1288 (2014).
- 1022 30. Aoyagi, A., *et al.* Abeta and tau prion-like activities decline with longevity in the Alzheimer's
1023 disease human brain. *Sci Transl Med* **11**(2019).
- 1024 31. Elmore, M.R., Lee, R.J., West, B.L. & Green, K.N. Characterizing newly repopulated
1025 microglia in the adult mouse: impacts on animal behavior, cell morphology, and
1026 neuroinflammation. *PLoS One* **10**, e0122912 (2015).
- 1027 32. Iba, M., *et al.* Synthetic tau fibrils mediate transmission of neurofibrillary tangles in a
1028 transgenic mouse model of Alzheimer's-like tauopathy. *J Neurosci* **33**, 1024-1037 (2013).
- 1029 33. Seeley, W.W., Crawford, R.K., Zhou, J., Miller, B.L. & Greicius, M.D. Neurodegenerative
1030 diseases target large-scale human brain networks. *Neuron* **62**, 42-52 (2009).
- 1031 34. Gustke, N., Trinczek, B., Biernat, J., Mandelkow, E.M. & Mandelkow, E. Domains of tau
1032 protein and interactions with microtubules. *Biochemistry* **33**, 9511-9522 (1994).
- 1033 35. Lei, F., *et al.* CSF1R inhibition by a small-molecule inhibitor is not microglia specific;
1034 affecting hematopoiesis and the function of macrophages. *Proc Natl Acad Sci U S A* **117**,
1035 23336-23338 (2020).
- 1036 36. Bellver-Landete, V., *et al.* Microglia are an essential component of the neuroprotective
1037 scar that forms after spinal cord injury. *Nat Commun* **10**, 518 (2019).
- 1038 37. Luo, J., *et al.* Colony-stimulating factor 1 receptor (CSF1R) signaling in injured neurons
1039 facilitates protection and survival. *J Exp Med* **210**, 157-172 (2013).
- 1040 38. Jul, P., *et al.* Hyperactivity with Agitative-Like Behavior in a Mouse Tauopathy Model. *J*
1041 *Alzheimers Dis* **49**, 783-795 (2016).

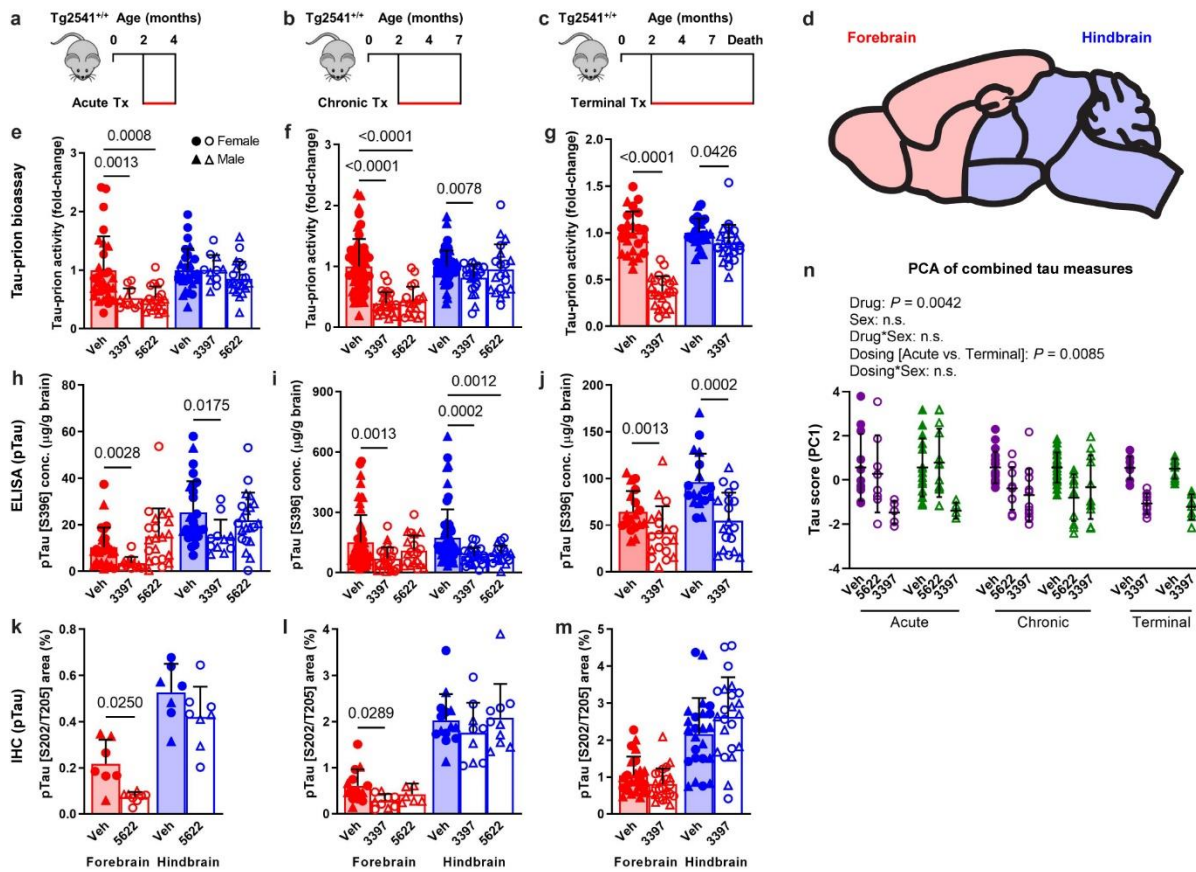
- 1042 39. Dumont, M., *et al.* Behavioral deficit, oxidative stress, and mitochondrial dysfunction precede tau pathology in P301S transgenic mice. *FASEB J* **25**, 4063-4072 (2011).
1043
1044 40. Wang, X., *et al.* Early intervention of tau pathology prevents behavioral changes in the
1045 rTg4510 mouse model of tauopathy. *PLoS One* **13**, e0195486 (2018).
1046 41. Bacioglu, M., *et al.* Neurofilament Light Chain in Blood and CSF as Marker of Disease
1047 Progression in Mouse Models and in Neurodegenerative Diseases. *Neuron* **91**, 56-66
1048 (2016).
1049 42. Ashton, N.J., *et al.* Increased plasma neurofilament light chain concentration correlates
1050 with severity of post-mortem neurofibrillary tangle pathology and neurodegeneration. *Acta*
1051 *Neuropathol Commun* **7**, 5 (2019).
1052 43. Rojas, J.C., *et al.* CSF neurofilament light chain and phosphorylated tau 181 predict
1053 disease progression in PSP. *Neurology* **90**, e273-e281 (2018).
1054 44. Benner, B., *et al.* Pexidartinib, a Novel Small Molecule CSF-1R Inhibitor in Use for
1055 Tenosynovial Giant Cell Tumor: A Systematic Review of Pre-Clinical and Clinical
1056 Development. *Drug Des Devel Ther* **14**, 1693-1704 (2020).
1057 45. Dong, X.X., Wang, Y. & Qin, Z.H. Molecular mechanisms of excitotoxicity and their
1058 relevance to pathogenesis of neurodegenerative diseases. *Acta Pharmacol Sin* **30**, 379-
1059 387 (2009).
1060 46. Liddelow, S.A., *et al.* Neurotoxic reactive astrocytes are induced by activated microglia.
1061 *Nature* **541**, 481-487 (2017).
1062 47. Watts, J.C., *et al.* Bioluminescence imaging of Abeta deposition in bigenic mouse models
1063 of Alzheimer's disease. *Proc Natl Acad Sci U S A* **108**, 2528-2533 (2011).
1064 48. Bellucci, A., *et al.* Induction of inflammatory mediators and microglial activation in mice
1065 transgenic for mutant human P301S tau protein. *Am J Pathol* **165**, 1643-1652 (2004).
1066 49. Ishizawa, K. & Dickson, D.W. Microglial activation parallels system degeneration in
1067 progressive supranuclear palsy and corticobasal degeneration. *J Neuropathol Exp Neurol*
1068 **60**, 647-657 (2001).
1069 50. Friedman, B.A., *et al.* Diverse Brain Myeloid Expression Profiles Reveal Distinct Microglial
1070 Activation States and Aspects of Alzheimer's Disease Not Evident in Mouse Models. *Cell*
1071 *Rep* **22**, 832-847 (2018).
1072 51. Keren-Shaul, H., *et al.* A Unique Microglia Type Associated with Restricting Development
1073 of Alzheimer's Disease. *Cell* **169**, 1276-1290 e1217 (2017).
1074 52. Mucha, P.J., Richardson, T., Macon, K., Porter, M.A. & Onnela, J.P. Community structure
1075 in time-dependent, multiscale, and multiplex networks. *Science* **328**, 876-878 (2010).
1076 53. Wang, C., *et al.* Microglial NF-kappaB drives tau spreading and toxicity in a mouse model
1077 of tauopathy. *Nat Commun* **13**, 1969 (2022).
1078 54. Hong, J., *et al.* Microglial Toll-like receptor 2 contributes to kainic acid-induced glial
1079 activation and hippocampal neuronal cell death. *J Biol Chem* **285**, 39447-39457 (2010).
1080 55. Heneka, M.T., *et al.* NLRP3 is activated in Alzheimer's disease and contributes to
1081 pathology in APP/PS1 mice. *Nature* **493**, 674-678 (2013).
1082 56. Krasemann, S., *et al.* The TREM2-APOE Pathway Drives the Transcriptional Phenotype
1083 of Dysfunctional Microglia in Neurodegenerative Diseases. *Immunity* **47**, 566-581 e569
1084 (2017).
1085 57. Dejanovic, B., *et al.* Changes in the Synaptic Proteome in Tauopathy and Rescue of Tau-
1086 Induced Synapse Loss by C1q Antibodies. *Neuron* **100**, 1322-1336 e1327 (2018).
1087 58. Yun, S.P., *et al.* Block of A1 astrocyte conversion by microglia is neuroprotective in models
1088 of Parkinson's disease. *Nat Med* **24**, 931-938 (2018).
1089 59. Kerkhofs, D., *et al.* Pharmacological depletion of microglia and perivascular macrophages
1090 prevents Vascular Cognitive Impairment in Ang II-induced hypertension. *Theranostics* **10**,
1091 9512-9527 (2020).

- 1092 60. Liu, Y., *et al.* Concentration-dependent effects of CSF1R inhibitors on oligodendrocyte
1093 progenitor cells *ex vivo* and *in vivo*. *Exp Neurol* **318**, 32-41 (2019).
- 1094 61. Zhan, L., *et al.* A MAC2-positive progenitor-like microglial population is resistant to CSF1R
1095 inhibition in adult mouse brain. *Elife* **9**(2020).
- 1096 62. Spangenberg, E.E., *et al.* Eliminating microglia in Alzheimer's mice prevents neuronal loss
1097 without modulating amyloid-beta pathology. *Brain* **139**, 1265-1281 (2016).
- 1098 63. Kodama, L., *et al.* Microglial microRNAs mediate sex-specific responses to tau pathology.
1099 *Nat Neurosci* **23**, 167-171 (2020).
- 1100 64. Guneykaya, D., *et al.* Transcriptional and Translational Differences of Microglia from Male
1101 and Female Brains. *Cell Rep* **24**, 2773-2783 e2776 (2018).
- 1102 65. Kang, S.S., *et al.* Microglial translational profiling reveals a convergent APOE pathway
1103 from aging, amyloid, and tau. *J Exp Med* **215**, 2235-2245 (2018).
- 1104 66. Colombo, G., *et al.* A tool for mapping microglial morphology, morphOMiCs, reveals brain-
1105 region and sex-dependent phenotypes. *Nat Neurosci* **25**, 1379-1393 (2022).
- 1106 67. Hampton, D.W., *et al.* Cell-mediated neuroprotection in a mouse model of human
1107 tauopathy. *J Neurosci* **30**, 9973-9983 (2010).
- 1108 68. Berve, K., West, B.L., Martini, R. & Groh, J. Sex- and region-biased depletion of
1109 microglia/macrophages attenuates CLN1 disease in mice. *J Neuroinflammation* **17**, 323
1110 (2020).
- 1111 69. Vinet, J., *et al.* Neuroprotective function for ramified microglia in hippocampal
1112 excitotoxicity. *J Neuroinflammation* **9**, 27 (2012).
- 1113 70. Busche, M.A., *et al.* Tau impairs neural circuits, dominating amyloid-beta effects, in
1114 Alzheimer models *in vivo*. *Nat Neurosci* **22**, 57-64 (2019).
- 1115 71. Badimon, A., *et al.* Negative feedback control of neuronal activity by microglia. *Nature* **586**,
1116 417-423 (2020).
- 1117 72. Liu, M., *et al.* Microglia depletion exacerbates acute seizures and hippocampal neuronal
1118 degeneration in mouse models of epilepsy. *Am J Physiol Cell Physiol* **319**, C605-C610
1119 (2020).
- 1120 73. Sosna, J., *et al.* Early long-term administration of the CSF1R inhibitor PLX3397 ablates
1121 microglia and reduces accumulation of intraneuronal amyloid, neuritic plaque deposition
1122 and pre-fibrillar oligomers in 5XFAD mouse model of Alzheimer's disease. *Mol*
1123 *Neurodegener* **13**, 11 (2018).
- 1124 74. Pinto, B., *et al.* Rescuing Over-activated Microglia Restores Cognitive Performance in
1125 Juvenile Animals of the Dp(16) Mouse Model of Down Syndrome. *Neuron* **108**, 887-904
1126 e812 (2020).
- 1127 75. Dagher, N.N., *et al.* Colony-stimulating factor 1 receptor inhibition prevents microglial
1128 plaque association and improves cognition in 3xTg-AD mice. *J Neuroinflammation* **12**, 139
1129 (2015).
- 1130 76. Hillmer, A.T., *et al.* Microglial depletion and activation: A [(11)C]PBR28 PET study in
1131 nonhuman primates. *EJNMMI Res* **7**, 59 (2017).
- 1132 77. Reu, P., *et al.* The Lifespan and Turnover of Microglia in the Human Brain. *Cell Rep* **20**,
1133 779-784 (2017).
- 1134 78. Horti, A.G., *et al.* PET imaging of microglia by targeting macrophage colony-stimulating
1135 factor 1 receptor (CSF1R). *Proc Natl Acad Sci U S A* **116**, 1686-1691 (2019).
- 1136 79. Lee, S.H., *et al.* Antibody-Mediated Targeting of Tau *In Vivo* Does Not Require Effector
1137 Function and Microglial Engagement. *Cell Rep* **16**, 1690-1700 (2016).
- 1138 80. Elmore, M.R., *et al.* Colony-stimulating factor 1 receptor signaling is necessary for
1139 microglia viability, unmasking a microglia progenitor cell in the adult brain. *Neuron* **82**,
1140 380-397 (2014).

- 1141 81. Barghorn, S., Biernat, J. & Mandelkow, E. Purification of recombinant tau protein and
1142 preparation of Alzheimer-paired helical filaments in vitro. *Methods Mol Biol* **299**, 35-51
1143 (2005).
- 1144 82. Zhang, Y., *et al.* Purification and Characterization of Progenitor and Mature Human
1145 Astrocytes Reveals Transcriptional and Functional Differences with Mouse. *Neuron* **89**,
1146 37-53 (2016).
- 1147 83. Wu, Y.E., Pan, L., Zuo, Y., Li, X. & Hong, W. Detecting Activated Cell Populations Using
1148 Single-Cell RNA-Seq. *Neuron* **96**, 313-329 e316 (2017).
- 1149 84. Chiu, I.M., *et al.* A neurodegeneration-specific gene-expression signature of acutely
1150 isolated microglia from an amyotrophic lateral sclerosis mouse model. *Cell Rep* **4**, 385-
1151 401 (2013).
- 1152 85. Tsugawa, H., *et al.* MS-DIAL: data-independent MS/MS deconvolution for comprehensive
1153 metabolome analysis. *Nat Methods* **12**, 523-526 (2015).
1154

1155 **FIGURES**

1156



1157

1158 **Fig. 1| CSF1R inhibition by three treatment paradigms reduces pathogenic tau levels in**

1159 **the brains of Tg2541 mice. a–c, Schematics of acute (a), chronic (b), or terminal (c) PLX**

1160 **treatment of Tg2541 mice from 2–4 mo of age, 2–7 mo of age, or 2 mo of age until death,**

1161 **respectively. d, Sagittal view of the mouse brain divided into two regions: the forebrain,**

1162 **containing the cortex, hippocampus, striatum, and olfactory bulb; and the hindbrain, containing**

1163 **the thalamus, hypothalamus, midbrain, cerebellum, and brain stem. e–g, Tau-prion levels in**

1164 **forebrain and hindbrain tissue homogenates of Tg2541 mice receiving acute (e), chronic (f), or**

1165 **terminal (g) treatment with vehicle, PLX3397 (275 mg/kg oral), or PLX5622 (1200 mg/kg oral),**

1166 **measured using the HEK293T cell tau-prion bioassay and normalized to the vehicle-treated**

1167 **group. h–j, Levels of pTau [S396] measured by ELISA in formic acid extracts of forebrain and**

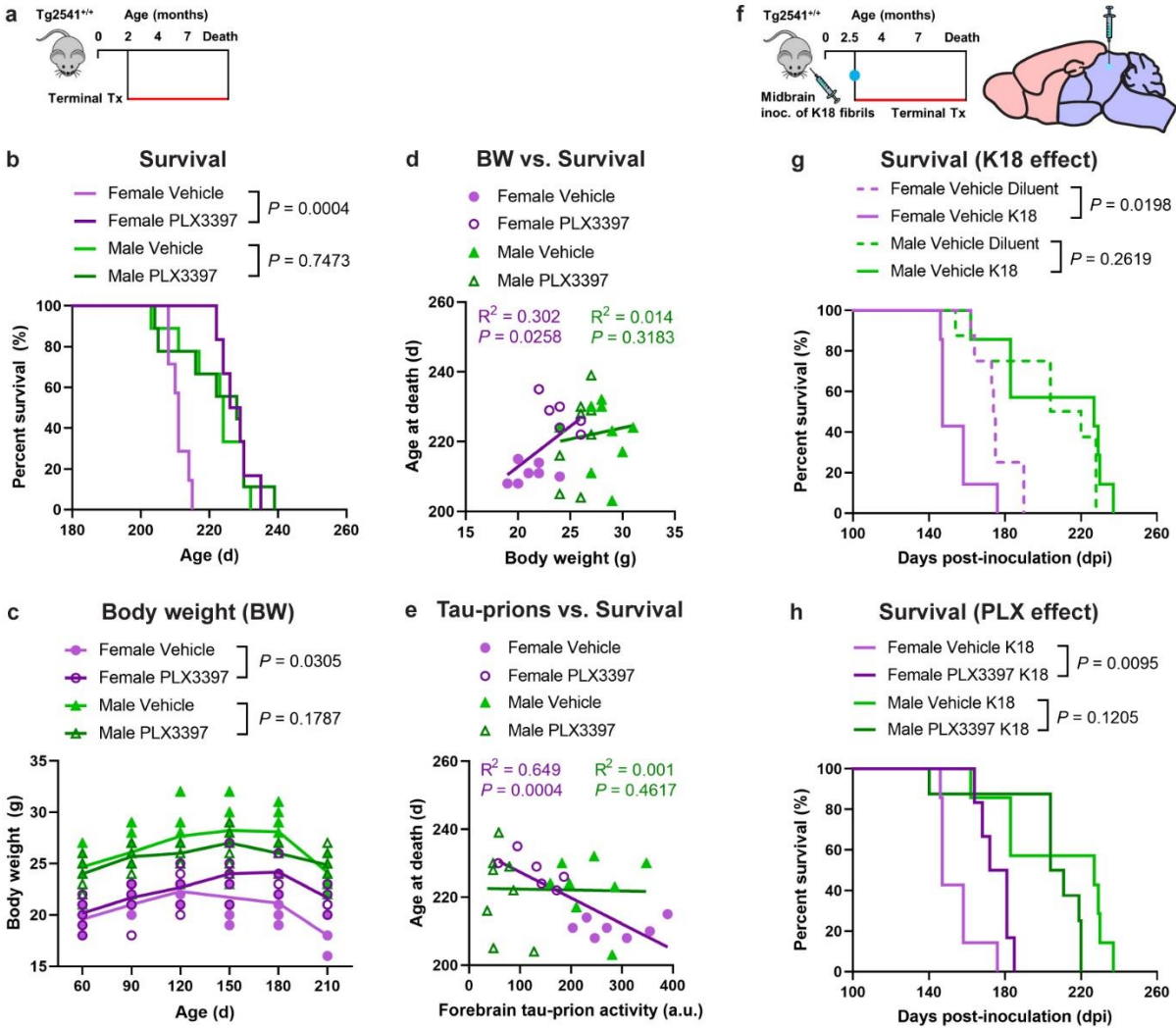
1168 **hindbrain tissue homogenates of Tg2541 mice receiving acute (h), chronic (i), or terminal**

1169 **treatment (j) with vehicle, PLX3397, or PLX5622, normalized to total protein concentration.**

1170 **k–m, Quantification of pTau [S202/T205]-positive area by IHC analysis of forebrain and**

1171 **hindbrain areas of Tg2541 mice receiving acute (k), chronic (l), or terminal (m) treatment with**

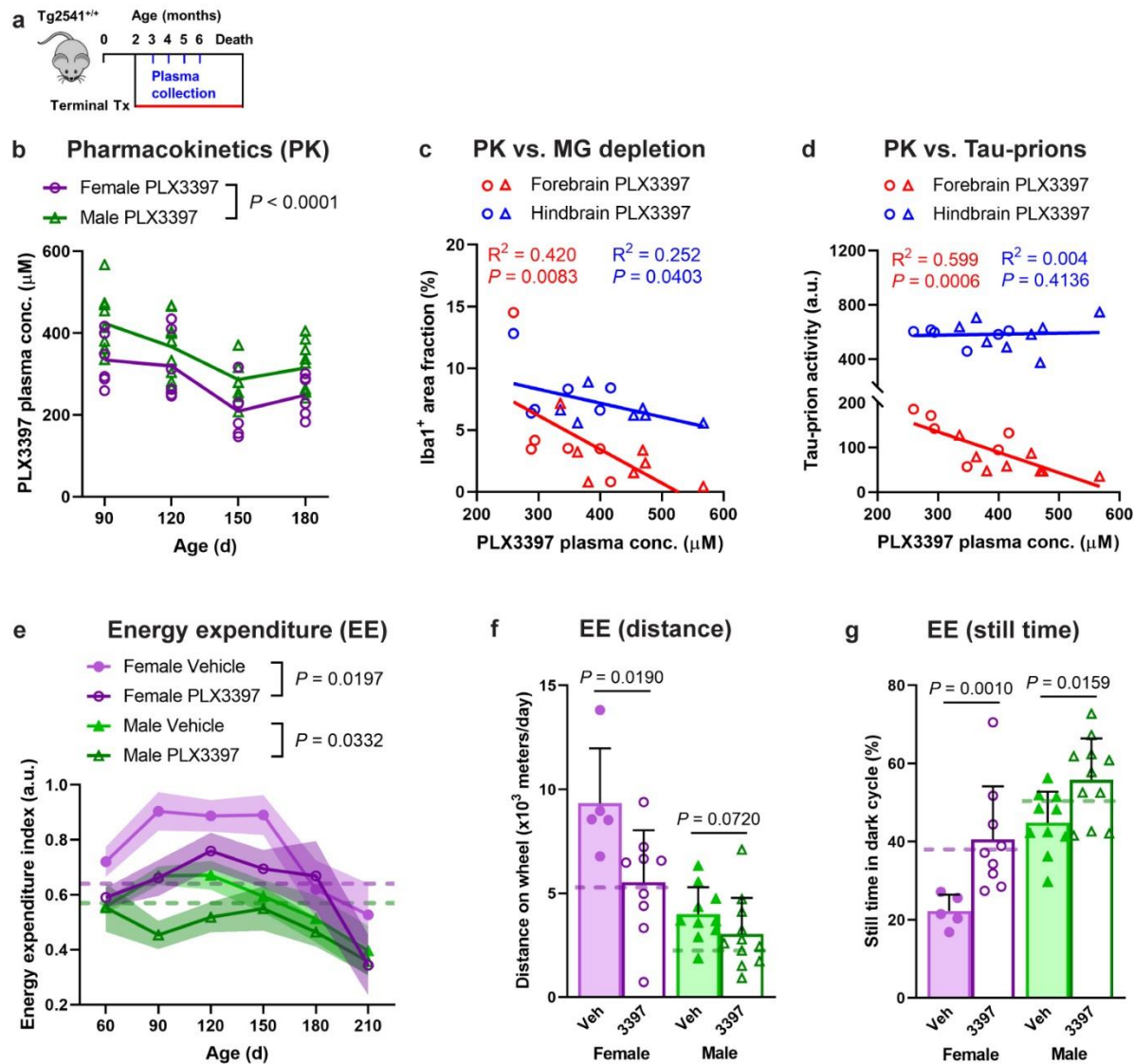
1172 vehicle, PLX3397, or PLX5622. Welch ANOVA with Dunnett T3 post hoc testing was used in **e**,
1173 **f**, **h**, **i**, and **l**. Two-way ANOVA with Holm-Šidák post hoc testing was used in **g**, **j**, **k**, and **m**. *P*
1174 values for all statistically significant differences ($P < 0.05$) are shown. **n**, Principal component
1175 analysis was performed, using all tau-prion and pTau[S396] data presented in Fig. 1e–j to
1176 calculate a ‘tau score’ that represents the amount of pathogenic tau in both the forebrains and
1177 hindbrains of Tg2541 mice. All data was first standardized to the respective vehicle-treated
1178 group of the same sex and same dosing paradigm. Then, two principal components (PC1 and
1179 PC2) were identified which accounted for 70.7% of the total variance in the data. Multiple linear
1180 regression was performed on PC1 of the drug-treated groups to evaluate the main effects sex
1181 and dosing paradigm, and the dosing*sex interaction effect. Multiple linear regression was
1182 performed on all groups to determine the main effect of drug and the drug*sex interaction effect.
1183 *P* values for all statistically significant differences ($P < 0.05$) are shown. n.s. indicates not
1184 statistically significant. PC2 was also evaluated, but only the drug main effect was statistically
1185 significant. In **e–n**, each symbol represents the forebrain or hindbrain of an individual mouse,
1186 with female mice shown as closed or open circles and male mice shown as closed or open
1187 triangles. Error bars represent the s.d. of the mean.



1188

1189 **Fig. 2| CSF1R inhibition extends survival of female Tg2541 mice.** **a**, Schematic of terminal
1190 PLX3397 treatment (275 mg/kg oral) of Tg2541 mice from 2 mo of age until death. **b**, Kaplan-
1191 Meier plot showing percent survival of female or male Tg2541 mice treated with vehicle or
1192 PLX3397. n=7 mice for Female Vehicle; n=6 mice for Female PLX3397; n=9 mice for Male
1193 Vehicle; n=9 mice for Male PLX3397. **c**, Body weights of female or male Tg2541 mice treated
1194 with vehicle or PLX3397. Differences in weight between vehicle and PLX3397 treatment in
1195 female or male mice were evaluated by mixed-effects analysis (Restricted maximum likelihood).
1196 Each symbol represents an individual mouse and lines indicate group means. **d**, **e**, Correlation
1197 plots for body weight at 180 d of age (**d**) or forebrain tau-prion activity at death (**e**) and survival
1198 for female or male Tg2541 mice treated with vehicle or PLX3397. Each symbol represents an
1199 individual mouse and linear regression lines are shown for female or male mice, with vehicle-
1200 and PLX3397-treated mice combined. Pearson's correlation analysis was performed and the

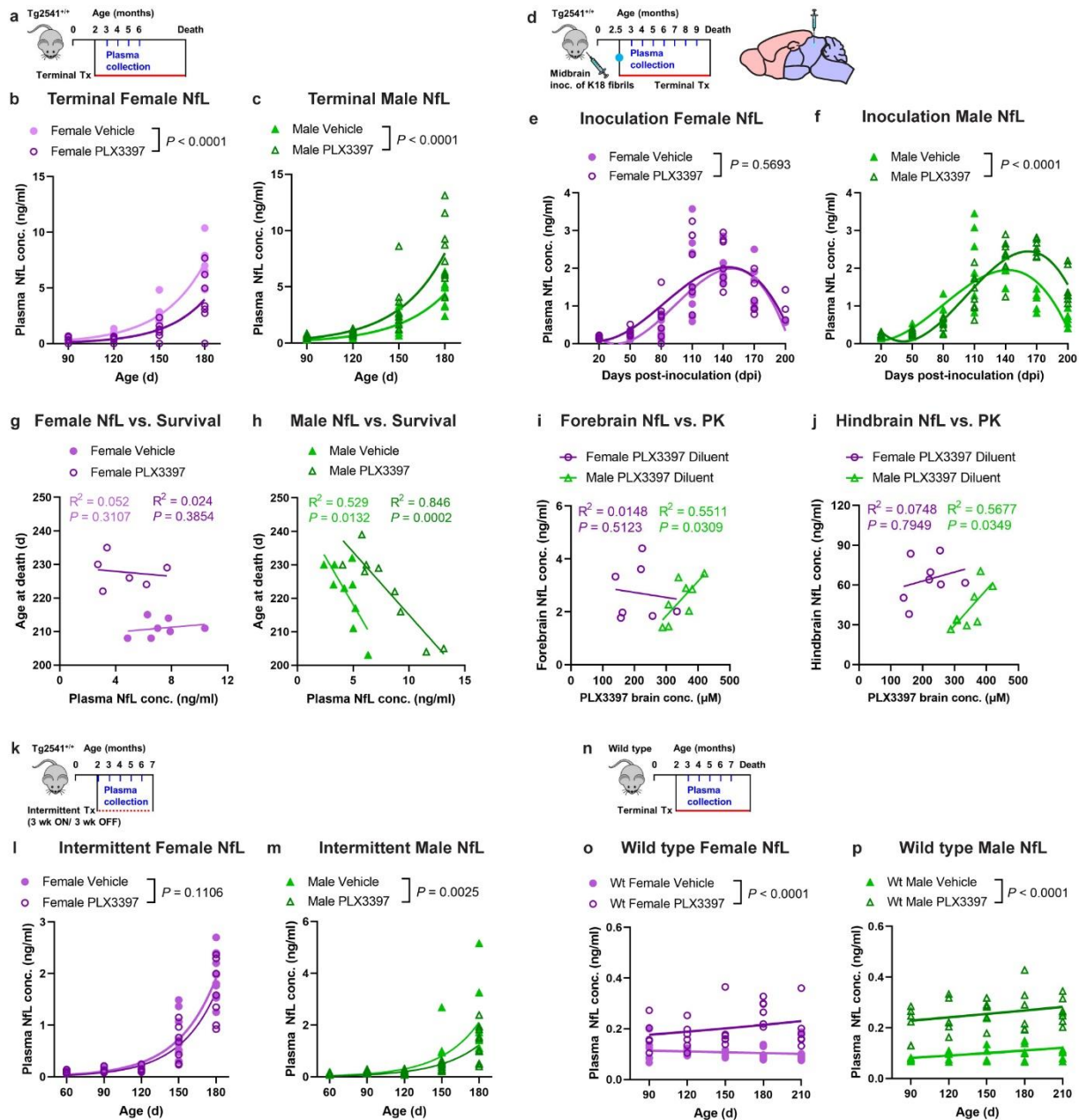
1201 results are shown. **f**, Schematic of terminal PLX3397 treatment of Tg2541 mice from 2.5 mo of
1202 age until death, following inoculation of K18 tau fibrils into the midbrain (hindbrain region) at 2.5
1203 mo of age. **g**, Kaplan-Meier plot showing percent survival of female or male Tg2541 mice
1204 inoculated with K18 tau fibrils or diluent. n=8 mice for Female Vehicle Diluent; n=7 mice for
1205 Female Vehicle K18; n=8 mice for Male Vehicle Diluent; n=7 mice for Male Vehicle K18.
1206 Differences in survival between diluent and K18 inoculation in male or female mice treated with
1207 vehicle were evaluated by Log-rank (Mantel-Cox) test. **h**, Kaplan-Meier plot showing percent
1208 survival of female or male Tg2541 mice inoculated with K18 tau fibrils and then receiving
1209 terminal treatment of vehicle or PLX3397 (275 mg/kg oral). n=7 mice for Female Vehicle K18;
1210 n=6 mice for Female PLX3397 K18; n=7 mice for Male Vehicle K18; n=8 mice for Male
1211 PLX3397 K18. In **b**, **g**, and **h**, differences in survival between treatment groups were evaluated
1212 by Log-rank (Mantel-Cox) test.



1213

1214 **Fig. 3| PLX3397 has sex-dependent pharmacokinetics and reduces hyperactivity in**
 1215 **Tg2541 mice.** **a**, Schematic of terminal PLX3397 treatment (275 mg/kg oral) of Tg2541 mice
 1216 from 2 mo of age until death and blood plasma collected at 3, 4, 5, and 6 mo of age. **b**, Plasma
 1217 concentration of PLX3397 in female or male Tg2541 mice. Each symbol represents an
 1218 individual mouse and the lines indicate group means. The difference between female and male
 1219 mice was assessed by two-way repeated measures ANOVA. **c**, **d**, Correlation plots for plasma
 1220 concentration of PLX3397 at 90 d age and Iba1 area fraction by IHC (**c**) or tau-prion activity (**d**)
 1221 in the forebrains or hindbrains of Tg2541 mice at death. Female mice are shown as open circles
 1222 and male mice shown as open triangles. Linear regression was performed with female and male
 1223 mice combined and best-fit lines are shown. Pearson's correlation analysis was performed and

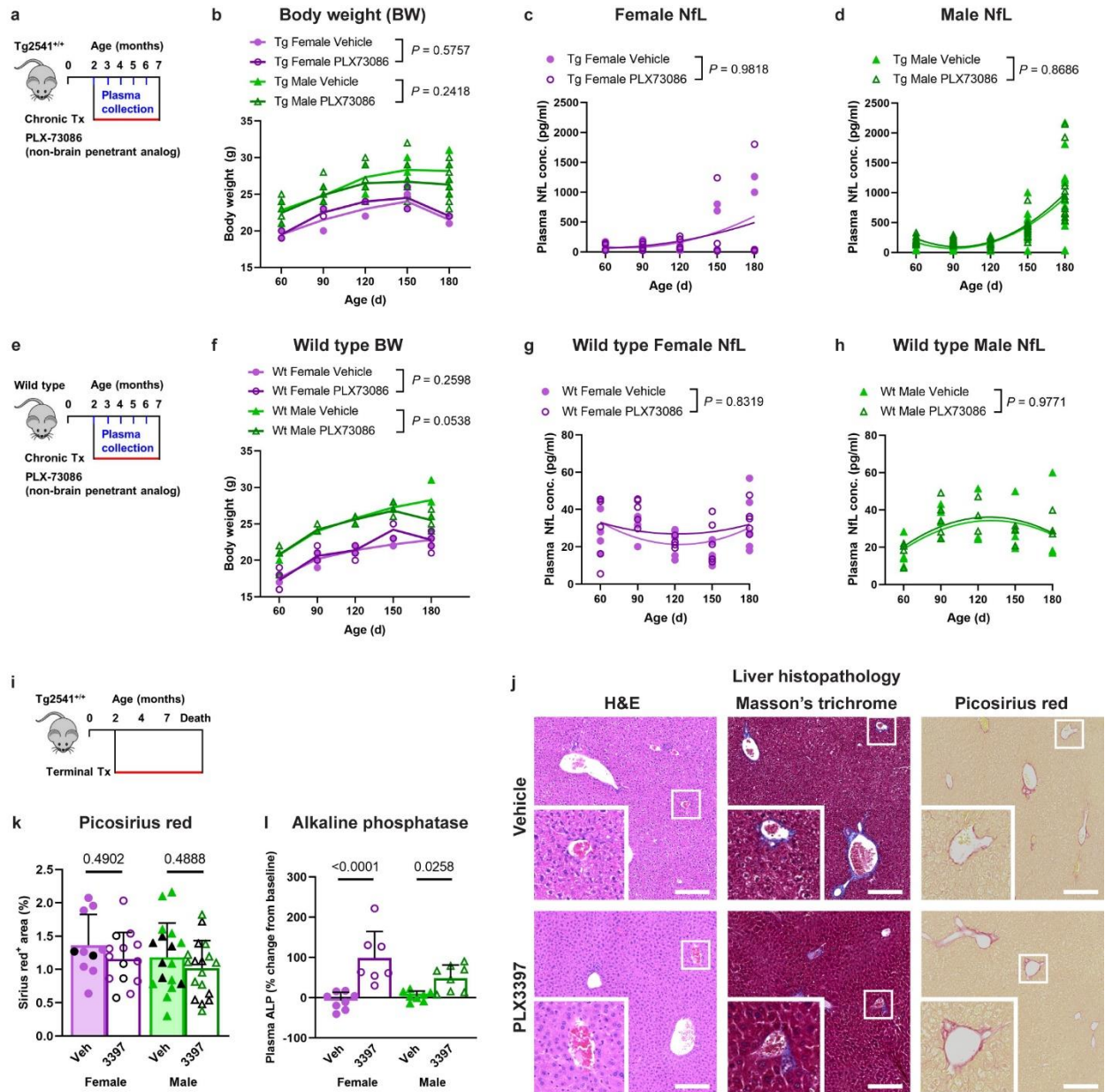
1224 the results are shown. **e**, Longitudinal energy expenditure indices (see Methods) of female or
1225 male Tg2541 mice treated with vehicle or PLX3397. Symbols represent the group means and
1226 shaded regions indicate the s.d. of the mean. Group sizes are the same as shown in **f** and **g**.
1227 Differences between vehicle and PLX3397 treatment in female or male mice were assessed by
1228 three-way repeated measures ANOVA. **f**, **g**, Average distance traveled on the running wheel (**f**)
1229 or still time during the dark cycle (**g**) in female or male Tg2541 mice treated with vehicle or
1230 PLX3397, and measured between 90-d-old and 150-d-old. Each symbol represents an
1231 individual mouse and the dashed lines indicate the same measurements in 90-d-old wild type
1232 mice. Differences between vehicle and PLX3397 treatment in female or male mice were
1233 assessed by Mann-Whitney test.



1234

1235 **Fig. 4| Plasma NfL levels are reduced by PLX3397 in female Tg2541 mice and increased**
 1236 **in male mice.** **a**, Schematic of terminal PLX3397 treatment (275 mg/kg oral) of Tg2541 mice
 1237 from 2 mo of age until death and blood plasma collected at 3, 4, 5, and 6 mo of age. **b, c**,
 1238 Plasma concentration of NfL in female (**b**) or male (**c**) Tg2541 mice treated with vehicle or
 1239 PLX3397. **d**, Schematic of terminal PLX3397 treatment of Tg2541 mice from 2.5 mo of age until
 1240 death, following inoculation of K18 tau fibrils into the midbrain (hindbrain region) at 2.5 mo of
 1241 age, and blood plasma collected monthly thereafter until death. **e, f**, Plasma concentration of
 1242 NfL in female (**e**) or male (**f**) Tg2541 mice inoculated with K18 followed by terminal treatment

1243 with vehicle or PLX3397, plotted over days post-inoculation (dpi). **g, h**, Correlation plots for
1244 plasma NfL concentration and survival in female (**g**) or male (**h**) Tg2541 mice. Each symbol
1245 represents an individual mouse. **i, j**, Correlation plots for brain concentration of PLX3397 and
1246 NfL concentration in the (**i**) forebrains or (**j**) hindbrains of Tg2541 mice receiving midbrain
1247 inoculation with diluent. Each symbol represents the forebrain or hindbrain of an individual
1248 mouse. In **g–j**, linear regression and Pearson’s correlation analysis were performed and the
1249 results are shown. **k**, Schematic of intermittent PLX treatment of Tg2541 mice from 2–7 mo of
1250 age, with three weeks on treatment followed by three weeks off of treatment, and blood plasma
1251 collected at 3, 4, 5, and 6 mo of age. **l, m**, Plasma concentration of NfL in female (**l**) or male (**m**)
1252 Tg2541 mice receiving intermittent treatment with vehicle or PLX3397. **n**, Schematic of terminal
1253 PLX treatment of C57BL/6J wild type mice (Wt) from 2 mo of age until death and blood plasma
1254 collected at 3, 4, 5, 6, and 7 mo of age. **o, p**, Plasma concentration of NfL in female (**o**) or male
1255 (**p**) Wt mice treated with vehicle or PLX3397. In **b, c, e, f, l, m, o, and p**, the differences
1256 between vehicle or PLX3397 treatment were evaluated by non-linear regression using
1257 exponential growth models (**b, c, l, m, o, and p**) or third-order polynomial models (**e and f**) and
1258 the best-fit lines and statistical results are shown. Each symbol represents an individual mouse.



1259

1260 **Fig. 5| Sex-dependent effects of CSF1R are not caused by peripheral toxicity. a,**

1261 Schematic of chronic treatment of Tg2541 mice from 2–7 mo of age with PLX73086 (200 mg/kg

1262 oral), a non-brain penetrant analog of PLX3397 and PLX5622. **b, c,** Plasma concentration of

1263 NfL in female (**b**) or male (**c**) Tg2541 mice treated with vehicle or PLX73086. **d,** Body weights

1264 of female or male T2541 mice treated with PLX73086. **e,** Schematic of chronic treatment of wild

1265 type (Wt) mice from 2–7 mo of age with PLX73086 (200 mg/kg oral). **f, g,** Plasma concentration

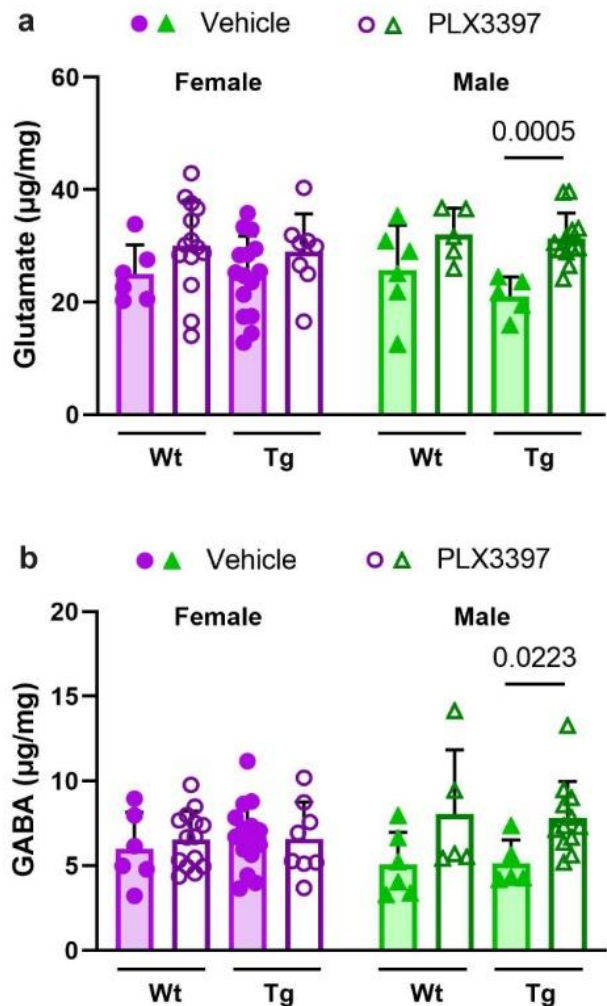
1266 of NfL in female (**f**) or male (**g**) Wt mice treated with vehicle or PLX73086. **h,** Body weights of

1267 female or male wild type mice treated with PLX73086. In **b, c, f,** and **g,** the differences between

1268 vehicle or PLX3397 treatment were evaluated by non-linear regression using quadratic models.

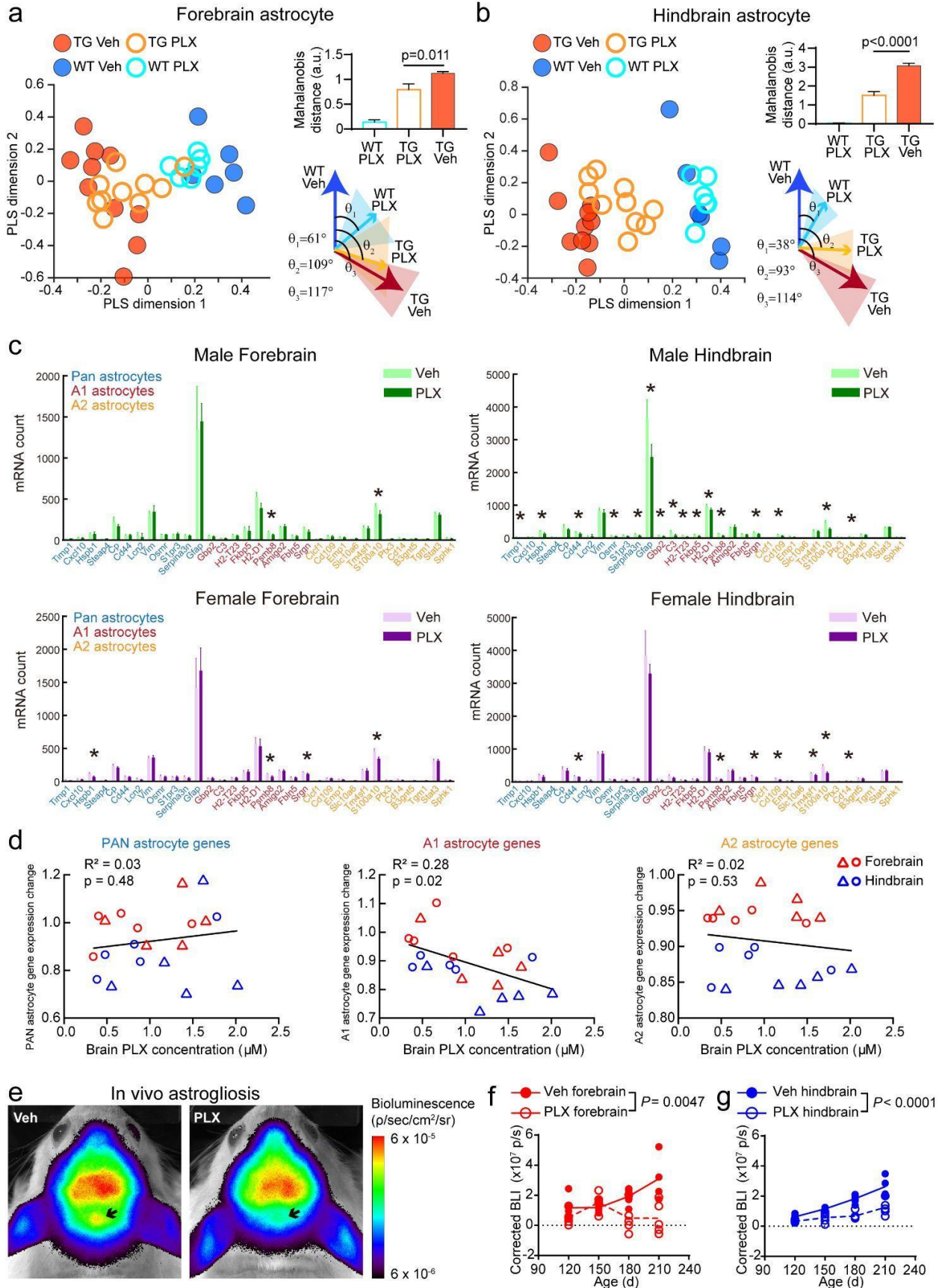
1269 Each symbol represents an individual mouse and the best-fit lines and statistical results are
1270 shown. In **d** and **h**, differences in weight between vehicle and PLX73086 treatment in male or
1271 female mice were evaluated by two-way repeated measures ANOVA and *P* values are shown.
1272 Each symbol represents an individual mouse and lines indicate group means. **i**, Schematic of
1273 terminal treatment of Tg2541 mice from 2 mo of age until death with PLX3397. **j**, Representative
1274 histopathology images of liver sections of Tg2541 mice receiving terminal treatment with vehicle
1275 or PLX3397, stained with hematoxylin and eosin (H&E), Masson's trichrome, or Picosirius red.
1276 High magnification insets are shown of the regions outlined with a white box. Scale bars, 200
1277 μm . **k**, Sirius red-stained liver sections of Tg2541 mice that received acute or terminal treatment
1278 with vehicle or PLX3397 were quantified for percent positive area. The acute and terminal
1279 treatment groups were combined for the analysis due to a limited sample size of terminal
1280 treatment groups and because the group means were similar for the two treatment paradigms.
1281 Mice receiving terminal treatment are shown as black symbols and mice receiving acute
1282 treatment are shown as purple or green symbols. **l**, Alkaline phosphatase (ALP) levels were
1283 measured at eight months of age in the plasma of Tg2541 mice receiving midbrain inoculation
1284 of diluent at 2.5 mo of age and then treated with vehicle or PLX3397 until death. The data are
1285 presented as a percent change from ALP levels at two months of age in the same mice. In **k**
1286 and **l**, the differences between vehicle and PLX3397 treatment were evaluated by ANOVA with
1287 Holm-Šidák post hoc analysis and *P* values are shown. Each symbol represents an individual
1288 mouse and error bars indicate the s.d. of the mean.

1292 mice for non-microglia gene expression patterns (1,599 genes for each mouse). Mice from the
1293 same treatment group (black boxes) show a high degree of correlations. Dashed boxes show
1294 correlations of Tg2541 mice and wild type vehicle group mice. **b**, Distributions of correlation
1295 coefficients in the two groups in dashed boxes in **a**. **c**, Partial least square (PLS) regression
1296 scores and projections of non-microglia gene expression patterns in different groups (1,599
1297 genes for each mouse). The first two dimensions are shown covering >95% of the total
1298 variance. Vehicle-treated mice (filled dots) were used for regression (five dimensions covering
1299 99.99% of the total variance) and PLX5622-treated (1200 mg/kg oral) mice (empty circles) were
1300 projected onto the regression dimensions. **d**, Mahalanobis population vector distances of gene
1301 expression patterns in PLS dimensions relative to the wild type vehicle group. Mann-Whitney
1302 test was used for statistical comparison. **e**, Population vector angles of gene expression
1303 patterns in PLS dimensions from different treatment groups. **f**, Example plots of measured brain
1304 PLX concentration against mRNA counts for a PLX-modulated gene (*Fos*) and a sex-modulated
1305 gene (*Uty*). Linear regression and Pearson's correlation analysis were performed and the
1306 results are shown. N/A indicates that there was no detectable expression of the *Uty* gene in
1307 female mice. See Supplementary Data File 2 for statistical comparisons between male and
1308 female PLX-treated mice of all genes. **g**, Variable importance in projection (VIP) scores in a PLS
1309 regression using non-microglial gene expression patterns to brain PLX concentration and sex.
1310 Genes with VIP scores above 2 are labeled. Red fonts indicate a subset that belongs to
1311 immediate early genes (IEGs). **h**, Scatter plot of measured vs. projected brain PLX
1312 concentration, which was based on a PLS regression with IEG expression. **i**, Correlation of
1313 brain PLX concentration and the population vector distances between PLX-treated individual
1314 mouse transcriptome pattern to WT, with and without the IEGs (1,599 and 1,543 genes for each
1315 mouse, respectively). Linear regressions were calculated for each group. **j**, Quantification of
1316 normalized expression levels from all IEGs (56 genes for each mouse) in the forebrain. Mann-
1317 Whitney tests were used for comparing between groups. **k**, Representative confocal images of
1318 *in situ* labeling of *MAPT* and *Fos* mRNA (RNAscope) in the forebrains of male and female
1319 Tg2541 mice treated with PLX3397 from 2 mo of age until death. Zoomed regions of interest are
1320 shown to the right. Arrows indicate labeled *Fos* puncta. **l**, Quantification of *Fos* mRNA levels
1321 measured in RNAscope images shown in **k**. Mann-Whitney tests were used for comparing
1322 between groups. In **c**, **f**, **h-j**, and **l**, each symbol represents an individual mouse.

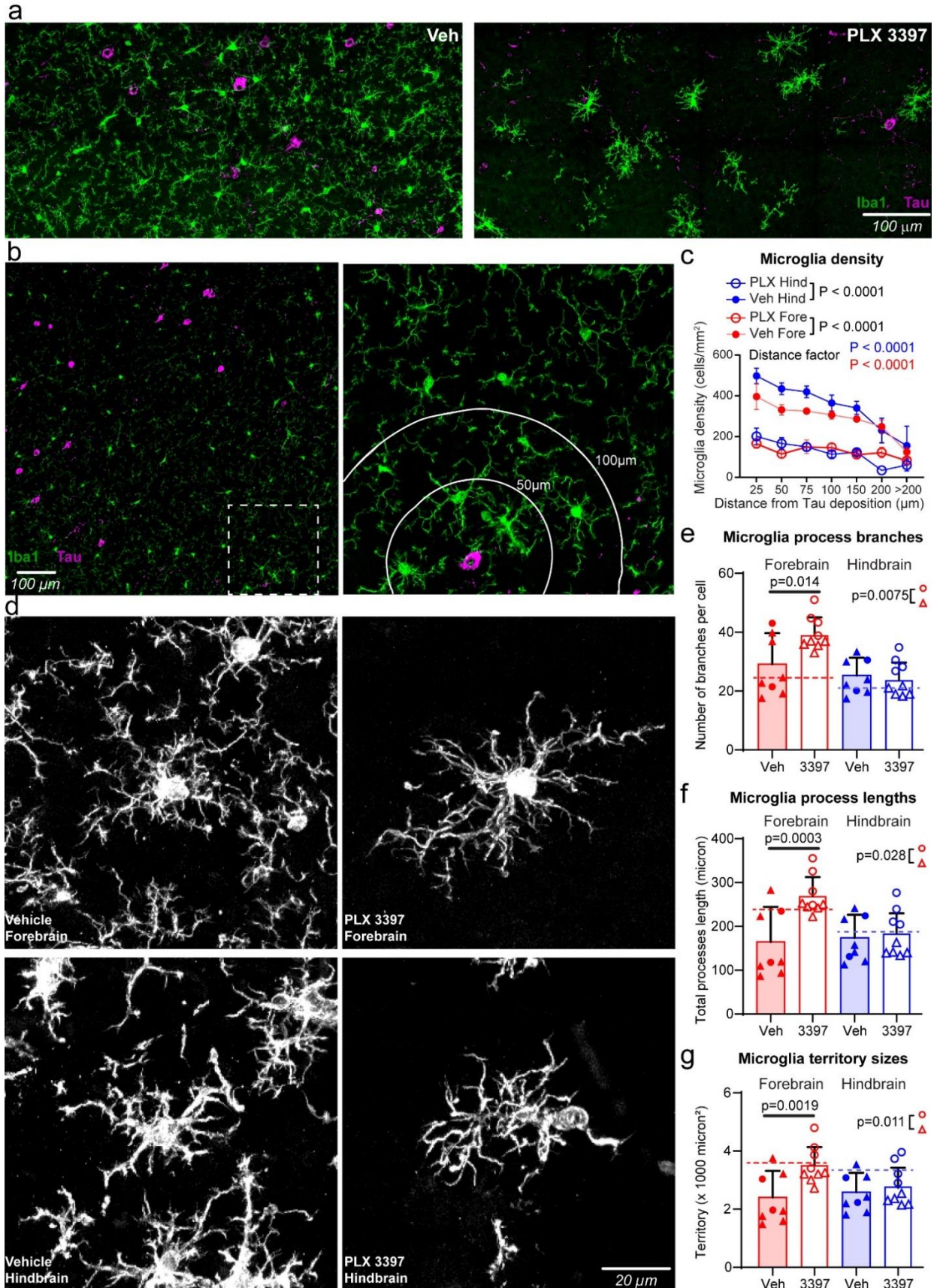


1323

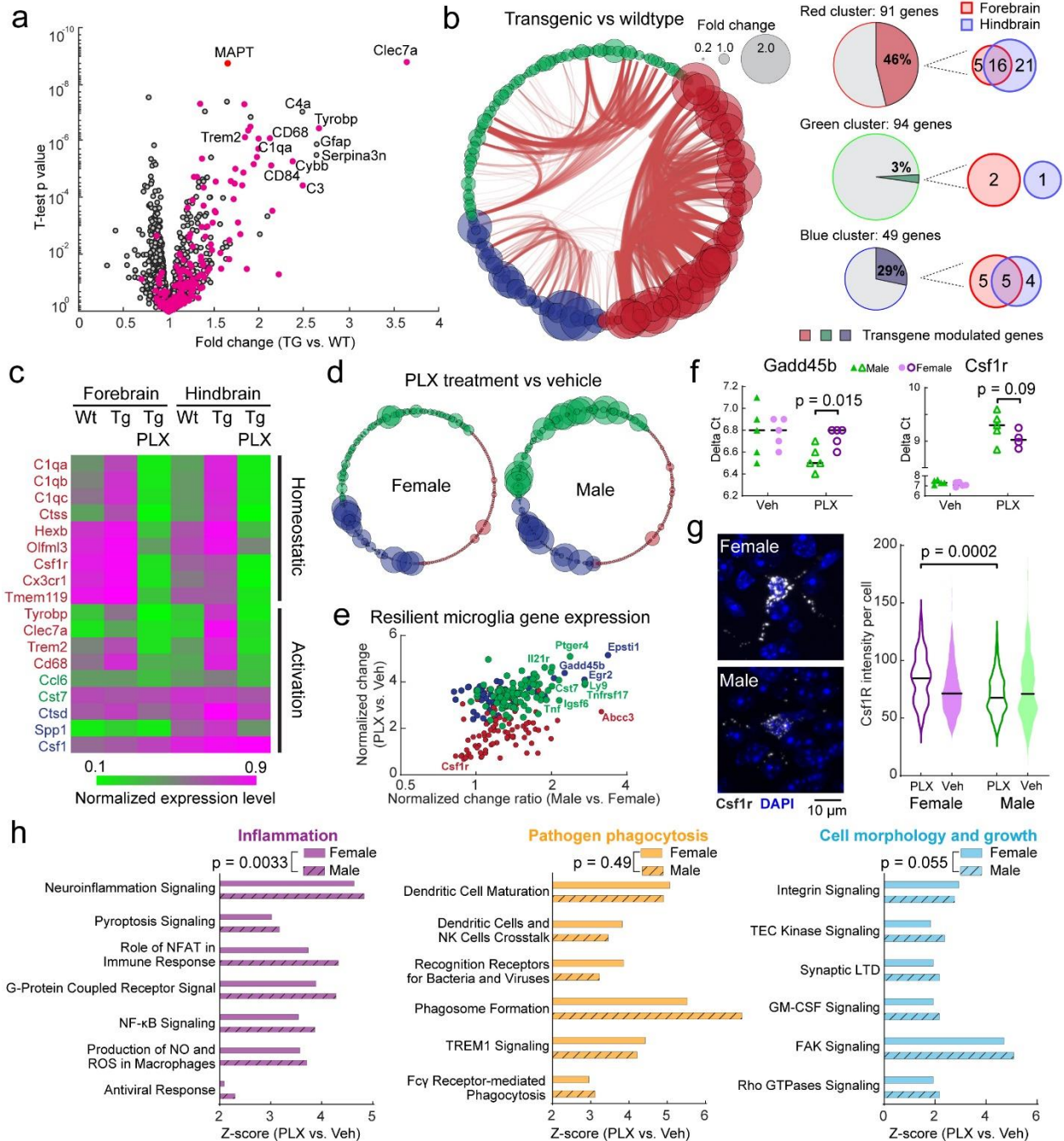
1324 **Fig. 7| PLX dysregulates neurotransmitter levels in the brains of male Tg2541 mice. a,**
1325 Glutamate levels in forebrain lysates of wild type (Wt) or Tg2541 (Tg) mice, dosed for 6-12
1326 weeks with PLX3397 (275 mg/kg oral) or vehicle beginning at 4 months of age, were measured
1327 by hydrophilic interaction liquid chromatography tandem mass spectrometry (HILIC-MS/MS). **b,**
1328 γ -Aminobutyric acid (GABA) levels in forebrain lysates of Wt or Tg mice, dosed for 6-12 weeks
1329 with PLX3397 (275 mg/kg oral) or vehicle beginning at 4 months of age, were measured HILIC-
1330 MS/MS. In **a** and **b**, Mann-Whitney tests were used for comparing vehicle and PLX3397
1331 treatment groups within mouse genotype and sex, and the *P* values of statistically significant
1332 differences ($P < 0.05$) are shown. Each symbol represents an individual mouse and error bars
1333 indicate the s.d. of the mean.



1335 **Fig. 8| CSF1R inhibition ameliorates tau-induced pathological astrocyte activation. a, b,**
1336 Analyses similar to Fig. 6c–e using astrocyte-specific genes (47 genes in each mouse) in (a)
1337 forebrain and (b) hindbrain regions. For other cell types and brain regions, see Supplementary
1338 Fig. 12. **c,** Quantifications of featured astrocyte genes in different conditions. Data are
1339 represented as mean \pm S.D. T-tests were used to compare vehicle and PLX-treated groups for
1340 each gene, with 5% false discovery rate correction for multiple comparisons. **d,** Correlation of
1341 brain PLX concentration and different groups of astrocyte gene expression. Based on a prior
1342 study⁴⁶, A1 genes are associated with neurotoxic astrocytes following lipopolysaccharide
1343 exposure and A2 genes are associated with neuroprotective function in an artery occlusion
1344 model. Linear regressions were calculated for each group. **e,** Representative images of *in vivo*
1345 bioluminescence imaging of GFAP activity in Tg2541 mice with vehicle or PLX3397 treatment.
1346 Arrows indicate hindbrain regions. **f, g,** Quantifications of longitudinal measurements of
1347 astrogliosis-driven bioluminescence in the (f) forebrains or (g) hindbrains of Tg2541 mice with
1348 vehicle or PLX3397 treatment. Differences in BLI signal between vehicle and PLX treatment
1349 were evaluated by mixed-effects analysis (Restricted maximum likelihood). In **a, b, d, f,** and **g**
1350 each symbol represents an individual mouse.



1352 **Fig. 9| PLX3397 treatment preferentially eliminates reactive microglia around tau**
1353 **deposits. a**, Representative confocal images of immunostaining of tau protein (magenta) and
1354 microglia (Iba1, green) in the brain of a vehicle-treated (left) or PLX3397-treated (right) 210-d-
1355 old Tg2541 mouse. **b**, Representative confocal images, similar to panel **a**, of a vehicle-treated
1356 210-d-old Tg2541 mouse. The right panel shows the zoomed image from the dashed box in the
1357 left panel. The white lines in the right panel show distances from the tau deposit at the center. **c**,
1358 Quantification of microglial densities at different distances from the nearest tau deposit in
1359 Tg2541 mice treated with vehicle or PLX3397 (275 mg/kg oral). Two-way ANOVA was used to
1360 compare statistical differences between treatment groups and distance bins. **d**, Representative
1361 confocal images of microglial processes labeled by Iba1 immunohistochemistry. **e-g**,
1362 Quantification of microglial processes branch numbers (**e**), total lengths (**f**) and territory sizes (**g**)
1363 in Tg2541 mice treated with vehicle or PLX3397. Each data point shows the average value of
1364 the microglia measured in an individual mouse. Error bars represent the s.d. of the mean.
1365 Circles indicate female mice and triangles indicate male mice. Dotted lines show the average
1366 measurements from microglia in wild type mice. Mann-Whitney tests were used to compare
1367 between groups. The forebrain regions of PLX3397-treated male and female mice were also
1368 compared directly and the *P* values are shown on each plot.

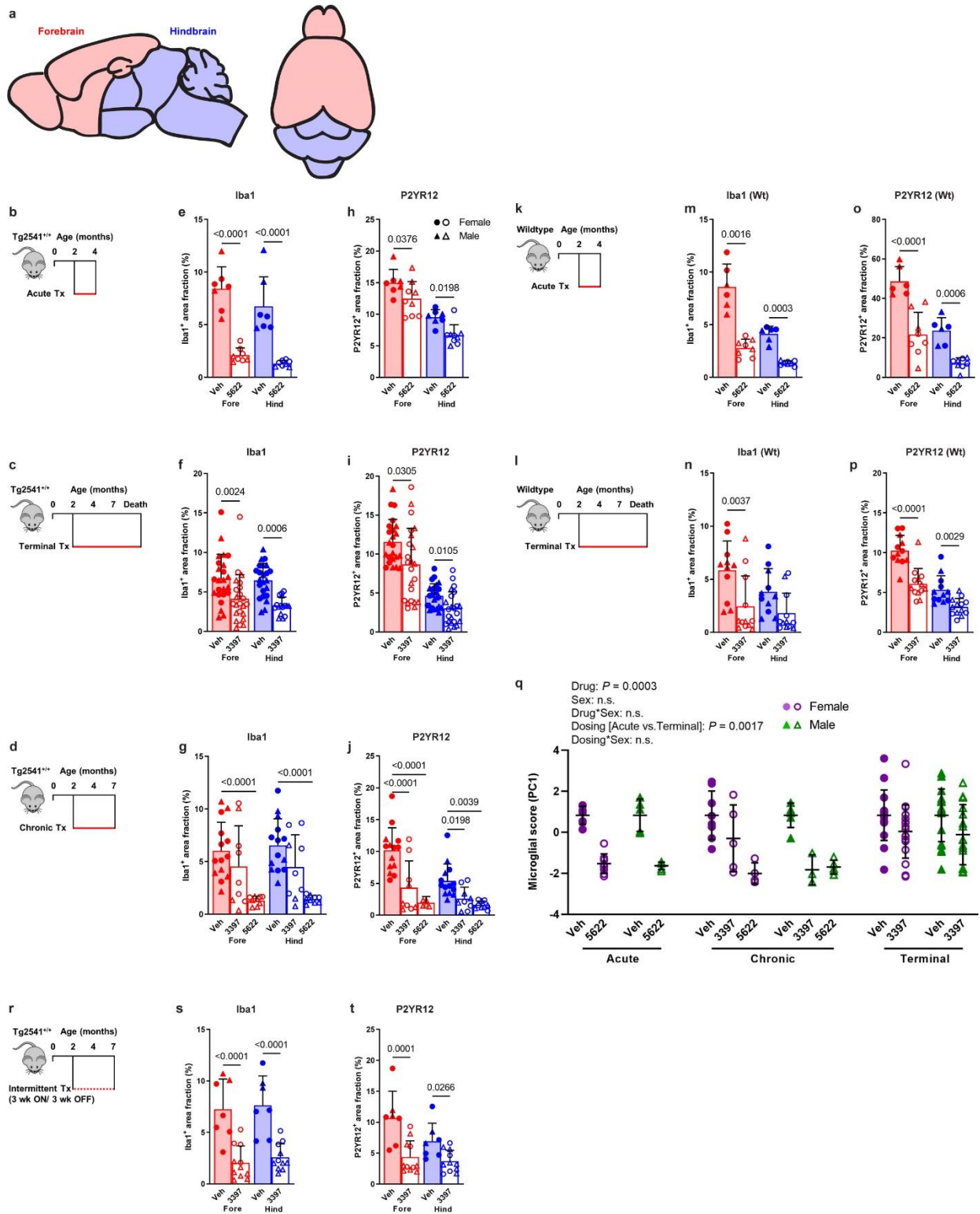


1369

1370 **Fig. 10| Selective ablation of tau-activated microglia gene expression by PLX5622. a,**
 1371 Volcano plot of gene expression changes between Tg2541 and wild type mice. Many microglial-
 1372 specific genes (magenta dots) show trends of up-regulation in Tg2541 mice. **b,** Schemaball
 1373 graphs of microglial-specific genes comparing Tg2541 to wild type. Individual circle sizes
 1374 indicate fold changes. Microglial-specific genes (242 genes in our dataset) are clustered into
 1375 three groups: red, green and blue. Connecting arcs between genes represent the degree of

1376 correlation. The pie charts on the right show the percentage of genes in each group that are
1377 differentially expressed in Tg2541 and wild type mice, and the Venn diagrams indicate the brain
1378 regions of differential expression. **c**, Heatmap showing expression level changes in DAM
1379 genes⁵¹. Gene names are color coded to show their group assignments. **d**, Schemaball graphs
1380 of microglial-specific genes comparing Tg2541 vehicle to PLX5622 treatment (1200 mg/kg oral)
1381 in male and female mice. **e**, Estimated gene expression levels in resilient microglia comparing
1382 between genders and treatment. Each dot represents a different gene, and is color-coded
1383 according to the cluster to which it belongs. **f**, Real-time PCR quantification of example
1384 microglial genes *Gadd45b* and *Csf1r* comparing vehicle to PLX5622 treatment in Tg2541 mice.
1385 Bars indicate medians and student's t-tests were used to compare groups. **g**, Representative
1386 images and quantification of *Csf1r* gene expression by *in situ* mRNA hybridization (RNAscope)
1387 analyses of Tg2541 mice treated with PLX3397 from 2 mo of age until death. Bars indicate
1388 medians and two-way ANOVA was used to compare groups. **h**, Ingenuity Pathway Analysis of
1389 the gene expression patterns in the resilient microglia in male and female mice. Paired t-tests
1390 were used in each category to compare sexes.

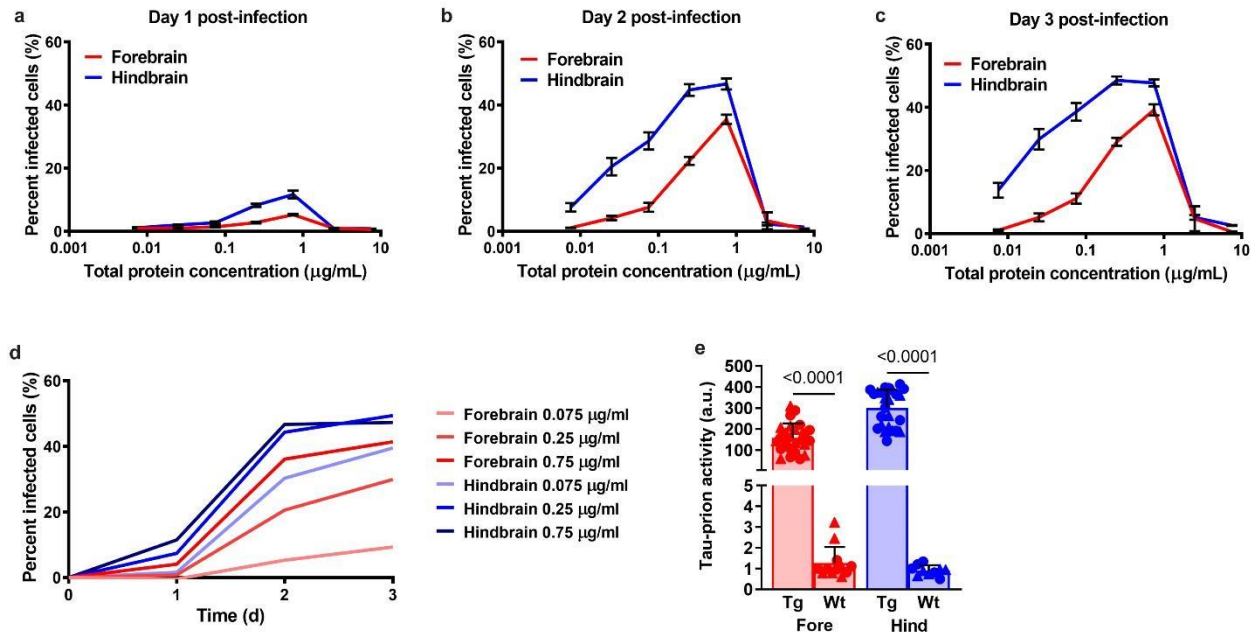
1391 SUPPLEMENTARY INFORMATION



1392

1393 Supplementary Fig. 1 | Microglial depletion by CSF1R inhibitors in Tg2541 and wild type

1394 **mice. a**, Sagittal and superior diagrams of the mouse brain divided into two regions: the
1395 forebrain, containing the cortex, hippocampus, striatum, and olfactory bulb; and the hindbrain,
1396 containing the thalamus, hypothalamus, midbrain, cerebellum, and brain stem. **b–d**, Schematics
1397 of acute (**b**), terminal (**c**), or chronic (**d**) PLX treatment of Tg2541 mice from 2–4 mo of age, 2
1398 mo of age until death, or 2–7 mo of age, respectively. **e–g**, Quantification of the Iba1-positive
1399 area fraction by IHC in the forebrains or hindbrains of Tg2541 mice receiving acute (**e**), terminal
1400 (**f**), or chronic (**g**) treatment with vehicle, PLX3397 (275 mg/kg oral), or PLX5622 (1200 mg/kg
1401 oral). **h–j**, Quantification of the P2yr12-positive area fraction by IHC in the forebrains or
1402 hindbrains of Tg2541 mice receiving acute (**h**), terminal (**i**), or chronic (**j**) treatment with vehicle,
1403 PLX3397, or PLX5622. **k, l**, Schematics of acute (**k**) or terminal (**l**) PLX treatment of C57BL/6J
1404 wild type mice (Wt) from 2–4 mo of age, or 2 mo of age until death, respectively. **m, n**,
1405 Quantification of the Iba1-positive area fraction by IHC in the forebrain and hindbrain of Wt mice
1406 receiving acute (**m**) or terminal (**n**) treatment with vehicle, PLX3397, or PLX5622. **o, p**,
1407 Quantification of the P2yr12-positive area fraction by IHC in the forebrains or hindbrains of Wt
1408 mice receiving acute (**o**) or terminal (**p**) treatment with vehicle, PLX3397, or PLX5622. *P* values
1409 for all statistically significant differences ($P < 0.05$) are shown. **q**, Principal component analysis
1410 was performed, using all data presented in **e–j** and **m–p** to calculate a ‘microglial score’ that
1411 represents the amount of Iba1 and P2yr12 staining in both the forebrains and hindbrains of
1412 Tg2541 and Wt mice. All data was first standardized to the respective vehicle-treated group of
1413 the same sex and same dosing paradigm. Then, two principal components (PC1 and PC2) were
1414 identified which accounted for 79.0% of the total variance in the data. Multiple linear regression
1415 was performed on PC1 of the drug-treated groups to evaluate the main effects sex and dosing
1416 paradigm, and the dosing*sex interaction effect. Multiple linear regression was performed on all
1417 groups to determine the main effect of drug and the drug*sex interaction effect. *P* values for all
1418 statistically significant differences ($P < 0.05$) are shown. n.s. indicates not statistically significant.
1419 PC2 was also evaluated, but only the drug main effect was statistically significant. **r**, Schematic
1420 of intermittent PLX treatment of Tg2541 mice from 2–7 mo of age, with three weeks on
1421 treatment followed by three weeks off of treatment. **s, t**, Quantification of the Iba1-positive (**s**) or
1422 P2yr12-positive (**t**) area fractions by IHC in the forebrains or hindbrains of Tg2541 mice
1423 receiving intermittent treatment with vehicle or PLX3397. In **e–j**, **m–p**, **s**, and **t**, each symbol
1424 represents the forebrain or hindbrain of an individual mouse, with female mice shown as closed
1425 or open circles and male mice shown as closed or open triangles. Error bars represent s.d. of
1426 the mean. Two-way ANOVA with Holm-Šidák post hoc testing was used in **e, f, h, i, m–p, s**, and
1427 **t**. Welch ANOVA with Dunnett T3 post hoc testing was used in **g** and **j**.



1428

1429 **Supplementary Fig. 2| Optimization of HEK293T cell bioassay for measuring tau-prions in**

1430 **Tg2541 mouse brain homogenates. a–c**, Percent of HEK293T cells expressing YFP-tau-

1431 RD*P301L/V337M with tau aggregates at one (a), two (b), or three (c) days post-infection with

1432 Tg2541 mouse forebrain or hindbrain homogenates at concentrations ranging from 0.0075–7.5

1433 µg/ml. Error bars represent s.e.m. of three terminal Tg2541 mice. d, Percent of cells infected

1434 with tau aggregates over time following infection with 0.075, 0.25, or 0.75 µg/ml Tg2541 mouse

1435 forebrain or hindbrain homogenates. Lines represent the means of three terminal Tg2541 mice.

1436 e, Tau-prion levels in 0.25 µg/ml forebrain or hindbrain homogenates of Tg2541 (Tg) or wild

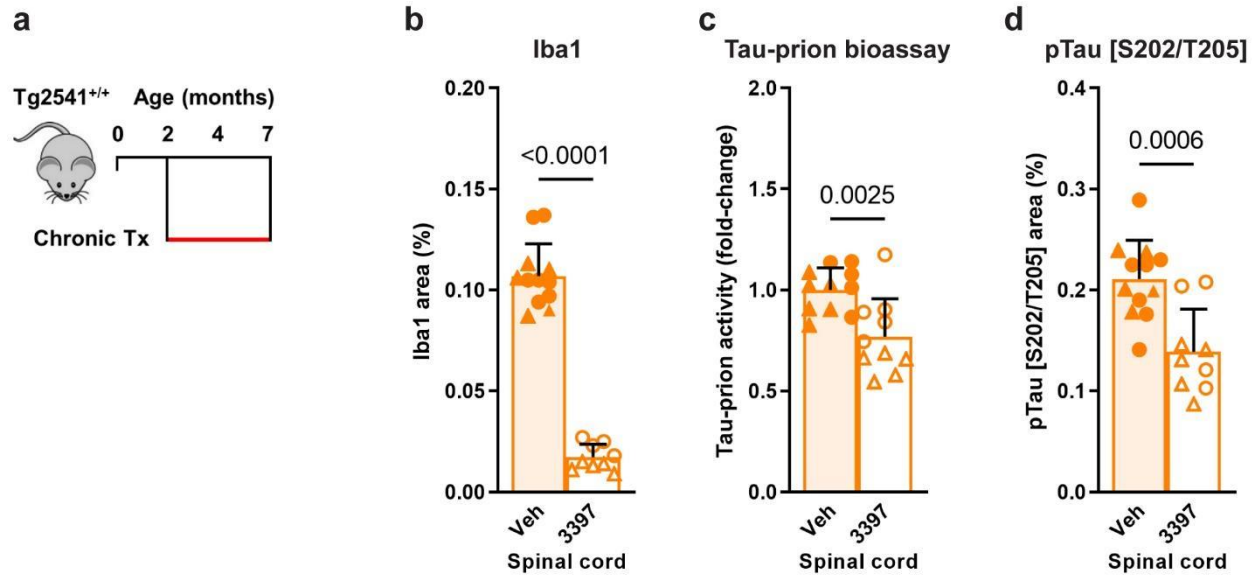
1437 type (Wt) mice, measured using the optimized HEK293T cell tau-prion bioassay. Each symbol

1438 represents the forebrain or hindbrain of an individual mouse and female mice are shown as

1439 closed circles while male mice are shown as closed triangles. Two-way ANOVA with Holm-

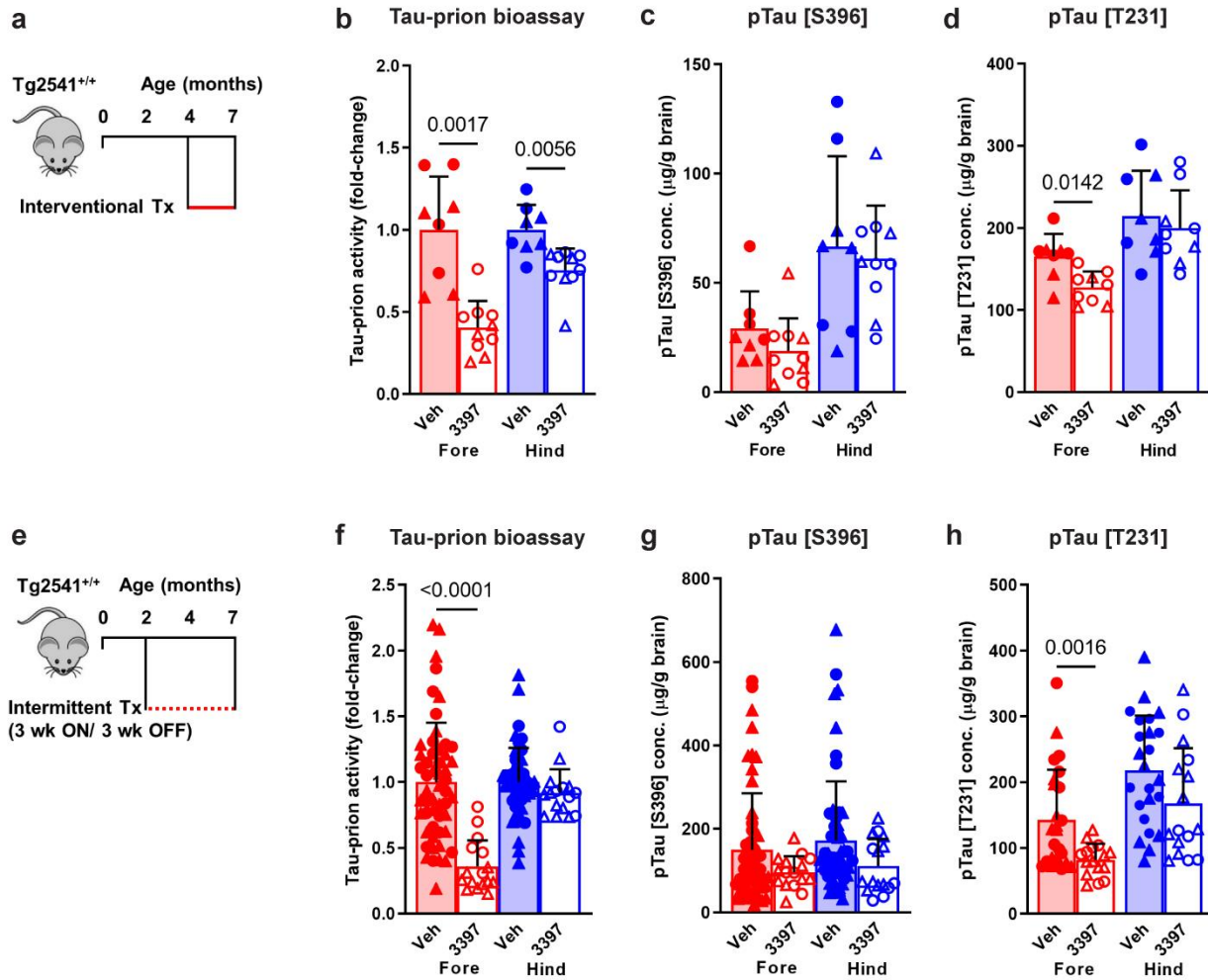
1440 Šidák post hoc testing was used and *P* values for all statistically significant differences (*P* <

1441 0.05) are shown.



1442

1443 **Supplementary Fig. 3| CSF1R inhibition reduces microglia and pathogenic tau levels in**
1444 **the spinal cords of Tg2541 mice. a**, Schematic of chronic PLX treatment of Tg2541 mice from
1445 2–7 mo of age. **b**, Quantification of the Iba1-positive area fraction by IHC in the spinal cords of
1446 Tg2541 mice receiving chronic treatment with vehicle or PLX3397 (275 mg/kg oral). **c**, Tau-
1447 prion levels in spinal cord tissue homogenates of Tg2541 mice receiving chronic treatment with
1448 vehicle or PLX3397, measured using the HEK293T cell tau-prion bioassay and normalized to
1449 the vehicle group. **d**, Quantification of pTau [S202/T205]-positive area by IHC in the spinal cords
1450 of Tg2541 mice receiving chronic treatment with vehicle or PLX3397. In **b–d**, each symbol
1451 represents an individual mouse, with female mice shown as closed or open circles and male
1452 mice shown as closed or open triangles. Error bars represent s.d. of the mean. Unpaired t tests
1453 were used and *P* values for all statistically significant differences (*P* < 0.05) are shown.



1454

1455 **Supplementary Fig. 4| Interventional or intermittent CSF1R inhibition reduces pathogenic**

1456 **tau levels in the brains of Tg2541 mice.** **a**, Schematic of interventional PLX treatment of

1457 Tg2541 mice from 4–7 mo of age. **b**, Tau-prion levels in forebrain and hindbrain tissue

1458 homogenates of Tg2541 mice receiving interventional treatment with vehicle or PLX3397 (275

1459 mg/kg oral), measured using the HEK293T cell tau-prion bioassay and normalized to the vehicle

1460 group. **c**, Levels of pTau [S396] measured by ELISA in formic acid extracts of forebrain and

1461 hindbrain tissue homogenates of Tg2541 mice receiving interventional treatment with vehicle or

1462 PLX3397, normalized to total protein concentration. **d**, Levels of pTau [T231] measured by

1463 ELISA in formic acid extracts of forebrain and hindbrain tissue homogenates of Tg2541 mice

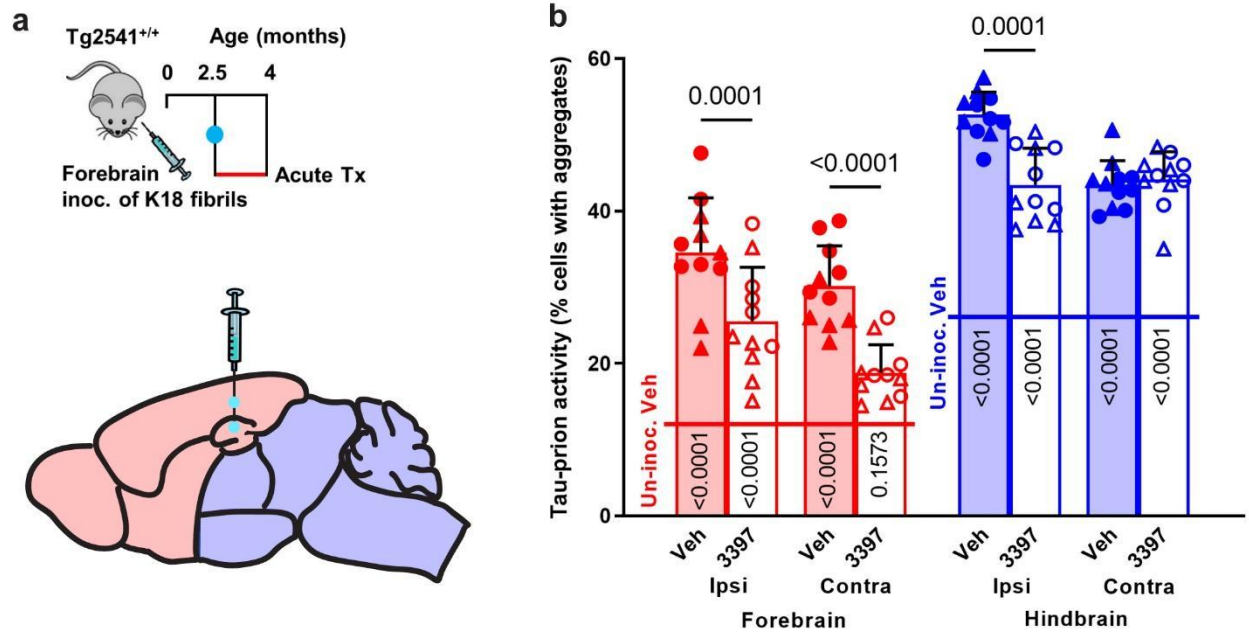
1464 receiving interventional treatment with vehicle or PLX3397, normalized to total protein

1465 concentration. **e**, Schematic of intermittent PLX treatment of Tg2541 mice from 2–7 mo of age,

1466 with three weeks on treatment followed by three weeks off of treatment. **f**, Tau-prion levels in

1467 forebrain and hindbrain tissue homogenates of Tg2541 mice receiving intermittent treatment

1468 with vehicle or PLX3397, measured using the HEK293T cell tau-prion bioassay and normalized
1469 to the vehicle group. **g**, Levels of pTau [S396] measured by ELISA in formic acid extracts of
1470 forebrain and hindbrain tissue homogenates of Tg2541 mice receiving intermittent treatment
1471 with vehicle or PLX3397, normalized to total protein concentration. **h**, Levels of pTau [T231]
1472 measured by ELISA in formic acid extracts of forebrain and hindbrain tissue homogenates of
1473 Tg2541 mice receiving intermittent treatment with vehicle or PLX3397, normalized to total
1474 protein concentration. In **b–d** and **f–h**, each symbol represents the forebrain or hindbrain of an
1475 individual mouse, with female mice shown as closed or open circles and male mice shown as
1476 closed or open triangles. Error bars represent s.d. of the mean. Two-way ANOVA with Holm-
1477 Šidák post hoc testing was used and *P* values for all statistically significant differences (*P* <
1478 0.05) are shown.



1479

1480 **Supplementary Fig. 5| CSF1R inhibition reduces pathogenic tau spreading following K18**

1481 **forebrain inoculation.** **a**, Schematic of acute PLX treatment of Tg2541 mice from 2.5–4 mo of

1482 age following inoculation of K18 tau fibrils into the hippocampus and overlying cortex (forebrain

1483 regions) at 2.5 mo of age. **b**, Tau-prion levels in the ipsilateral (inoculated side) or contralateral

1484 (un-inoculated side) forebrain or hindbrain tissue homogenates of Tg2541 mice receiving acute

1485 treatment with vehicle or PLX3397 (275 mg/kg oral) following K18 forebrain inoculation,

1486 measured using the HEK293T cell tau-prion bioassay and presented as percent of cells with tau

1487 aggregates. Horizontal lines across bars indicate the mean tau-prion level in forebrain (12.54%

1488 cells with aggregates) or hindbrain (26.06% cells with aggregates) tissue homogenates of

1489 Tg2541 mice that did not undergo K18 inoculation and received acute treatment with vehicle

1490 (Un-inoc. Veh). Each symbol represents the ipsilateral or contralateral forebrain or hindbrain of

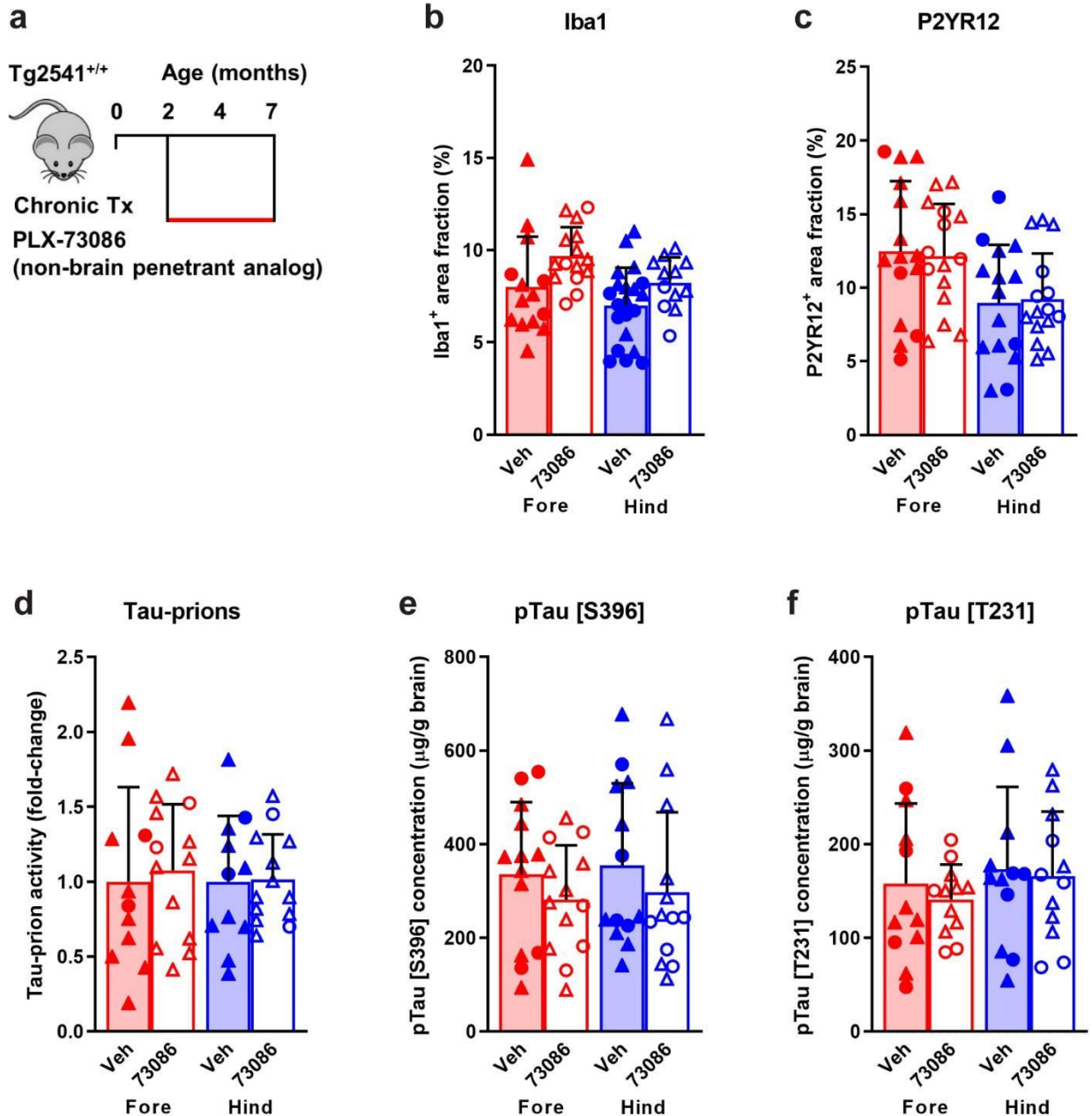
1491 an individual mouse, with female mice shown as closed or open circles and male mice shown

1492 as closed or open triangles. Error bars represent s.d. of the mean. Three-way ANOVA with

1493 Holm-Šidák post hoc testing was used and *P* values for all statistically significant differences (*P*

1494 < 0.05) between Veh and 3397 are shown above the bars. *P* values for all differences between

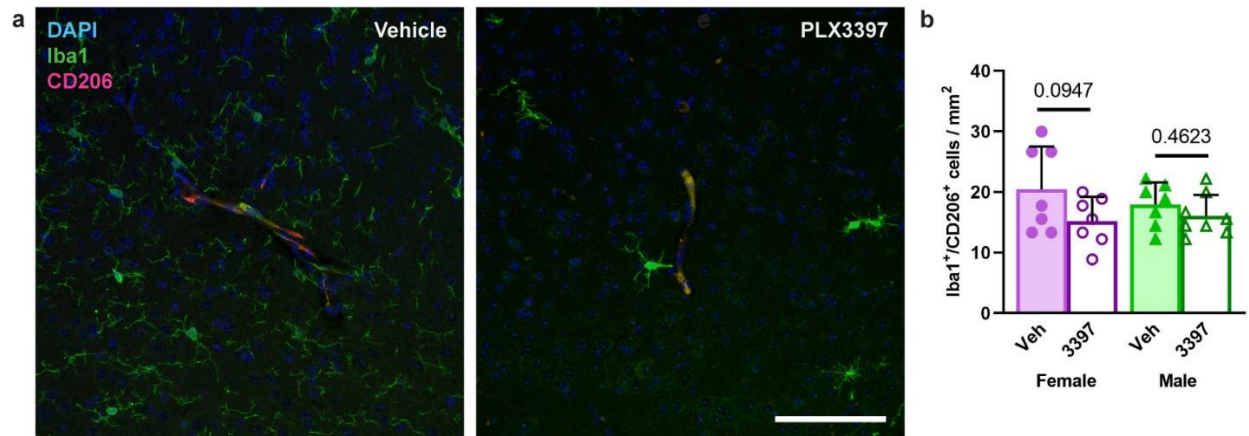
1495 each group and the respective brain region of Un-inoc. Veh mice are shown on the bars.



1496

1497 **Supplementary Fig. 6| Non-brain penetrant analog of CSF1R inhibitors does not reduce**
1498 **microglia or pathogenic tau levels in the brains of Tg2541 mice.** a, Schematic of chronic
1499 treatment of Tg2541 mice from 2–7 mo of age with PLX73086, a non-brain penetrant analog of
1500 PLX3397 and PLX5622. b, c, Quantification of the Iba1-positive (b) or P2yr12-positive (c)
1501 area fractions by IHC in the forebrains or hindbrains of Tg2541 mice receiving chronic treatment with
1502 vehicle or PLX73086 (200 mg/kg oral). d, Tau-prion levels in forebrain and hindbrain tissue
1503 homogenates of Tg2541 mice receiving chronic treatment with vehicle or PLX73086, measured

1504 using the HEK293T cell tau-prion bioassay and normalized to the vehicle group. **e, f**, Levels of
1505 pTau [S396] (**e**) or pTau [T231] (**f**) measured by ELISA in formic acid extracts of forebrain and
1506 hindbrain tissue homogenates of Tg2541 mice receiving chronic treatment with vehicle or
1507 PLX73086, normalized to total protein concentration. In **b–f**, each symbol represents the
1508 forebrain or hindbrain of an individual mouse, with female mice shown as closed or open circles
1509 and male mice shown as closed or open triangles. Error bars represent s.d. of the mean. Two-
1510 way ANOVA with Holm-Šidák post hoc testing was used and *P* values for all statistically
1511 significant differences ($P < 0.05$) are shown.



1512

1513 **Supplementary Fig. 7| Pharmacological CSF1R inhibition does not deplete perivascular**

1514 **macrophages.** a, Representative immunofluorescence images of Tg2541 mouse cortical blood

1515 vessels labeled for perivascular macrophages (Iba1+/CD206+) and microglia (Iba1+/CD206-).

1516 Iba1 labels both PVMs and microglia. Mice were treated with PLX3397 from 2.5 mo of age until

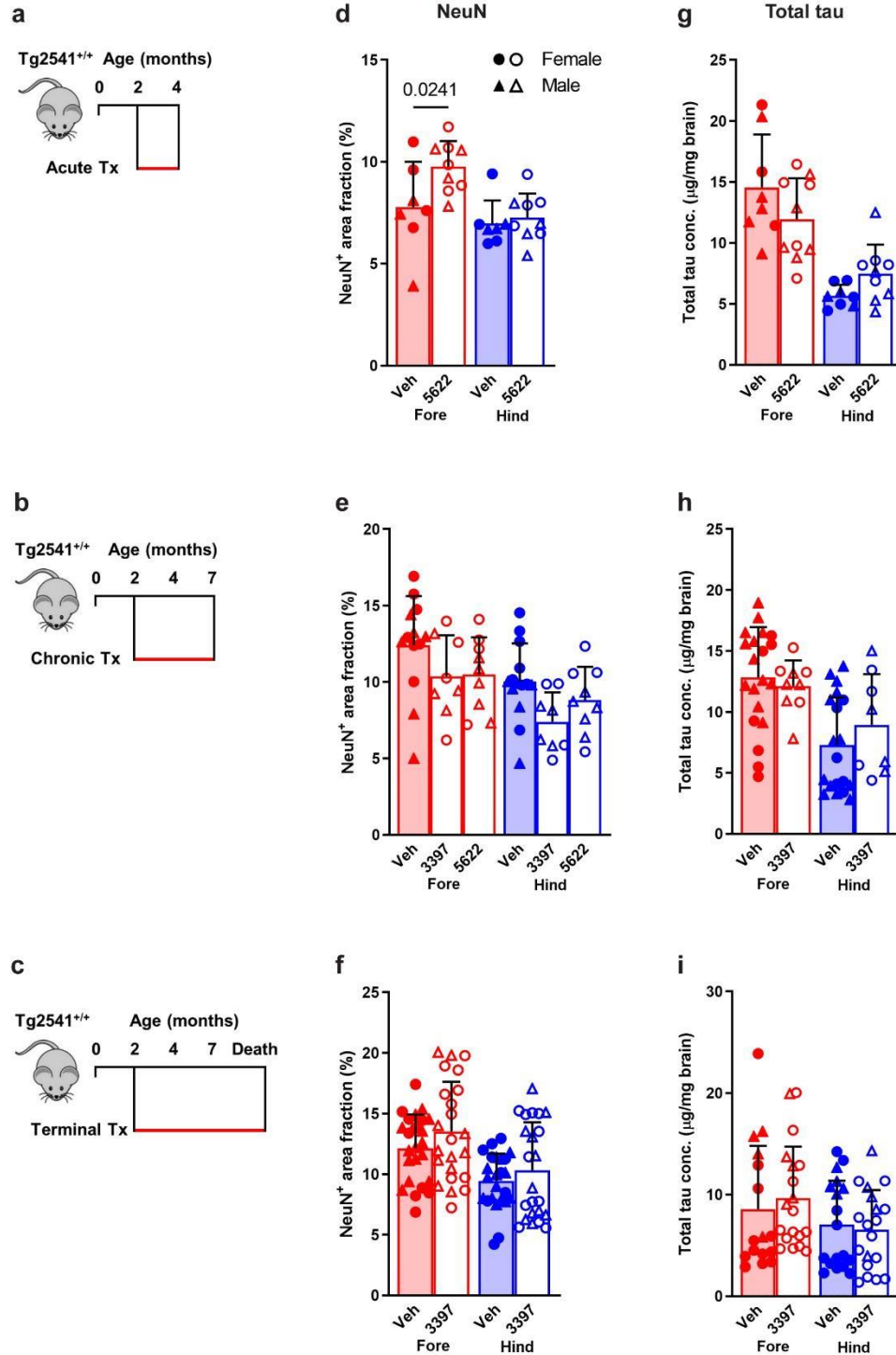
1517 death, following inoculation of K18 tau fibrils into the midbrain (hindbrain region) at 2.5 mo of

1518 age. Scale bar, 100 μ m. b, Quantification of Iba1+/CD206+ cell density in images of Tg2541

1519 mouse cortical blood vessels. Each symbol represents the average of six blood vessel images

1520 from each individual mouse. Error bars represent s.d. of the mean. Two-way ANOVA was used

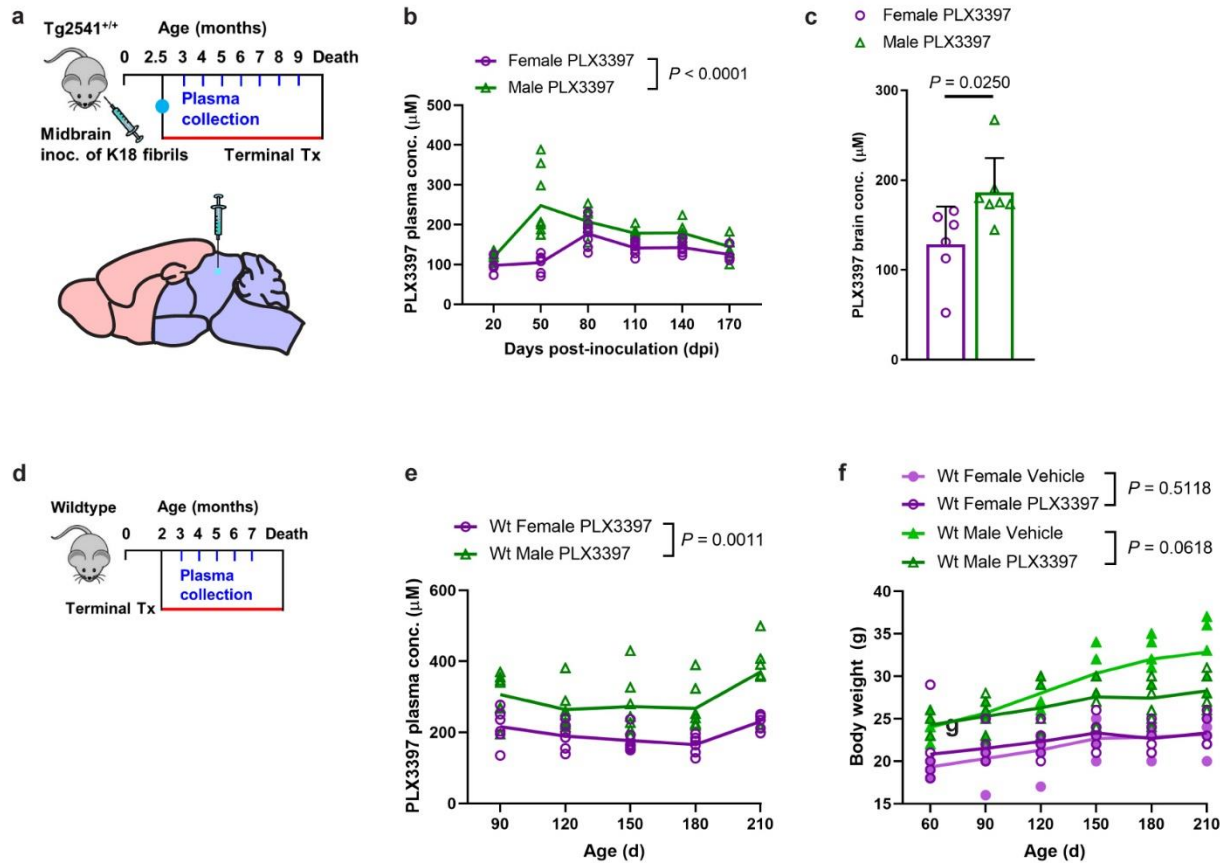
1521 and the *P* values for Holm-Šidák post hoc testing between treatment groups are shown.



1522

1523 **Supplementary Fig. 8| CSF1R inhibition by three treatment paradigms does not affect**
 1524 **neurons or total tau levels.** a–c, Schematics of acute (a), chronic (b), or terminal (c) PLX
 1525 treatment of Tg2541 mice from 2–4 mo of age, 2–7 mo of age, or 2 mo of age until death,
 1526 respectively. d–f, Quantification of neuronal nuclei (NeuN)-positive area fraction by IHC analysis

1527 of forebrain and hindbrain areas of Tg2541 mice receiving acute (**d**), chronic (**e**), or terminal (**f**)
1528 treatment with vehicle, PLX3397 (275 mg/kg oral), or PLX5622 (1200 mg/kg oral). **g–i**, Levels of
1529 total tau measured by ELISA in forebrain and hindbrain tissue homogenates of Tg2541 mice
1530 receiving acute (**g**), chronic (**h**), or terminal treatment (**i**) with vehicle, PLX3397, or PLX5622,
1531 normalized to total protein concentration. In **d–i**, each symbol represents the forebrain or
1532 hindbrain of an individual mouse, with female mice shown as closed or open circles and male
1533 mice shown as closed or open triangles. Error bars represent s.d. of the mean. Two-way
1534 ANOVA with Holm-Šidák post hoc testing was used in **d**, and **f–i**. One-way ANOVA with Holm-
1535 Šidák post hoc testing was used in **e**. *P* values for all statistically significant differences (*P* <
1536 0.05) are shown.



1537

1538 **Supplementary Fig. 9| PLX3397 levels are increased in male Tg2541 and wild type mice.**

1539 **a**, Schematic of terminal PLX3397 treatment of Tg2541 mice from 2.5 mo of age until death,

1540 following inoculation of K18 tau fibrils into the midbrain (hindbrain region) at 2.5 mo of age.

1541 Blood plasma was collected at monthly intervals from 3–9 mo of age. **b**, Plasma concentration

1542 of PLX3397 in female or male Tg2541 mice inoculated with K18 followed by terminal treatment

1543 with PLX3397, plotted over days post inoculation (dpi). Mixed-effects analysis (Restricted

1544 maximum likelihood) was used to compare female and male mice and the P value is shown. **c**,

1545 Brain concentration of PLX3397 at death in female or male Tg2541 mice inoculated with K18

1546 followed by terminal treatment with PLX3397. Unpaired t test was used to compare female and

1547 male mice and the P value is shown. Each symbol represents an individual mouse and the error

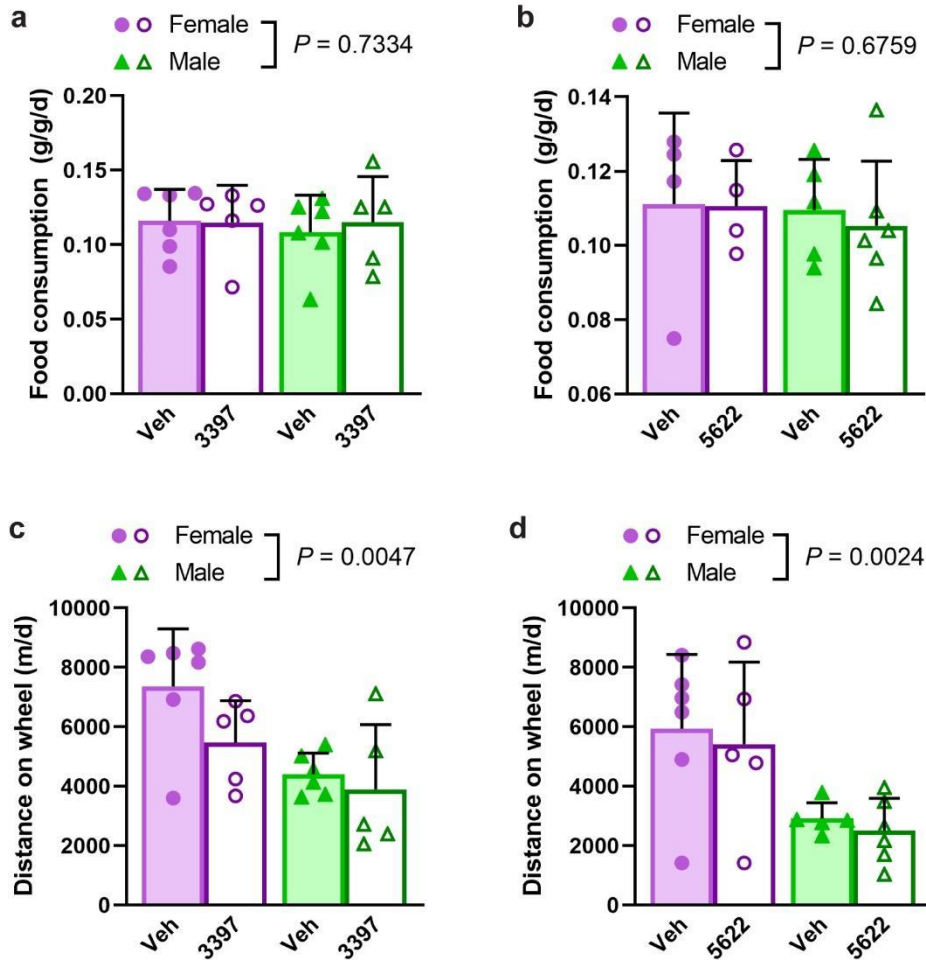
1548 bars represent the s.d. of the mean. **d**, Schematic of terminal PLX treatment of C57BL/6J wild

1549 type mice (Wt) from 2 mo of age until death and blood plasma collected at 3, 4, 5, 6, and 7 mo

1550 of age. **e**, Plasma concentration of PLX3397 in female or male Wt mice. The difference between

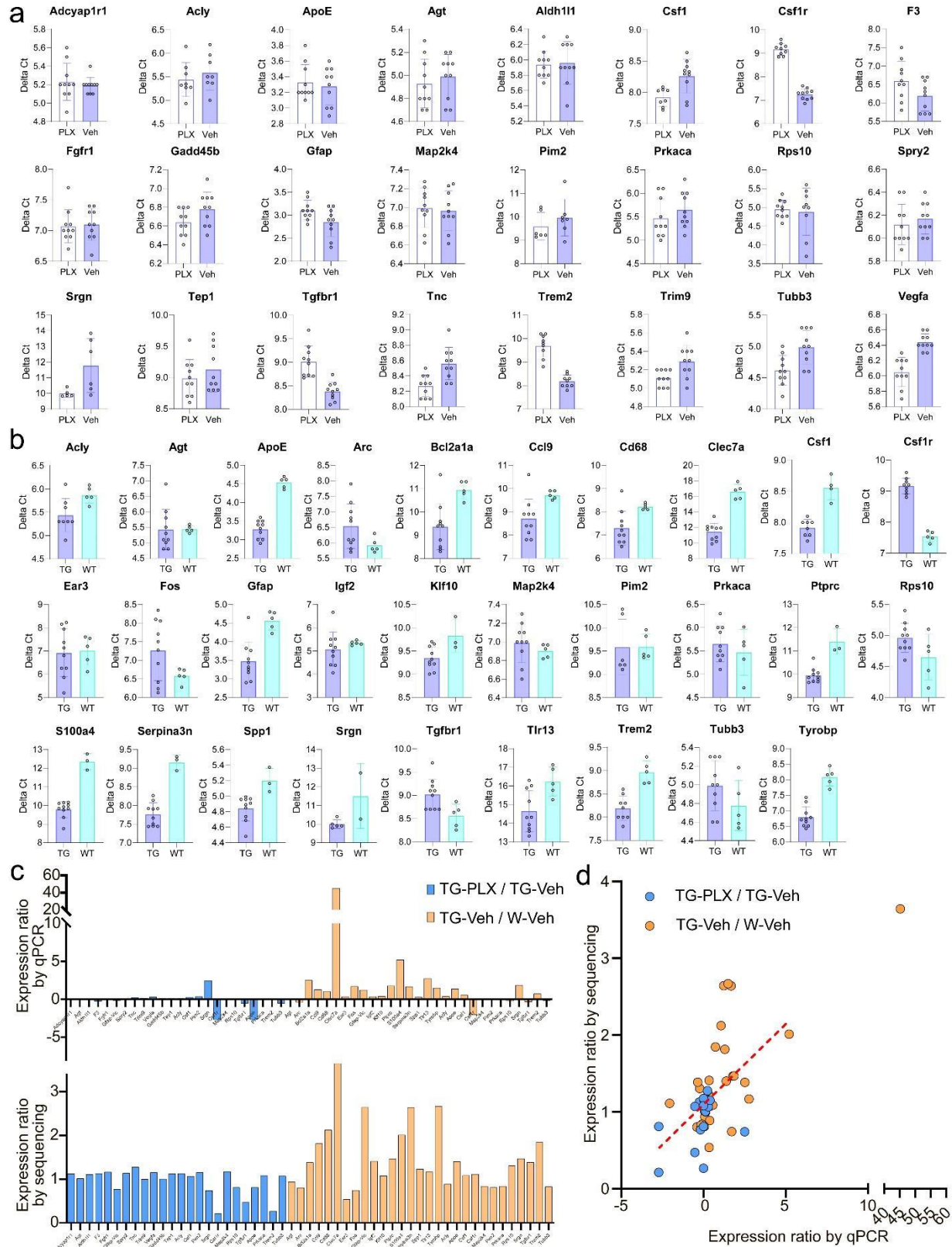
1551 female and male mice was assessed by two-way repeated measures ANOVA and the P value is

1552 shown. **f**, Body weights of female or male Wt mice treated with vehicle or PLX3397. Differences
1553 in weight between vehicle and PLX3397 treatment in male or female mice were evaluated by
1554 two-way repeated measures ANOVA and *P* values are shown. In **b**, **e**, and **f**, each symbol
1555 represents an individual mouse and the lines represent the group means.



1556

1557 **Supplementary Fig. 10| Food consumption and activity of Tg2541 mice treated with**
1558 **CSF1R inhibitors. a, b,** Food consumption measured in Tg2541 mice receiving terminal
1559 treatment with vehicle or PLX3397 (275 mg/kg oral) (a), or vehicle or PLX5622 (1200 mg/kg
1560 oral) (b), reported as grams of food per gram of mouse body weight per day (g/g/d). c, d,
1561 Running wheel activity measured in Tg2541 mice receiving terminal treatment with vehicle or
1562 PLX3397 (c), or vehicle or PLX5622 (d), reported as total distance traveled in meters per day
1563 (m/d). In a-d, each symbol represents an individual mouse, with female mice shown as closed
1564 or open circles and male mice shown as closed or open triangles. Error bars represent s.d. of
1565 the mean. Two-way ANOVA was used to compare female and male mice and P values are
1566 shown.



1567

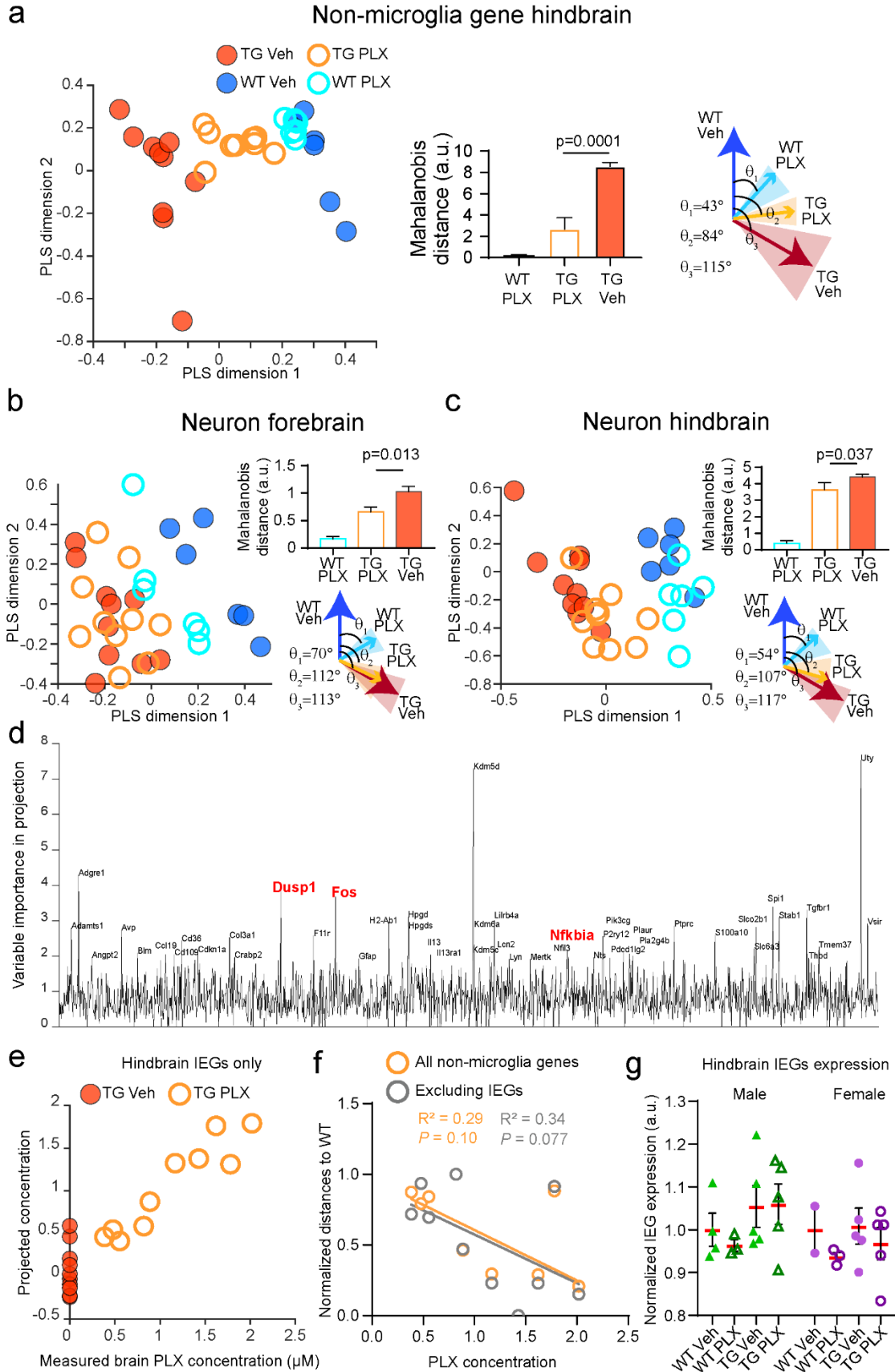
1568

1569

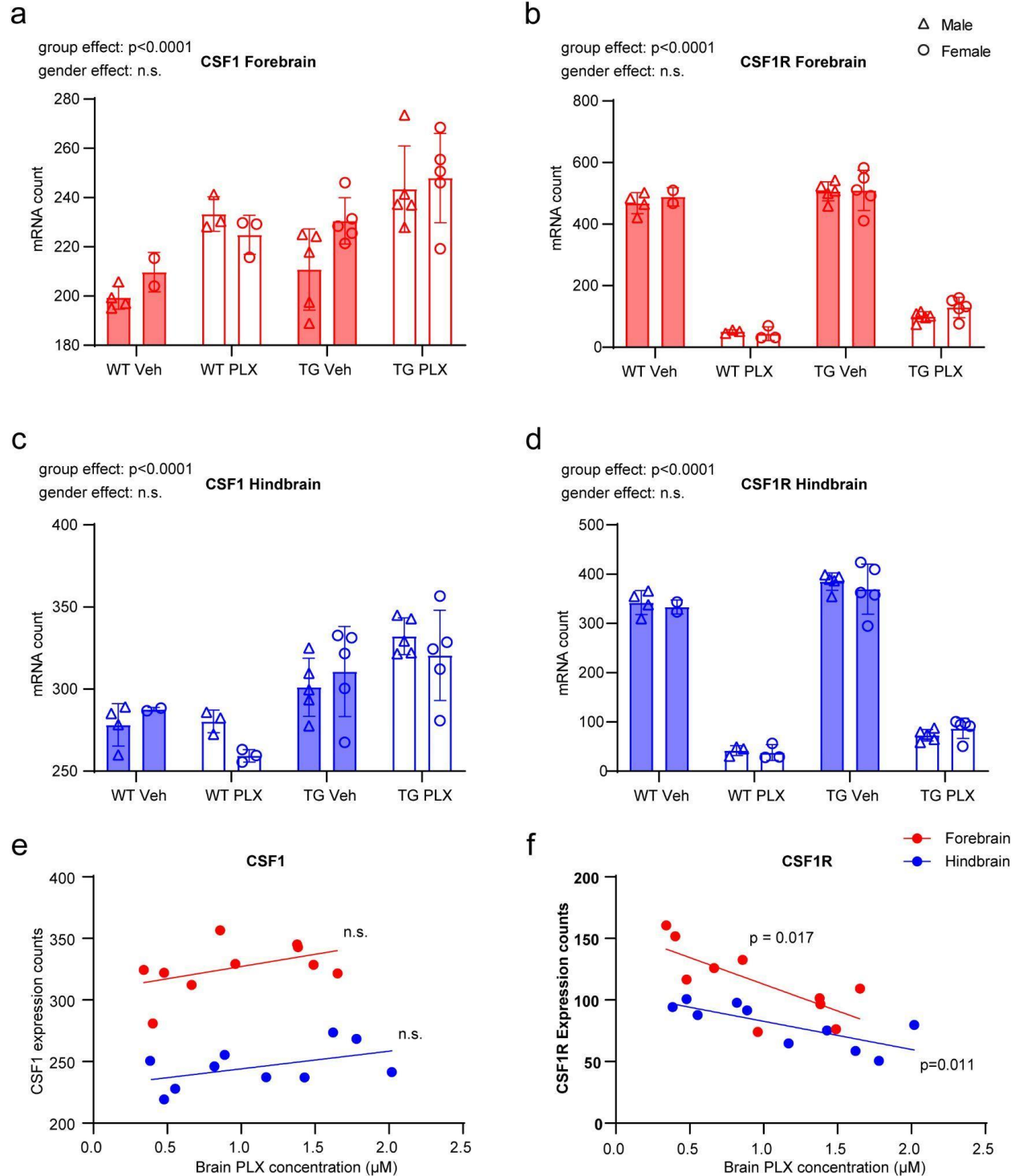
Supplementary Fig. 11| Validation of Nanostring sequencing results with real-time PCR.

a, Delta Ct values of 24 selected genes in hindbrains of Tg2541 mice treated with PLX5622

1570 (1200 mg/kg) and vehicle. A lower Delta Ct reading indicates higher expression level. **b**, Delta
1571 Ct values of 29 selected genes in hindbrains of Tg2541 and wild type mice treated with vehicle.
1572 A lower Delta Ct reading indicates higher expression level. **c**, Expression ratios of the 53 genes
1573 in **(a)** and **(b)** as measured by qPCR and Nanostring sequencing. **d**, Scatter plot of the data in
1574 **(c)**. Red dotted line shows a linear trend line.



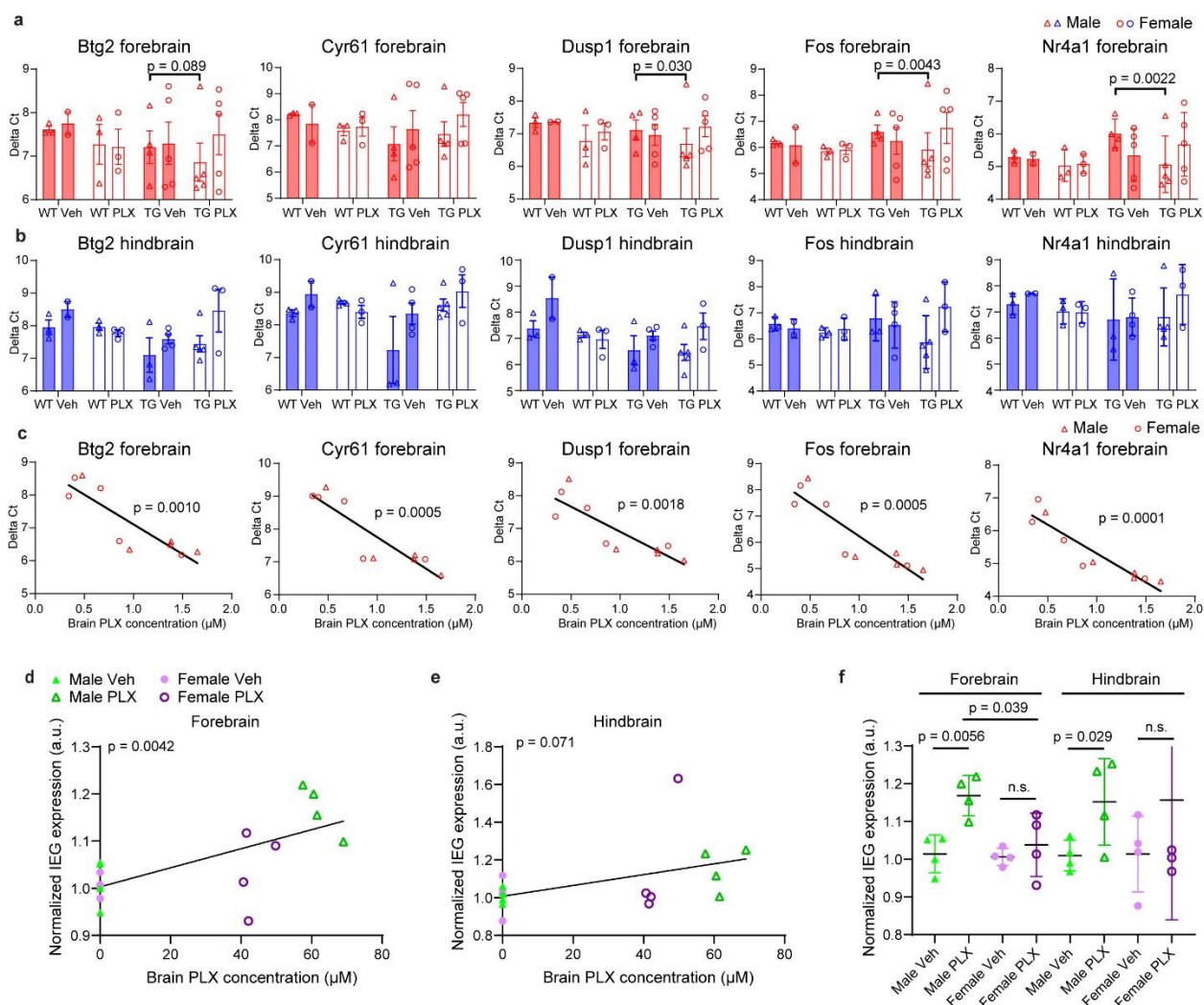
1576 **Supplementary Fig. 12| Gene expression pattern analyses of non-microglial and neuron-**
1577 **specific genes. a–c,** Analyses similar to Fig. 6c–e, using (a) all non-microglial genes in
1578 hindbrain, or neuron-specific genes in (b) forebrain and (c) hindbrain. **d–g,** Analyses similar to
1579 Fig. 6g–j, using data from hindbrains.



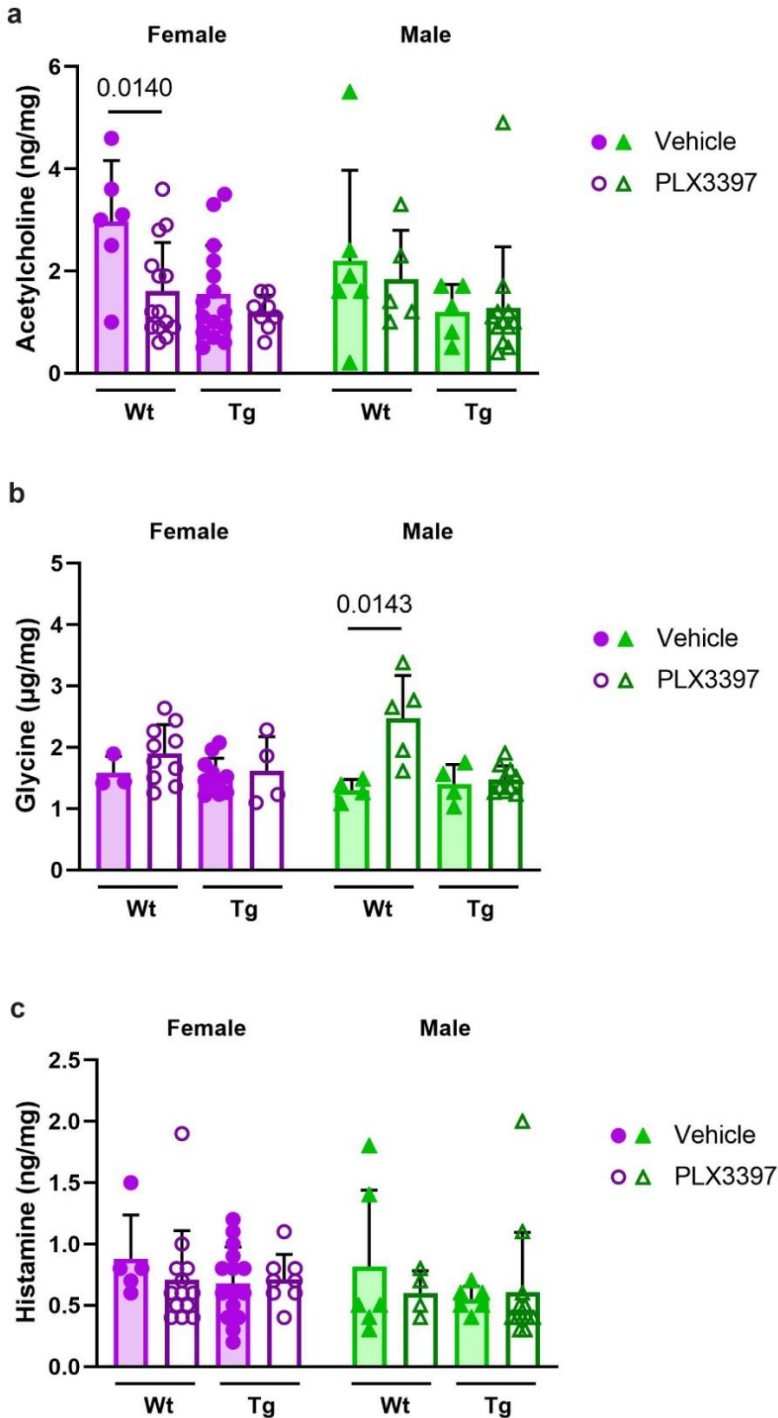
1580

1581 **Supplementary Fig. 13| PLX treatment led to increased CSF1 expression and decreased**
 1582 **CSF1R expression.** Quantification of CSF1 expression showed slight increase after PLX
 1583 treatment, while CSF1R expression showed marked decrease. Two-way ANOVA was used for

1584 statistical tests. Bottom panels showed scatter plots of brain PLX concentration against CSF1 or
1585 CSF1R expression. Linear regressions were calculated for each group.



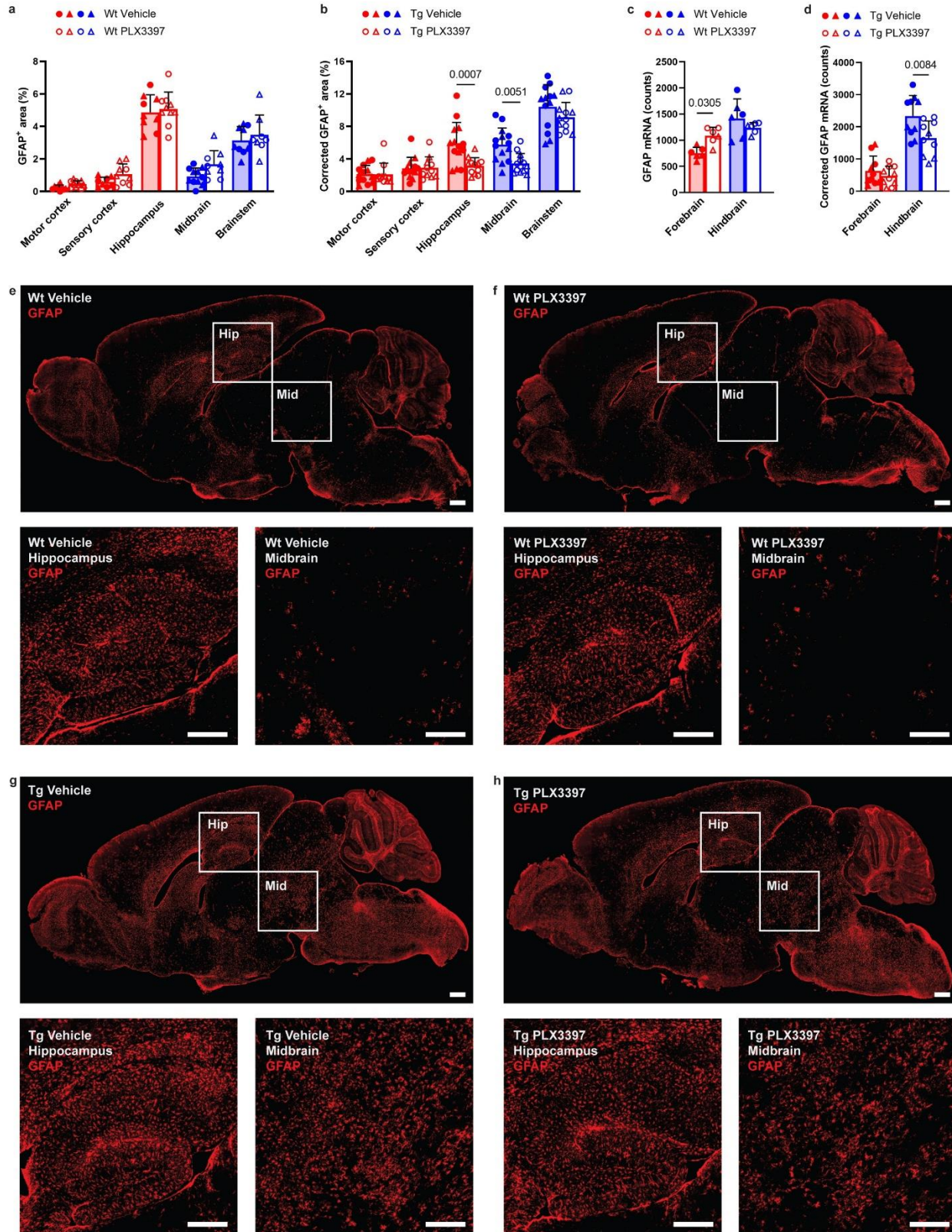
1586
 1587 **Supplementary Fig. 14| Validation of IEG up-regulation following PLX treatment. a, b,**
 1588 Real-time PCR quantifications of the mRNA levels of five IEGs in forebrains (**a**) and hindbrains
 1589 (**b**) from PLX5622- or vehicle-treated Tg2541 or wildtype mice. **c**, Correlation of brain PLX
 1590 concentration and expression levels from the five immediate early genes in the forebrains from
 1591 PLX5622-treated Tg2541 mice. **c, d**, Correlation of brain PLX concentration and normalized
 1592 expression levels from all immediate early genes (IEGs, 56 genes for each mouse) in the (**d**)
 1593 forebrains and (**e**) hindbrains of vehicle- and PLX3397-treated Tg2541 mice. Pearson's
 1594 correlation analysis was performed and the *P* values are shown. **f**, Quantification of normalized
 1595 expression levels from all IEGs (56 genes for each mouse) in the forebrain and hindbrain of
 1596 vehicle- and PLX3397-treated Tg2541 mice. Mann-Whitney tests were used for comparisons
 1597 between groups. Each symbol represents an individual mouse.



1598

1599 **Supplementary Fig. 15| Brain neurotransmitter levels unaffected by PLX3397 in male**
1600 **Tg2541 mice.** **a**, Forebrain lysates of wild type (Wt) or Tg2541 (Tg) mice, dosed for 6-12 weeks
1601 with PLX3397 (275 mg/kg oral) or vehicle beginning at 4 months of age, were measured by
1602 hydrophilic interaction liquid chromatography tandem mass spectrometry (HILIC-MS/MS). **b**,

1603 HILIC-MS/MS analysis of the same samples for glycine. **c**, HILIC-MS/MS analysis of the same
1604 samples for histamine. **a–c**, Mann-Whitney tests were used for comparing vehicle and PLX3397
1605 treatment groups within mouse genotype and sex, and the *P* values of statistically significant
1606 differences ($P < 0.05$) are shown. Each symbol represents an individual mouse and error bars
1607 indicate the s.d. of the mean.



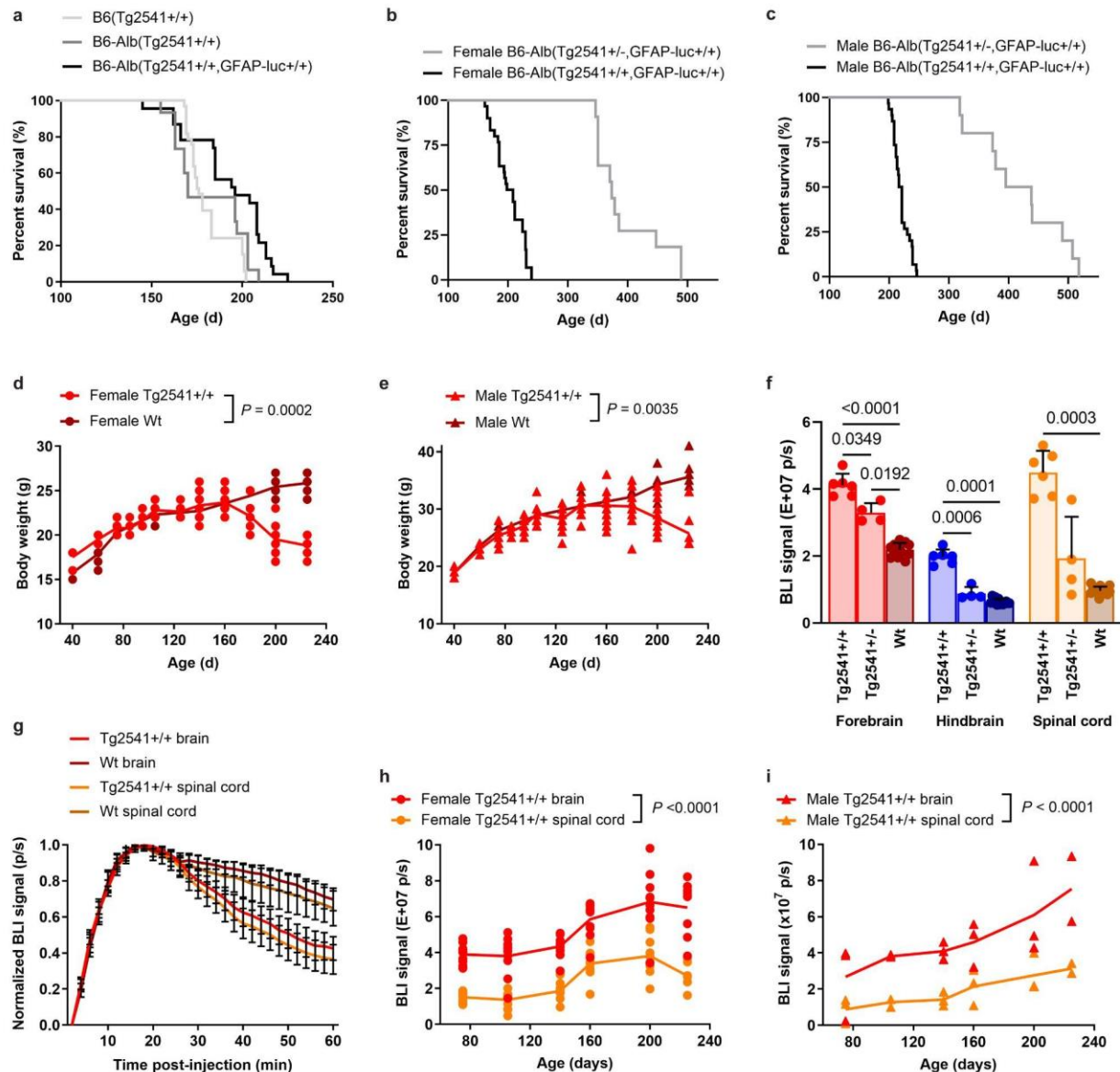
1608

1609

1610

Supplementary Fig. 16| GFAP expression is reduced by PLX3397 treatment in Tg2541 mice. a, b, GFAP levels measured by IHC in five different brain regions, three forebrain regions

1611 and two hindbrain regions, of **(a)** wild type (Wt) and **(b)** Tg2541 mice treated with PLX3397 (275
1612 mg/kg oral) or vehicle. GFAP levels in Tg2541 mice were corrected for the average levels in
1613 each brain region of PLX3397- and vehicle-treated Wt mice. **c, d**, GFAP mRNA levels
1614 measured by Nanostring in the forebrain or hindbrain of **(c)** wild type and **(d)** Tg2541 mice
1615 treated with PLX3397 (275 mg/kg oral) or vehicle. GFAP mRNA levels in Tg2541 mice were
1616 corrected for the average levels in each brain region of PLX3397- and vehicle-treated Wt mice.
1617 In **a–d**, Two-way ANOVA with Holm-Šidák post hoc testing was used to evaluate the differences
1618 between vehicle- and PLX3397-treated groups within each brain region and *P* values of
1619 statistically significant differences ($P < 0.05$) are shown. Each symbol represents an individual
1620 mouse with female mice shown as closed or open circles and male mice shown as closed or
1621 open triangles. **e–h**, Representative GFAP IHC images of a brain section from **(e)** a Wt vehicle-
1622 treated mouse, **(f)** a Wt PLX3397-treated mouse, **(g)** a Tg2541 vehicle-treated mouse, and **(h)** a
1623 Tg2541 PLX3397-treated mouse. High-magnification images of the indicated hippocampus
1624 (Hip) and midbrain (Mid) regions are shown below each image. Scale bars, 500 μm .



1625

1626 **Supplementary Fig. 17| Generation, optimization, and validation of bigenic Tg2541/GFAP-**

1627 **luciferase mice for in vivo bioluminescent imaging (BLI) of astrocytosis. a,** Kaplan-Meier

1628 plot shows that the survival curve (kinetics of disease) is unchanged for Tg2541 homozygous

1629 mice bred to B6-albino background and homozygous for the reporter GFAP-luciferase

1630 transgene. **b, c,** Kaplan-Meier plots for **(b)** female and **(c)** male mice showing that survival

1631 curves of homozygous and hemizygous B6-albino bigenic Tg2541 mice is not sex-dependent;

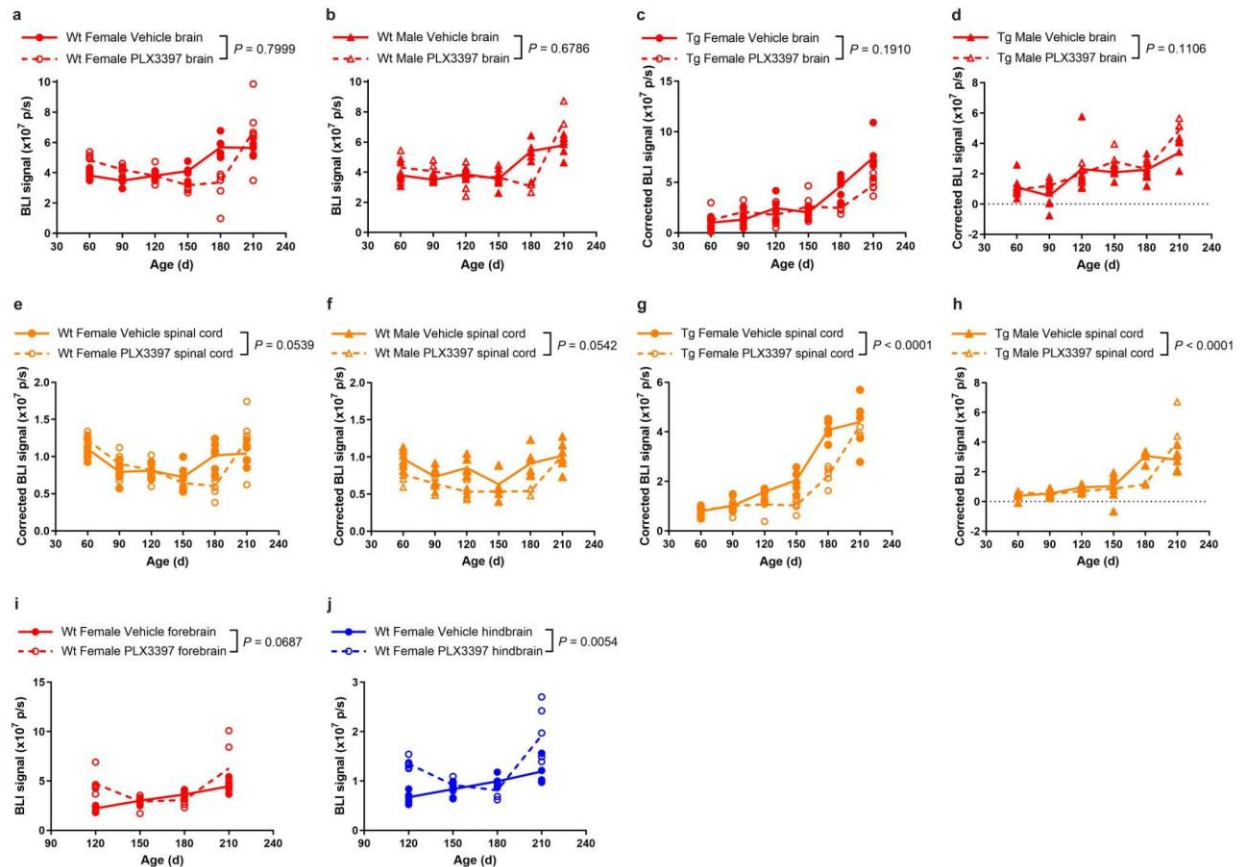
1632 homozygous Tg2541 mice have a median survival of 212 days, and hemizygous Tg2541 mice

1633 have a median survival of 378 days. **d, e,** As a crude surrogate of general health, longitudinal

1634 measurements of mouse body weight (grams) shows that in contrast to Wt mice, **(d)** female and

1635 **(e)** male Tg2541 mice lose weight as a result of decreased food intake from increasing

1636 paraparesis with disease progression. Because earlier studies gave a standard volume of d-
1637 luciferin substrate regardless of changes in individual mouse weight, we optimized the protocol
1638 to give a 25mg/kg of CycLuc1 to increase consistency in BLI measurements. **f**, To validate the
1639 GFAP-luciferase reporter gene and the synthetic luciferin substrate (CycLuc1) *in vivo*, we
1640 performed BLI in Tg2541 homozygous mice (~200 days old) with advanced disease pathology
1641 and showed the BLI signal is significantly increased in the forebrain, hindbrain and spinal cord
1642 as compared to similar aged Tg2541 hemizygous and Wt mice. Welch ANOVA with Dunnett T3
1643 post hoc testing was used to compare groups and *P* values for all statistically significant
1644 differences ($P < 0.05$) are shown. Error bars represent the s.d. of the mean. **g**, Time-lapse
1645 imaging (two-minute intervals) of BLI signal from brain and spinal cord in Tg and Wt mice
1646 showed that peak BLI signal occurred between 14 and 20 minutes after CycLuc1 injection to the
1647 peritoneum. Thus, to decrease variability in our study, we collect images at 14, 16, and 18
1648 minutes post-injection and average all three time points to account for subtle differences in time
1649 of injection and individual mouse pharmacokinetic of CycLuc1. **h**, **i**, Longitudinal BLI plots in (**h**)
1650 female and (**i**) male mice show kinetics of gliosis in the Tg2541 brain and spinal cord (3 mice
1651 per field of view). **j**, Example image of the field of view (magnification) used to capture both the
1652 brain and spinal cord in three mice per time point. In **d**, **e**, **h**, and **i**, differences between groups
1653 were evaluated by repeated measures ANOVA and *P* values are shown. Each symbol
1654 represents an individual mouse and lines indicate group means.



1655

1656

Supplementary Fig. 18| Brain and spinal cord BLI of PLX3397-treated wild type and

1657 **Tg2541 mice. a, b,** Longitudinal brain BLI plots of (a) female and (b) male wild type (Wt) mice

1658 treated with PLX3397 (275 mg/kg oral) or vehicle. **c, d,** Longitudinal brain BLI plots of (c) female

1659 and (d) male Tg2541 mice (Tg) treated with PLX3397 (275 mg/kg oral) or vehicle. The data

1660 were corrected for brain BLI levels of PLX3397- and vehicle-treated Wt mice, shown in a and b.

1661 Due to resolution and/or sensitivity of this magnification, we did not observe any differences

1662 between PLX3397 and vehicle groups. Higher magnification imaging on single mice from the

1663 same cohort was performed as shown in Fig. 8e-g. **e, f,** Longitudinal spinal cord BLI plots of (e)

1664 female and (f) male Wt mice treated with PLX3397 (275 mg/kg oral) or vehicle. **g, h,**

1665 Longitudinal spinal cord BLI plots of (g) female and (h) male Tg2541 mice (Tg) treated with

1666 PLX3397 (275 mg/kg oral) or vehicle. The data were corrected for spinal cord BLI levels of

1667 PLX3397- and vehicle-treated Wt mice, shown in e and f. **i, j,** High magnification BLI plots of the

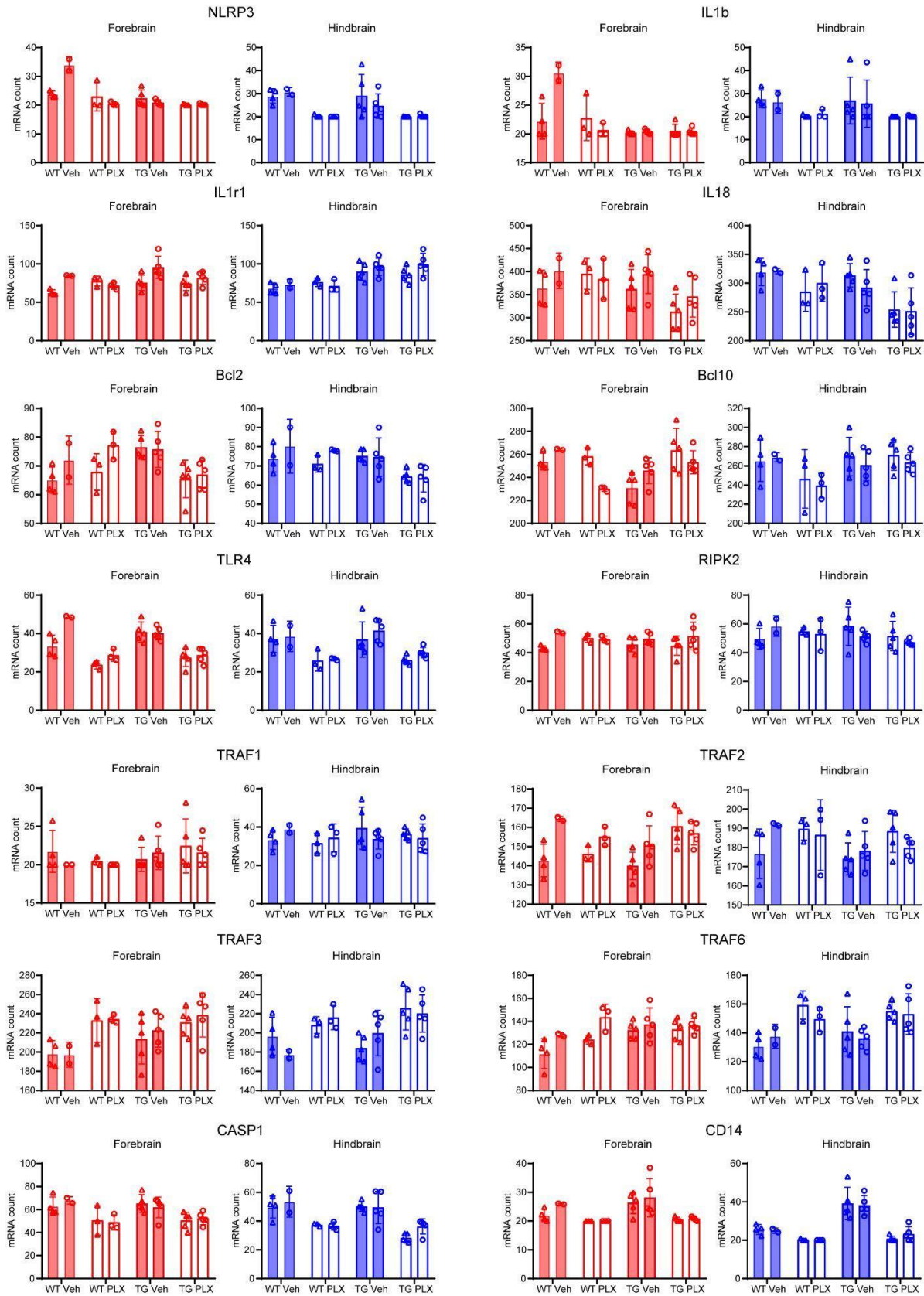
1668 (i) forebrain and (j) hindbrain of female Wt mice treated with PLX3397 (275 mg/kg oral) or

1669 vehicle, and used to correct the BLI data of female Tg2541 mice presented in Fig. 8f,g. In a-j,

1670 differences between vehicle and PLX3397 treatment were evaluated by repeated measures

1671 ANOVA and P values are shown. Each symbol represents an individual mouse and lines

1672 indicate group means.



1678 **Supplementary Fig. 20| Tau pathology or PLX treatment did not lead to marked alteration**
1679 **of inflammasome-related genes.** Quantification of 14 inflammasome-related genes in different
1680 experimental groups.

1681 **Supplementary Data File 1| Statistical tests of sex-specific drug effects on microglia, tau,**
1682 **and neurons. a,** Statistical test results for 3-way ANOVA analyses for each figure panel where
1683 female and male mice were combined. Statistical test results include the type III sum-of-squares
1684 (SS), the F statistic, and the *P* value for the main effect of sex and for the sex*drug interaction
1685 effect. **b, c,** Statistical test results for 2-way ANOVA analyses for **(b)** female or **(c)** male mice
1686 separately, for each figure panel where female and male mice were combined. Statistical test
1687 results include the type III sum-of-squares (SS), the F statistic, and the *P* value for the main
1688 effect of drug, and the *P* value for the multiple comparisons post-hoc testing of each drug
1689 compared to the vehicle in the forebrain, hindbrain, or spinal cord. 'na' indicates that the data is
1690 not available because the drug was not tested in that particular experiment.

1691
1692 **Supplementary Data File 2| Differentially expressed genes in male and female PLX-**
1693 **treated Tg2541 mice.** Forebrain samples from male and female Tg2541 mice were analyzed
1694 for gene expression by Nanostring following chronic treatment with PLX5622. The data
1695 represent the average expression levels of five male and five female mice, which were then
1696 compared by unpaired t-test and the *P* value is shown. Please note that the entire transcriptome
1697 dataset which also includes hindbrain data, wild type mice, and vehicle-treated mice are
1698 available from Github with the following link: [https://gitfront.io/r/user-](https://gitfront.io/r/user-8849465/665dd65fd9d9e78650ed02b9f30236d99240de39/UCSF-PLX-nanostring/)
1699 [8849465/665dd65fd9d9e78650ed02b9f30236d99240de39/UCSF-PLX-nanostring/](https://gitfront.io/r/user-8849465/665dd65fd9d9e78650ed02b9f30236d99240de39/UCSF-PLX-nanostring/)

1700